PERFORMANCE OF CONCRETE SLABS WITH EMBEDDED HYDRONIC LOOPS FOR GEOTHERMALLY BASED BRIDGE DE-ICING APPLICATIONS

by

Mark Hurley

Presented to the Faculty of the Graduate School of

The University of Texas at Arlington in Partial Fulfillment

of the Requirements

for the Degree of

MASTER OF SCIENCE IN CIVIL ENGINEERING

THE UNIVERSITY OF TEXAS AT ARLINGTON

May 2019

ACKNOWLEDGEMENTS

First and foremost, I want to acknowledge my advisor, Dr. Xinbao Yu, for giving me the opportunity to be a part of a research project intended to facilitate the growth, development, and safety of bridges and roadways using an innovative approach. Also, his guidance, support, continual feedback, and effective communication along the way helped me mature in the field of Engineering and paved the way for new opportunities in the future.

I am deeply gratified for all the funding support provided by TX-DOT to facilitate the growth and development of a new field of research. Without their funding support and assistance with extending the project to the next phase, the opportunity to achieve such success would be greatly compromised.

I would like to acknowledge Dr. Anand Puppala, for assisting with the research progression and funding support during the initial phase of the project. I am gratified for the time invested by Dr. Anand Puppala and Dr. Laureano Hoyos to support me as committee members, and the constructive criticism and feedback provided to ensure the quality of this thesis is not compromised. I greatly appreciate the group effort by Omid Habibzadeh-Bigdarvish, Gang Lei, and Teng Li regarding assistance with laboratory experiments, editing, and other project related tasks.

Finally, I am grateful for all the support from my family and friends- All the advice, wisdom, and humor over the years has contributed immensely to my progression as a Graduate Student.
The quality of this thesis is a function of the predecessors who have paved the way for the opportunities what we are accustomed to, and everyone who have helped refine my work over the span of my graduate studies.

May 10, 2019

Abstract

PERFORMANCE OF CONCRETE SLABS WITH EMBEDDED HYDRONIC LOOPS FOR GEOTHERMALLY BASED BRIDGE DE-ICING APPLICATIONS

Mark Hurley, MS

The University of Texas at Arlington, 2019

Supervising Professor: Xinbao Yu

Geothermal energy has always been available as a renewable thermal reserve, however, only recently has it been unlocked as a potential source of energy to de-ice bridges and roadways. The ability to efficiently extract the geothermal reserves has been accomplished with the advent of new technology. Each progressing year, the refinement of technology has led to a reduction in the input required to achieve a desired output. For the case of bridge de-icing, the extracted input of thermal energy must exceed the required demands to permit de-icing. The conventional approach to de-icing (using chemicals, salt, and sand) works as a mediator of the freeing point to melt ice, however, there is absence of thermal energy. Therefore, various methods have been devised to generate heat using different sources of energy with the intended goal of efficient de-icing.

The focus for this thesis is to experimentally simulate the derivation of geothermal energy via a hydronic loop de-icing system. A small-scale bridge slab was subjected to multiple winter scenarios in a controlled setting to obtain a prediction of the thermal reserves required to permit de-icing. An additional slab was placed in an outdoor environment to test the performance of the system under cyclic conditions over the span of a winter period. The vertical and lateral thermal distribution across the slab was determined to gauge the temperature variation in reference to the

pipe geometry. The thermal minimum was also determined to obtain the maximum heat input requirement. The negative influence of sustained wind was studied to attain a relationship of thermal demands as a function of wind magnitude. A thermal rebound study is provided to determine the recovery rate of thermal energy in respect to a negative incremental change in wind magnitude. By compiling the steady-state response of the slab for a wide range of winter scenarios and creating an error bound estimate, the thermal demands could be predicted with a higher degree of precision. The final aim is to formulate a design criterion to estimate the required inlet temperature to achieve efficient ice removal across the entire slab area.

Table of Contents

List of Figures

List of Tables

CHAPTER 1

1.1 Background of Project

Texas is especially prone to freezing rain conditions during the winter months, which lead to a host of consequences that need to be mitigated for the future generations to progress toward a safer, more robust society. Through extensive research and development, multiple solutions have been proposed to minimize the negative implications arising from icy conditions. Conventional practices such as utilizing plows and de-icing chemicals have proved detrimental in the long run, due to the corrosion and residual environmental effects (figure 1-3 b). The structural integrity of bridges and roads will diminish over time due to intermittent exposure of de-icing chemicals, which increasing the likelihood of structural collapse and adds to the cost and time demands regarding maintenance. For instance, rock salt is HYGROSCOPIC, meaning that it draws in extra water during the de-icing process and hence, creates a slurry salt/water mix that consequently expands within concrete (Callum Graham and Jessica Snow, 2017). This can eventually lead to unnecessary pit holes which creates a vicious cycle of water infiltration (figure 1-3 a). Moreover, using heavy machinery such as plows can further degrade roadways over time. Therefore, automated solutions to the current issue have increasingly been proposed. One such instance which proved the limitation of a conventional approach occurred in 2014 for the DFW area (Figure 1-1). A major winter event created very treacherous travel conditions due to heavy accumulation of ice. Multiple accidents were reported over the span of the event, which could have been mitigated if proper de-icing methods were emplaced. To prevent the recurring events from causing safety concerns, a de-icing system must be developed that can extract the thermal demands necessary to counter any such scenario.

Figure 1- 1 Cobblestone Ice Creates Dangerous Travel Conditions during Record Ice Event (Yu et al., 2017)

One alternative approach is to extract geothermal energy from the sub-surface via a hydronic heating system embedded within boreholes. A closed pipe network extends within the borehole to extract heat and transfer the energy to the underside of a pre-existing bridge. For newly designed bridges, it is more efficient to embed the pipe network within the slab to minimize the energy demands required for de-icing. At a depth that exceeds 30 feet, the mean earth temperature is relatively constant as shown in figure 1-2. In the DFW region, the mean earth temperature is roughly 68 ° F (Reysa, 2005). Therefore, the number of boreholes needed to permit de-icing can be determined. By circulating water with an anti-freeze agent via a circulation pump, the extracted thermal energy can continually transmit to the base of the slab to initiate the de-icing process. To idealize the system, a heat pump is attached to the proposed de-icing system for additional heat if needed. To prevent heat loss at the base, an insulative material is added to encapsulate the pipe network to maintain higher efficiency.

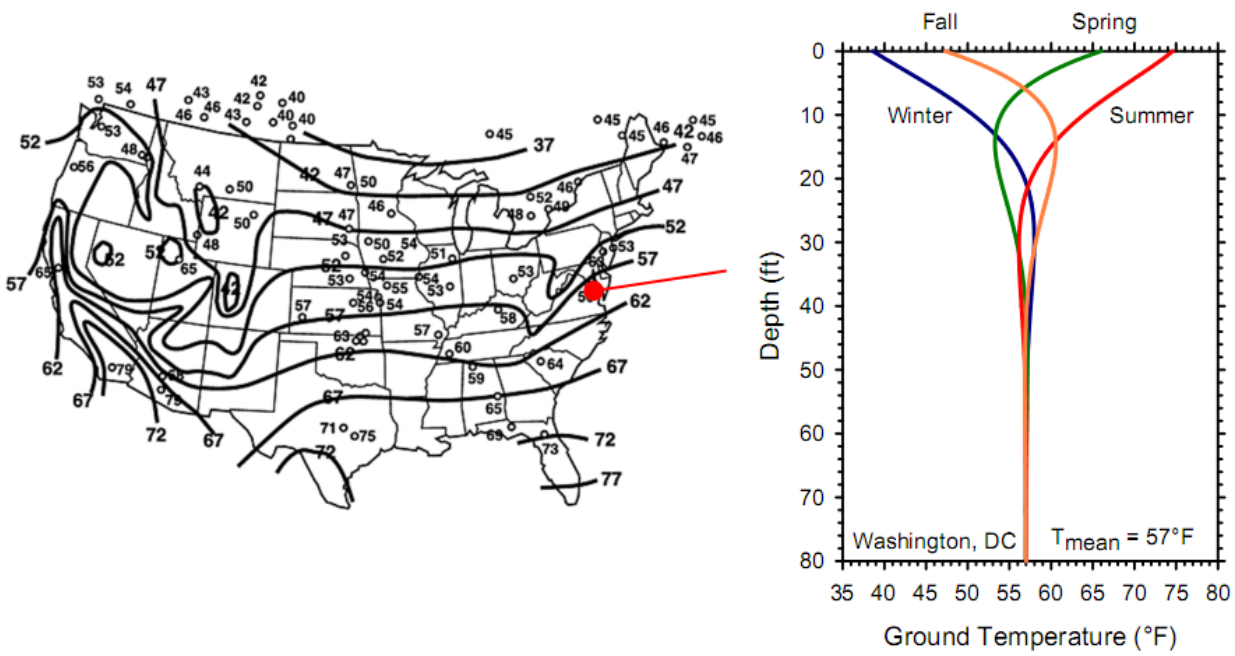

Figure 1- 2 Seasonally ground temperature (Sutman and Olgun, 2013)

Figure 1- 3 (a) De-icing Salt causing Pits (Ryan Kartchner Concrete Construction) (b) Column deterioration from chemical solution contamination (C. Michael Lee, 2017)

1.1.1. External Versus Internal Model

Although the rapid advancement in technology has facilitated growth and development across multiple sectors, there remains a growing concern of maintaining pre-existing structures such as bridges. In Texas, preferential black ice is very problematic during Winter months, which contributes to traffic accidents and consequently, fatalities. Therefore, utilizing various technological advances to create a renovative solution for bridge de-icing is a necessary condition to prevent reoccurrence of these issues. Internally heated bridge decks are accompanied by three typical methods for generating thermal energy: electric, heat pipe, and hydronic methods. Electric heating is induced by transmitting a voltage (signal) through conductor such a concrete that is incased with electric resistant material or impurities to increase the generation of heat. The loss in energy of the current results in the generation of heat via the law of conservation of energy (Minsk, 1999). The heat pipe method utilizes a working fluid such as co2, which is vaporized at the heat source. The fluid is then transferred to the cold end of the pipe where it condenses, and releases stored energy in form of heat. A capillary wick network running along the length of the pipe is encased to provide the necessary force of adhesion to allow the working fluid to return to heat source completing the loop. Lastly, hydronic heating utilizes circulated water typically mixed with glycol (antifreeze agent) to transmit the heat throughout a pipe network embedded within the concrete slab. Hydronic heating can be translated to the base of pre-existing bridges for external source heating. The goal of this thesis is to determine the performance and overall efficiency of an externally heated system using a novel approach and provide necessary recommendations to enhance the efficiency going forward. Figure 1-4 differentiates the external heating method for existing bridges (a) versus the internal heating method for new bridges (b). The internal method encapsulates the pipe network within the concrete prior to the curing process. Because the pipe is closer to the surface, less heat demands are required for de-icing relative to the external approach, which secures the pipe network to the base of the slab with an additional foam layer at the interface. The external method hasn’t been studied as extensively as the internal method. Therefore, a thorough investigation will be provided regarding its effectiveness at countering winter weather scenarios.

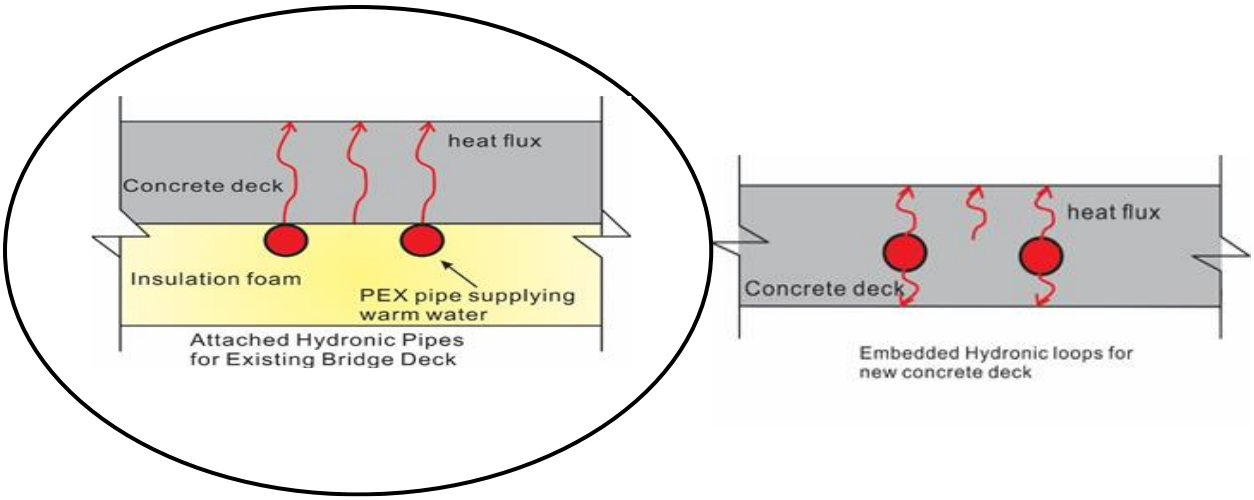

Figure 1- 4 (a) Proposed externally heated system for pre-existing bridges, (b) Internally heated system for new bridges

1.1.2. Steady-State and Transient Studies

To properly simulate sub-freezing conditions in the field, a laboratory study is initially conducted in a controlled environment. In the field, there exists cyclic transient conditions, which can be separated into two sub-sets based on the peak and trough periods. The least likelihood of de-icing will tend to occur as the trough period (minimum diurnal temperature) is approached. Transient conditions, however, are very difficult to analyze due to the variability of wind as a negative influence factor. Moreover, a time lag will exist within the slab in response to transient ambient conditions, which implies that there is a higher likelihood of de-icing relative to steady-state conditions if wind is not considered as a factor. Therefore, an experimental study confined to static conditions will be conducted to determine the feasibility of de-icing and predict the required thermal energy to ensure the process is complete. To attain static conditions, a freezer box is utilized which maintains a relatively constant temperature for the duration of each test. The wind is negligible unless an external source is applied. The objective is to obtain steady-state conditions within the slab so that the thermal demands can be accurately estimated. By testing the performance of the simulated geothermal de-icing system as a measure of validity, the field model can be implemented with confidence. An additional study was conducted to measure the slab response to transient outdoor conditions to gauge the range of possible circumstances that may be encountered.

1.2. Scope and Objective

The use of geothermal energy as a renovative solution to mitigate potential road hazards due to preferential ice accumulation, snow, and freezing rain conditions is the final aim. A preceding experimental study is conducted to bridge the gap between testing the performance of the system and field implementation. For this study, a fabricated de-icing system attached to a concrete slab is subjected to various environmental conditions ranging from static to variable states. The main objective of the experimental study is to test the reliability of the system and predict the required energy demands given a Winter scenario. To determine the reliability of the system, multiple Winter weather scenarios were simulated to gauge the proficiency of the system to counteract potential freezing events. Multiple factors that potentiate the loss in efficiency derived from the system were considered. One such factor that cannot be overlooked is the negative influence of wind on convective heat transfer. A statistical analysis is performed to validate the prediction of energy demands required for de-icing.

1.3. Thesis Structure

This thesis is a compilation of two journal papers awaiting submission. The main body is divided into chapters according to the following structure:

Chapter 1 presents the project background, scope, and objectives.

Chapter 2 presents a brief literature review as a building block for the overall research progression. It covers the principles of extracting geothermal energy using renovative solutions such as energy piles. Also, multiple case studies are provided to summarize some of the research progress up to date in different regions across the globe. Lastly, a brief cost benefit analysis is provided to weigh the benefits of using a geothermal de-icing system relative to conventional approaches.

Chapter 3 and 4 investigate the performance of experimental bridge de-icing system subjected to controlled sub-freezing conditions (Paper A) and outdoor conditions (Paper B). The literature review and methodology section will comprise of most references utilized in each paper.

Chapter 2. LITERATURE REVIEW

2.1. Introduction

Bridge overpasses are highly susceptible to preferential ice accumulation during winter months, which is typically unseen by the naked eye. Roads are insulated below by the earth, and hence, are less susceptible to ice accumulation relative to bridges which are exposed to cold air over a larger surface area. Therefore, it is imperative to implement reliable de-icing methods to enhance safety and traffic flow of the motorists. Conventional snow and ice removal system (CSRS) perpetuate common issues associated with bridges such as reducing structural integrity, promoting negative environmental impact, and requiring intensive labor. Application of de-icing salt as the most common deicer for pavements, provoke a phenomenon known as “chloride attack” which initially corrodes the steel reinforcement in the deck and eventually causes the deterioration of bridge deck or even failure of the structure (Gode and Paeglitis, 2014). There is a growing concern regarding the deterioration of infrastructure, and their condition assessment is always a challenge (Brown et al., 2002). Overall, application of deicing salt is not an efficient solution for de-icing the bridge deck, because not only it accelerates the bridge deck corrosion, also causes travel delays for motorist which lead to great financial cost due to excessive fuel consumption (Bigdarvish et al. 2017).

In a world moving toward utilization of renewable energy, geothermal energy is recognized as a reliable source of green energy which can reduce the demand for fossil fuels (International Energy Agency, 2014). As ground temperature below a certain depth are constant (Brandl, 2006), a variety of different methods are employed to extract shallow geothermal energy, namely: borehole, deep and shallow foundations, diaphragm walls, tunnel liners and anchors, for cooling and heating purposes (Bigdarvish et al. 2017). In recent years, a new application for geothermal energy is developed. In this method, geothermal heat pump de-icing system (GHDS) is utilized for heating and de-icing the bridge deck. In this system, with contribution of heat pump, sufficient energy is provided to melt snow and ice on the bridge deck surface. Heat carrier fluid is circulating between ground loop heat exchangers and hydronic pipes in contact with the deck to transfer heat from

ground to bridge surface (Fig. 2-1). The traditional type of GHDS is using internal hydronic pipe embedded in the concrete slab, however, a new method has been developed by utilizing external hydronic pipe, attached to the base of the bridge deck and encapsulated in a layer of insulation foam to retain heat (Lei et al., 2018). In this method, application of this system is not limited only to new bridges and can be utilized for pre-existing bridges. Moreover, Habibzadeh-Bigdarvish et al., (2019) performed a life-cycle cost-benefit analysis on these systems and showed application of this system are economically viable, even without considering the environmental impact costs. Their analysis illustrates the geothermal heat pump deicing system (GHDS) has a cost-to-benefit ratio of 2.6 for the base case.

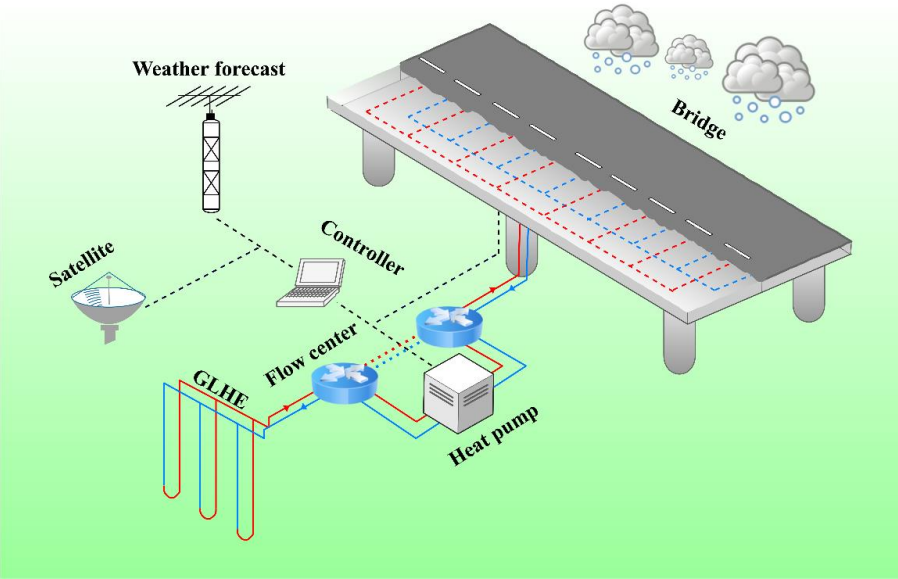

Figure 2- 1 Conceptual illustration of the geothermal heat pump de-icing system (GHDS) (Source: Bigdarvish et al., 2019)

Although there is extensive research pertaining to the success of geothermal de-icing systems for newly developed bridges, there is a limited scope of research corresponding to the study of an external de-icing system attached to pre-existing bridges. Li et al., (2018) investigated the feasibility of an externally heated geothermal bridge deck through numerical analysis. Their analysis involves a finite element model for both internal and external bridge deck heating system and studies the effect of a series parameters (e.g. ambient and inlet temperature, fluid velocity and wind speed) on both systems respectively. The result of the simulations demonstrates that the proposed externally heated geothermal bridge deck can achieve above freezing temperature in a mild winter weather condition, however, it require more heating time in compare with internal

bridge deck heating system. In a similar approach, Lei et al., (2018) studied the externally heated geothermal bridge deck using numerical simulation with more focus on the design of such system. The output of the analysis shows applicability of this system and contributing factors to the ideal performance. However, although these studies, investigates the de-icing potential for a geothermal heat pump de-icing system (GHDS) applied externally to pre-existing bridges using the numerical analysis but they lack information regarding validation of the result and actual performance of this system.

2.2. Geothermal Energy as a De-Icing Source

2.2.1. Introduction

The benefits of tapping into geothermal energy reserves are profound. The growing technological advancement has provided the necessarily tools to unlock the full potential of thermal energy for bridge de-icing mechanisms. Geothermal energy provides a sustained clean source of energy without the negative environmental consequences encountered via chemical de-icing agents. Therefore, the demands have risen exponentially to find a more reliable solution for mitigating future complications. Various attempts at replicating a geothermal de-icing system for bridge pavement slabs have been documented using an experimental approach. Thus far, there has been numerous applications for the purpose of de-icing such as underground heat exchangers, geothermal energy piles, and soil borehole thermal energy storage (BTES) (Yu et al., 2017). Ground heat exchangers are critical components in any GSHP system since they comprise the elements that extract and transfer maximum heat reserves from the ground. They can be connected to the heat pump by open or closed loops (Pagola, 2018). To ensure the demands for the system are justified, a long-term cost benefit assessment is provided.

This section presents a brief overview of current innovative solutions to the common problem of bridge de-icing using hydronic heating. Multiple advancements have been made for newly designed bridges, however, solutions for pre-existing bridges are limited. The current demand for externally heated bridges has accelerated due to the escalating consequences induced by conventional methods. Analytical approaches regarding estimating the heat flux demand for de-icing and the convective heat transfer coefficient are introduced.

2.3. Hydronic System

There have been promising results regarding increasing the efficiency of hydronic heating systems over time. To maximize the thermal energy output extracted from the ground, the use of pile heat exchanger coupled with a ground source heat pump has been devised as an alternative to borehole heat exchangers. The heat pump may potentially be needed under drastic weather circumstances, which can be readily determined using an automated weather control unit. This will ensure overall costs are minimized while provided enough energy to de-ice effectively. Yet, if the thermal energy potential is maximized from the geothermal energy reserves, then utilization of only a fluid pump may be sufficient. That is, the extraction of thermal energy from the sub-surface is enough to counter the winter conditions. Typically, an additional heat exchanger is connected to the pump system so de-icing can be permissible under a wider range of conditions. Thus, predicting the thermal demands with reasonable accuracy is a critical element when deciding whether a heat exchanger is required. This will ensure unnecessary energy is not wasted over time. Borehole heat exchangers typically consists of a U-shaped pipe unit embedded within the borehole encapsulated by a thermally conductive material. An energy pile is a heat exchange unit which can encompass an increased surface area of pipe relative to the borehole heat exchanger. Energy pile is a recent development which takes advantage of deep foundations for new structures. It greatly reduces the costs of installation needed for borehole heat exchangers. The use of energy piles as an alternative source of heat transfer has been increasing in demand. Multiple parametric studies using various models have been conducted to test its efficiency. The following key findings have been discovered using a finite element method to determine the factors that maximize the pile efficiency (Francesco Cecinatoa, c and Fleur A. Loveridge (2015).

1) The most important factor in relation to pile efficiency is the total pipe surface area, implying that maximizing the number of pipes distributed within the cross-sectional area is highly recommended provided that the pipe spacing is within a reasonable distance.
2) Maximizing the concrete thermal conductivity will yield greater energy exchange. The use of graphene to enhance the thermal properties and rigidity of concrete would be quite useful to maximize the pipe efficiency.

It was also discovered that fluid velocity yields a negligible influence on energy pile efficiency (Francesco Cecinatoa, c and Fleur A. Loveridge, 2015). The potential for de-icing is a function of the thermal load extracted from the geothermal energy loads, which is defined as the thermal energy irrespective of other heat sources such as the environment. Therefore, replicating a geothermal de-icing system experimentally will prove very useful to estimate the heat flux required to maintain a snow/ice free slab. Figure 2-2 shows a schematic view of a pile heat exchanger system using ground loops inserted in vertical boreholes. Note that Figure 3 is not to scale, and the boreholes need only to be 4 to 8 in. (100 to 200 mm) in diameter (Yu et al., 2017).

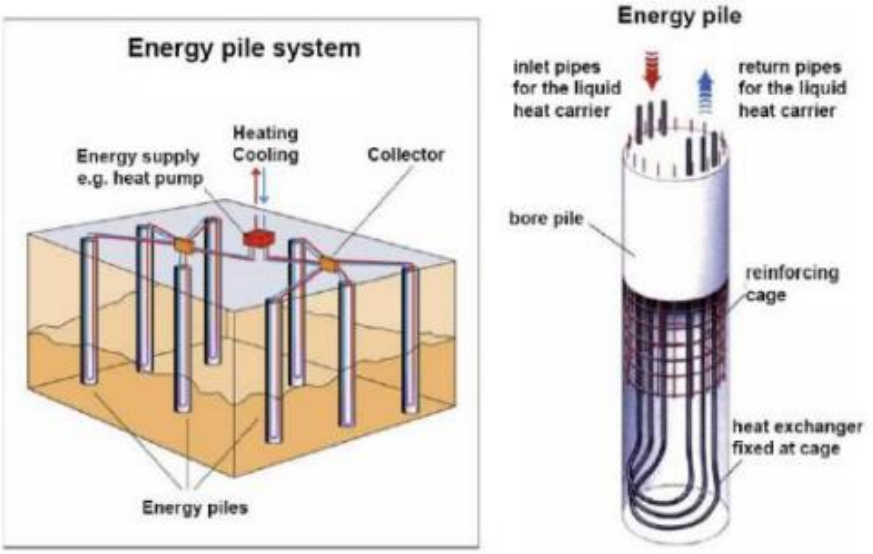

Figure 2- 2 Schematic plot of a GSHP for space heating and cooling; (b) Energy piles as the host of the absorber pipes (Yu et al., 2011)

2.4. Thermal Demand

In this section, a brief synopsis regarding the thermal energy demands required for hydronic snow melting will be presented. Case studies relating to the principles of bridge de-icing will be presented to outline the current breakthroughs. Prior to the implementation stage of any de-icing system, extensive testing needs to be conducted to ensure that the capacity of the unit achieves the intended goal. Multiple studies have been performed to predict the thermal output required for the snow melting process as follows.

2.4.1. Performance of Pile Heat Exchange Unit

Kong et al investigated the thermal performance of an energy pile heat exchange unit under various snow conditions. The aim was to determine the net rate of change corresponding to the snow melting process if the de-icing system works contemporaneously with conventional methods (use of de-icing chemicals). The system was deemed successful if there was a noticeable difference relative to relying solely on de-icing chemicals to initiate the process. The de-icing system consisted of a five U-shaped Polethylene (PERT) loops connected in series from the pile shaft to the bridge deck. The pipe network was embedded within a reinforced concrete layer of the bridge deck for heat exchange (Kong et al, 2018). Prior to testing, it was predetermined that a 20 m long energy pile can generate a max heat flux of 80 W/m^2 if no heat pump was employed. The heated slab surface area for the study was 15m^2. For the testing process, only one panel (3.5m by 10m) was reserved for the snow melting as exemplified in figure 2-3. The heat exchange tubes were installed in proximity to car wheels to save geothermal energy.

The following equations were utilized to determine whether the accumulated snow process would be effectively eliminated.

$$q_0 = q_s + q_m + A_r * (q_h + q_e) \quad \text{.....(1)}$$

Where q_s and q_m are the sensible and latent heat flux (W/m^2), A_r is the snow-free area ratio, q_h is the convective heat flux (W/m^2), and q_e is evaporative heat flux (W/m^2).

To measure the hydronic thermal energy inputted into the system, the following equation is utilized for transient conditions.

$$q_{hydronic} = mc_p(T_{in} - T_{out}) \quad \text{.....(2)}$$

Where m = mass flow rate (kg/s), c_p is the heat capacity of working fluid, and $(T_{in} - T_{out})$ is the temperature gradient between the inlet and outlet sections of pipe network.

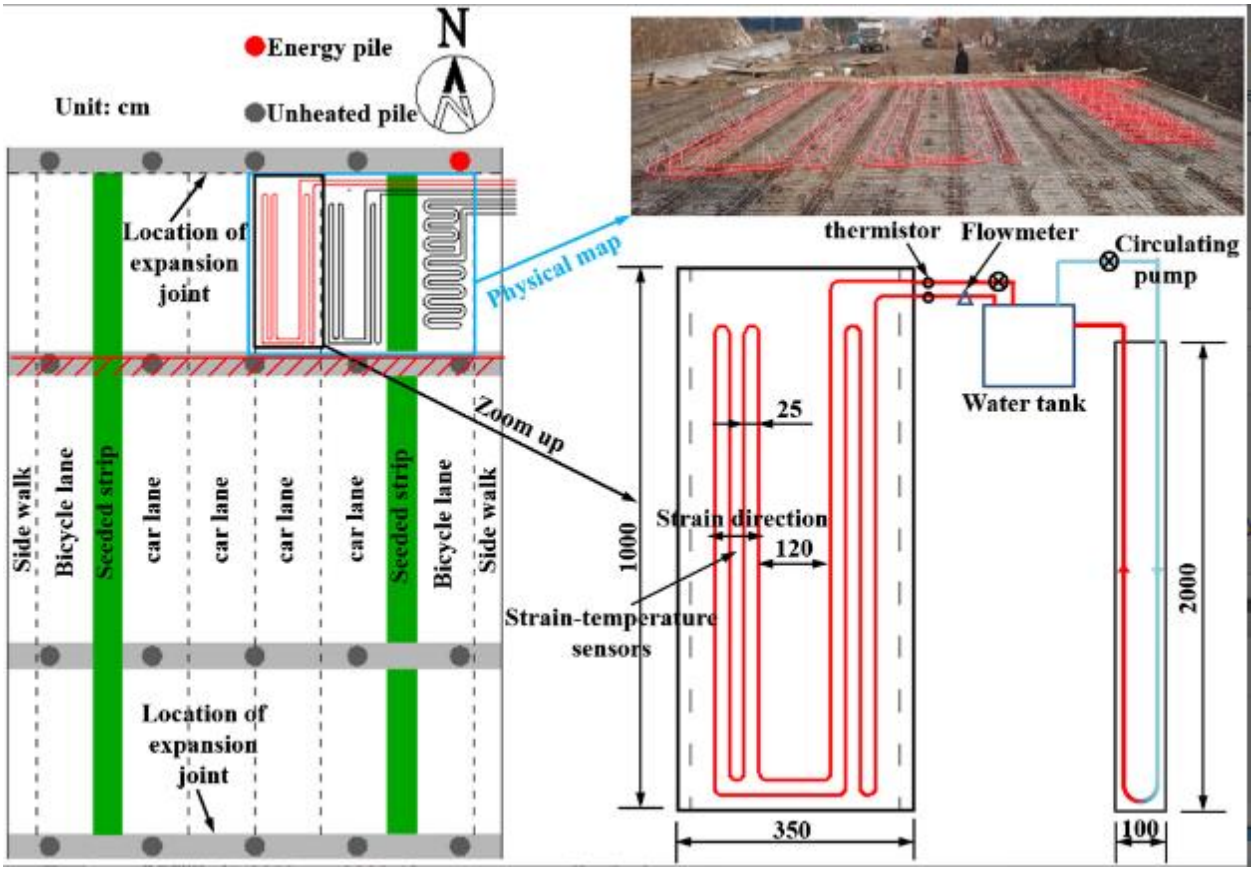

Figure 2- 3 Schematic diagram of the energy pile-based bridge deck deicing system (*Kong* et al, 2018)

The main design objective of a geothermal heating system is to achieve a certain limit of snow melting, which is adjusted according to societal demands. The snow-free area ratio (Ar), which is defined as the ratio of snow-free area of a surface to its total area, relates to snow melting performance (Yu et al, 2017). Accordingly, Chapman (1956) presented definitions of snow-melting performance classes as follows:

- Class 1 (residential): During the snowfall, the entire surface may be covered with snow (Ar=0). After the snowfall, the system is expected to melt the accumulated snow.
- Class 2 (commercial): During the snowfall, 50% of the surface may be covered with snow (Ar=0.5).
- Class 3 (industrial): During the snowfall, the entire surface is kept free from snow accumulation (Ar=1).

Since the objective of the study was to accelerate the snow melting process after cessation of snow fall, A_r was taken as zero. Using equation (1), the required heat flux to efficiently melt snow (100%) at a recorded rate of .94 mm/hr was 85.82 W/m^2. Table 2-1 displays the typical snowfall rates according to the SAE Deicing Committee (Fahey, 2008). Using equation (2), the following relation was determined experimentally: $q_{hydronic} \approx 70 \frac{W}{m^2} < q_{theoretical,max} = 80 \frac{W}{m2}$. A possible reason for the discrepancy between analytical and experimental results would be the loss of thermal energy along the surface area of the pile foundation. The hydronic thermal demands are illustrated in figure 2-4. Although the snow wasn't completely eliminated at the last recorded period as shown in figure 2-5 (27 hour mark), there was sufficient evidence for accelerated snow melting, predominately along the effective area (Kong et al, 2018). Therefore, an energy pile based de-icing system without a heat pump can reliably accelerate the snow melting process, however, additional piles and a heat pump would be required to effectively keep the slab snow-free during a snow event.

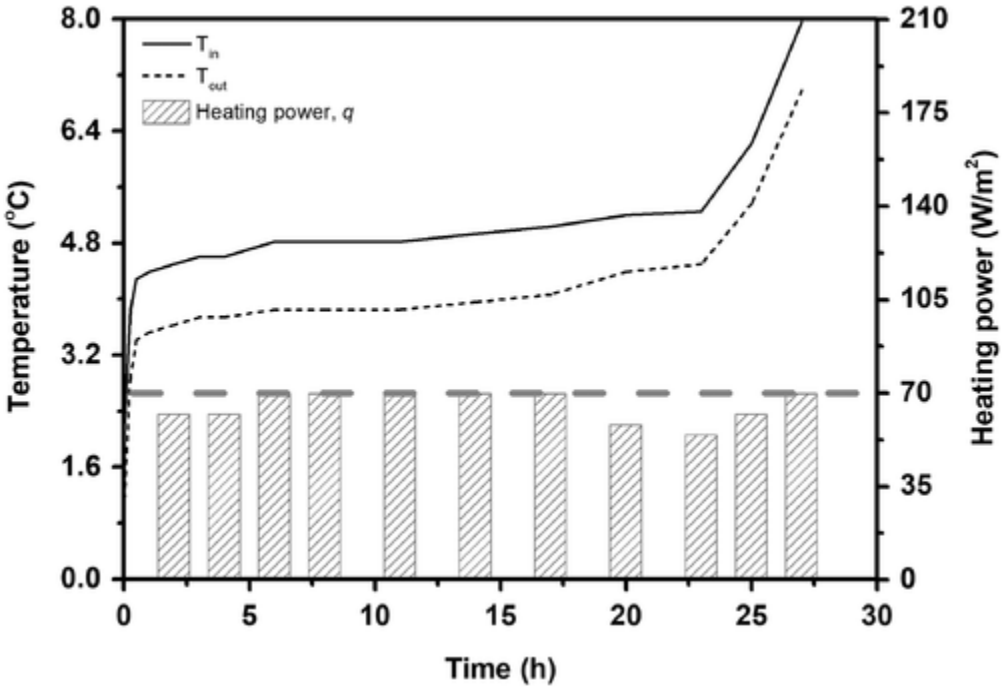

Figure 2- 4 Hydronic heating power of de-icing system (Kong et al, 2018)

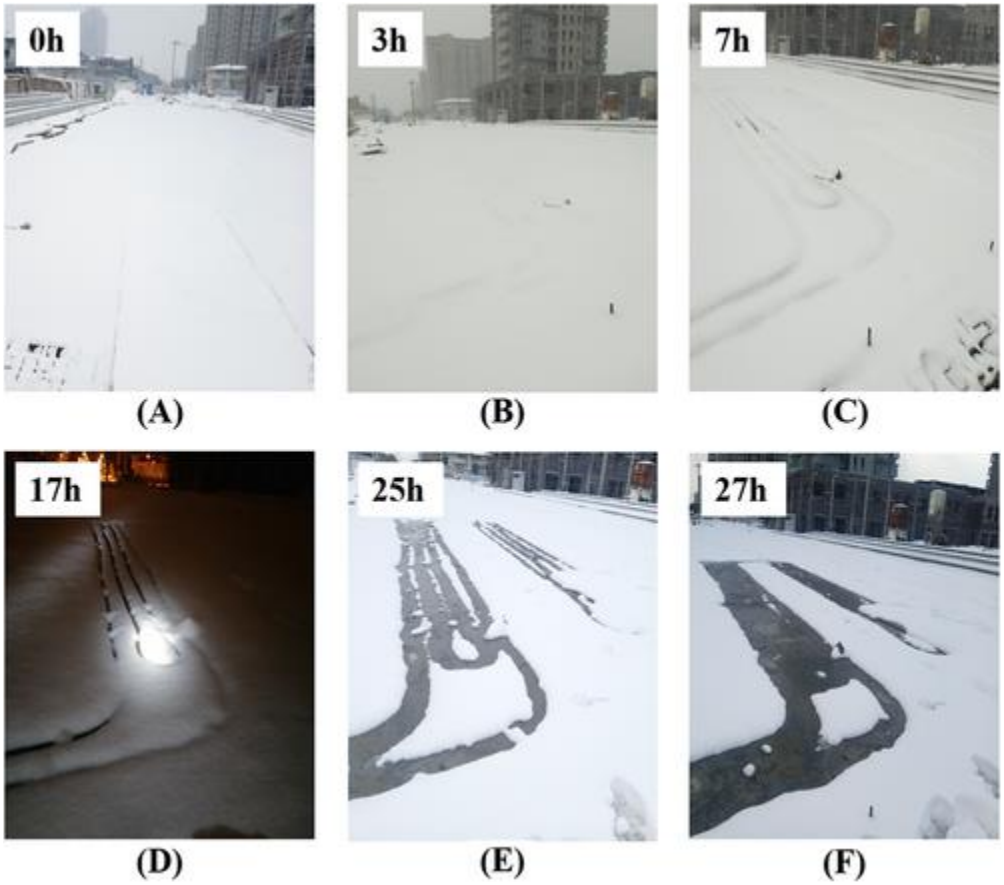

Figure 2- 5 Bridge conditions after time interval: 0, 3, 7, 17, 25, and 27 hours (Kong et al, 2018)

Table 2- 1: LWE Snowfall Intensity (Fahey, 2008)

Snowfall Rate, R (mm/hr)	Classification
< 1	Light
1 < R < 2.5	Moderate
R > 2.5	Heavy

2.4.2. Feasibility Study of Bridge De-icing using Energy Pile

The intended goal of the following feasibility study was to replicate the de-icing process for a Virginia bridge. Multiple thermistors were installed within the experimental slab to determine the performance of the system under encountered Winter conditions. Two layers of rebar were

utilized to reinforce the slab and increase the thermal capacity. The slab was split into two halved sections defined according to pipe spacing at 8 and 12 inches as shown by figure 2-7. The PEX pipe series of loops was attached to the upper level of rebar reinforcement. The relative performance of the system was measured using a control slab with no heating source. The system was powered using two circulation pumps such that flow (water and glycol) could be independent per section, or together in either series or parallel (Bowers, 2016). The pile plan is shown in figure 2-6, in which four observational boreholes were utilized to monitor thermal output from the sub-surface.

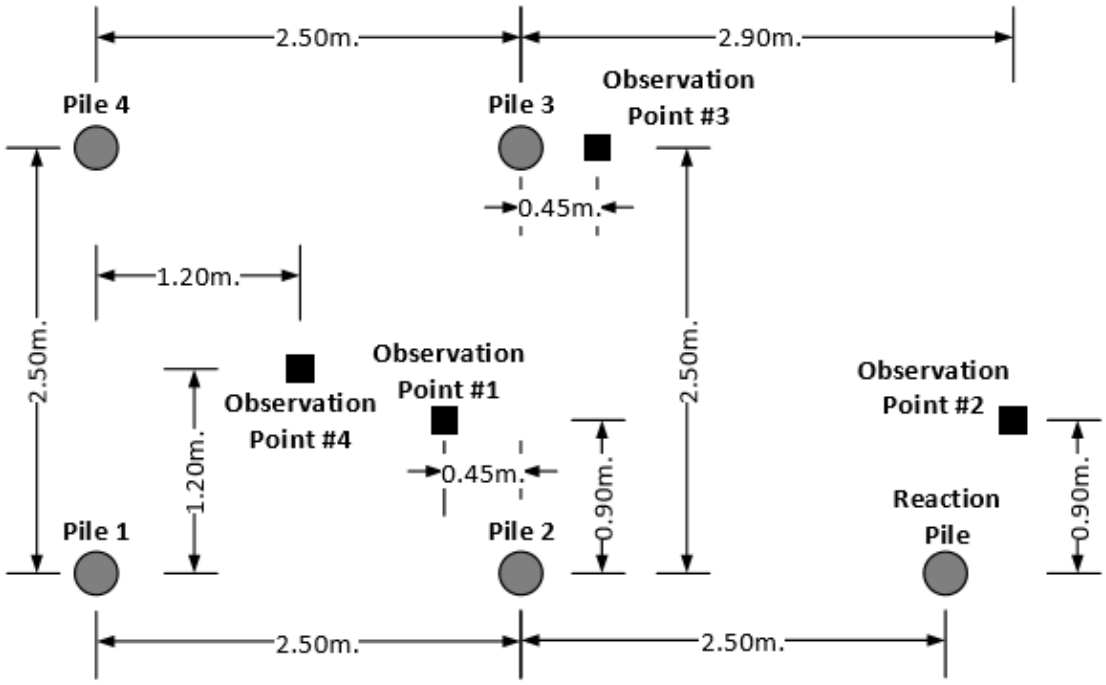

Figure 2- 6 Field layout of the energy piles and observations wells (Bowers, 2016)

Figure 2- 7 Experimental Bridge Deck during Construction Process (Bowers, 2016)

The experimental study proved that the energy pile driven de-icing system was capable of sufficiently countering a mild snowfall event with very low ambient conditions (15 ° F) without the aid of an additional heat pump. The extracted inlet water temperature was around 45 ° F, which was sufficient to completely eliminate all snowfall precipitation after a short duration as indicted in figure 2-8 (a) and (b). The non-heated slab relative to the heated slab exemplifies the reliability of the system, however, the system was turned on prior to the event (Bowers, 2016). If the system was run contemporaneously with the initiation of the snow event, slab de-icing likely wouldn't occur. If the ambient conditions were close to freezing, there would be no need to pre-run the system. Based on multiple Winter events ranging from light to severe, the ability of the de-icing system to melt the accumulated snow during the event was greatly hindered as the level of severity increased, however, the snow was eliminated once the event ceased. Therefore, energy piles are a very efficient method for de-icing bridge slabs so long the accumulation rates aren't too heavy.

Figure 2- 8 Photographs of the heated bridge deck at 9:15 (top) and 10:00 (bottom) on the morning of 2/24/2014 (Bowers, 2016)

2.5. Determination of Convective Heat transfer Coefficient

The overall performance of any geothermal de-icing system is negatively influenced by wind, which displaces the thermal energy at a rate proportional to the wind magnitude. Thus, determination of the convective heat flux is an important consideration to relate to the thermal demands of the system to permit de-icing. The heat input can then be altered accordingly, depending on the winter conditions. The following equations are utilized to solve the convective heat transfer coefficient to gauge how much energy will be lost due to wind.

$$q = \frac{Q}{A} = k * (T_s - T_\infty)/\ \delta \quad \text{.....(3)}$$

$$q = \frac{Q}{A} = h * (T_s - T_\infty\ ) \quad \text{.....(4)}$$

By rearranging equations (4) and (5) to solve for q, the following equation is attained to solve h:

$$h = \ k/\delta \quad \text{.....(5)}$$

Where k = thermal conductivity ($\frac{W}{m^2 * K}$), h = convective heat transfer coefficient, T_s = surface temperature of slab, $T\infty$ = ambient temperature, and δ = thickness of thermal boundary layer (mm). If the thermal conductivity and thickness of boundary layer are known, then the heat

transfer coefficient can be readily determined. The following experimental study was performed to estimate the thermal boundary layer using a testing prototype within an enclosed wind tunnel. The test prototype which is illustrated in figure 2-9 consisted of a heater, insulated box (cavity) and a base to mount the proof walls. The test walls were built from red brick blocks, tepetate (limestone) and adobe, each of which were pasted with a mixture of cement, sand and lime (Galán, 2014). Multiple sensors were installed transverse along the wall centerline and perpendicular to the wind direction as shown in figure 2-10. The prototype slab was subjected to various wind conditions ranging from 0 to 10 m/s.

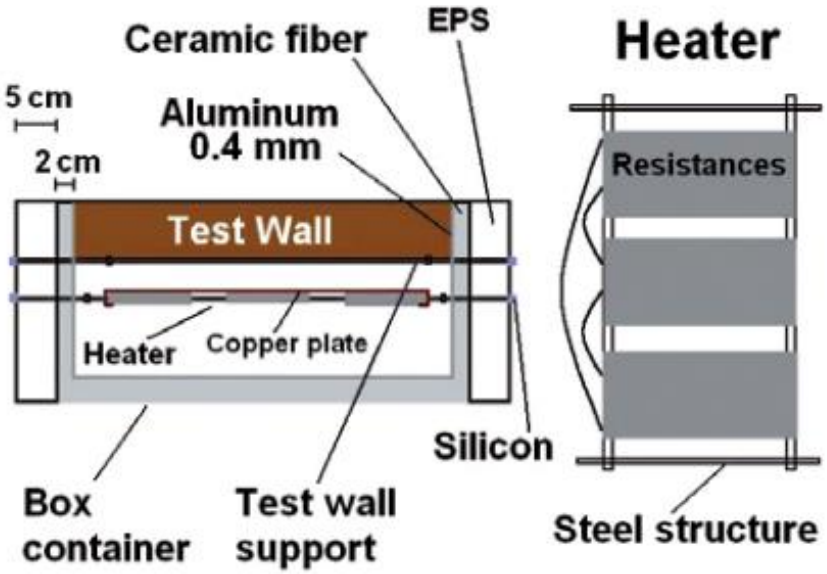

Figure 2- 9 Testing prototype Design (Galán et al, 2014).

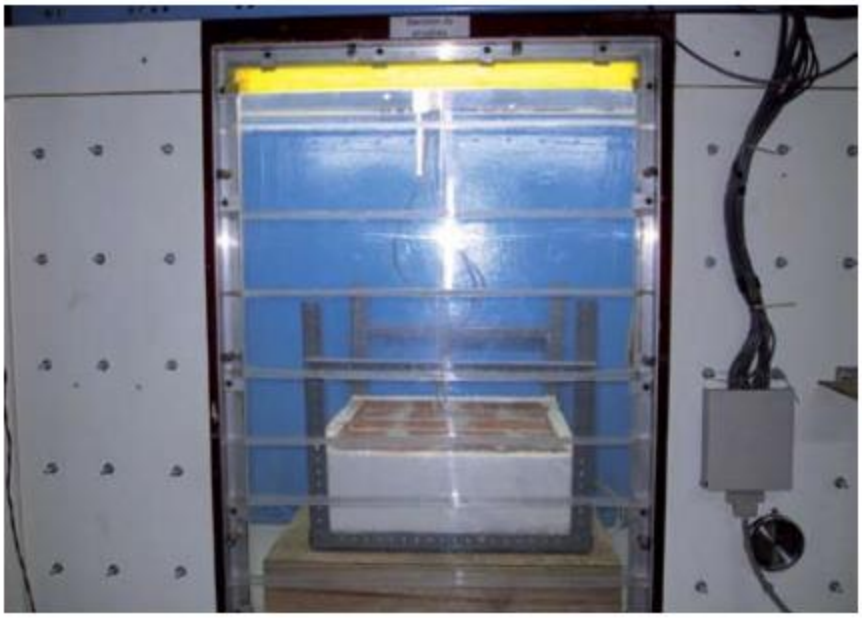

Figure 2- 10 Test prototype within Wind Tunnel (Galán et al, 2014).

To measure the thickness of the thermal boundary layer, the temperature distribution above the plate subjected to wind at 8m/s was recorded. The results confirm that the temperature rapidly converges toward the minimum external temperature within the first 4.5 mm (Galán et al, 2014). The same relationship held for wind speeds at 6 and 10 mph, however due to the limitation in the test set-up, the boundary could not be defined for speeds below 6 mph. To obtain the convective coefficient over the entire wind range, the sensors would need to be installed at a greater depth to achieve convergence for lower magnitudes. The results matched well with experimental correlations, implying that the prototype set-up was reliable. Thus, the convective coefficient can be reasonably estimated if the testing conditions are well controlled.

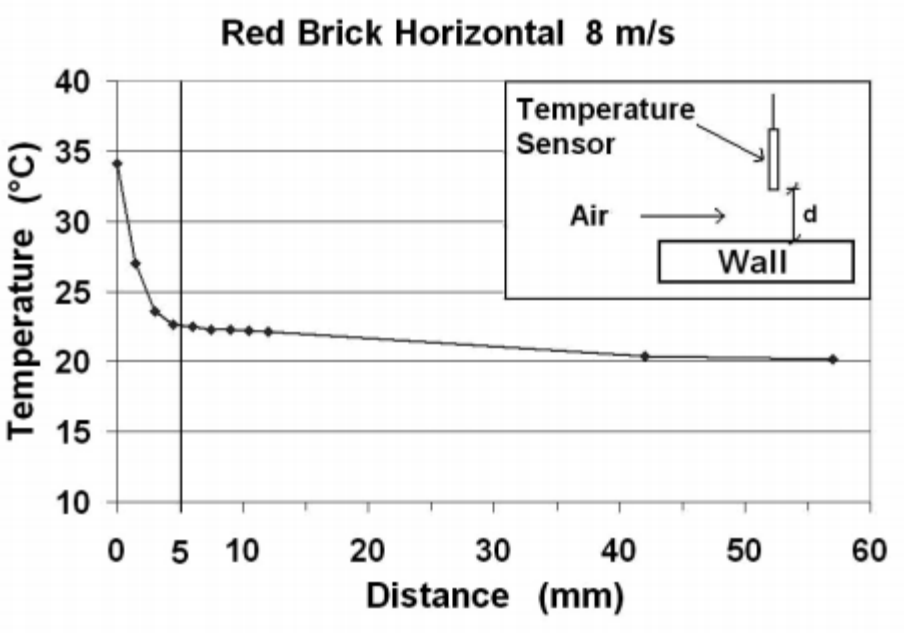

Figure 2- 11 Temperature Profile for wind = 8 m/s (Galán et al, 2014).

2.6. Case Studies

This section introduces case studies across Europe and Asia for the purpose of utilizing the potential for geothermal energy to de-ice pavement slabs for bridges. Each sub-section will include a brief summary of the system development and success over the span of the project. A more extensive review of case studies can be found in the paper by Nagai et al (2009).

2.6.1. Geothermal Heated Well System (Japan)

Yoshitake, et al (2011) developed a new heating pipe system capable of extracting geothermally heated water from an underground storage tank. A closed loop pipe network was then extended from the storage unit and encapsulated within concrete pavement without the use of electrical resistance or boiler unit. The construction cost of the system was reduced by roughly 50% relative to comparable systems (Yu, et al, 2017). A schematic of the overall heating system is shown in figure 2-12. Figure 2-13 and 2-14 exemplify the success of the system in countering a winter weather event by verifying the performance of the system on a relative scale. The thermal image indicates the heating potential of the system to efficiently extract heat from the underground storage tank.

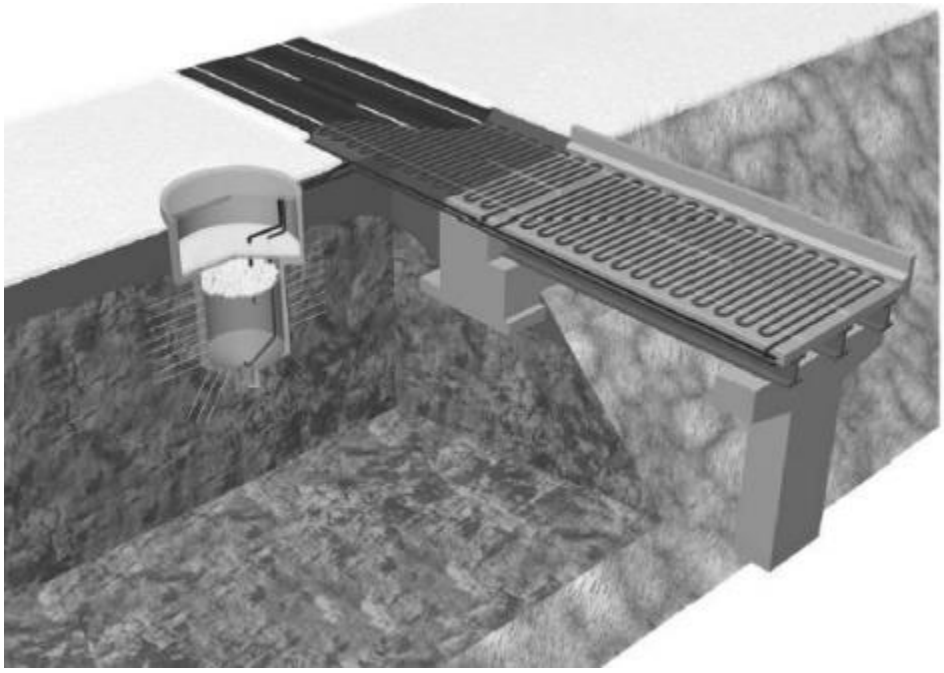

Figure 2- 12 Schematic of Geothermal Heated Well System (Yoshitake et al, 2011)

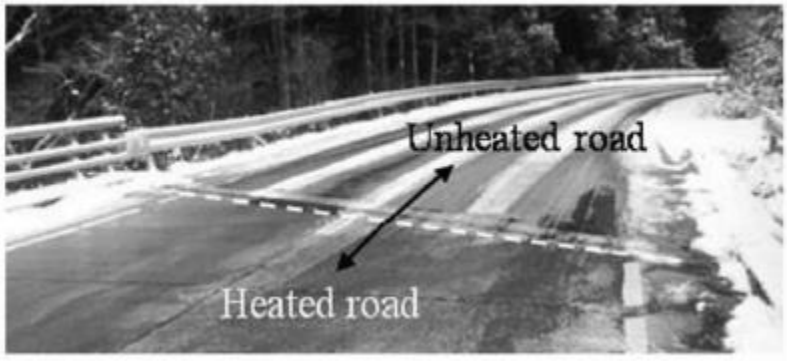

Figure 2- 13 Result of De-icing installation on part of road (Yoshitake et al, 2011)

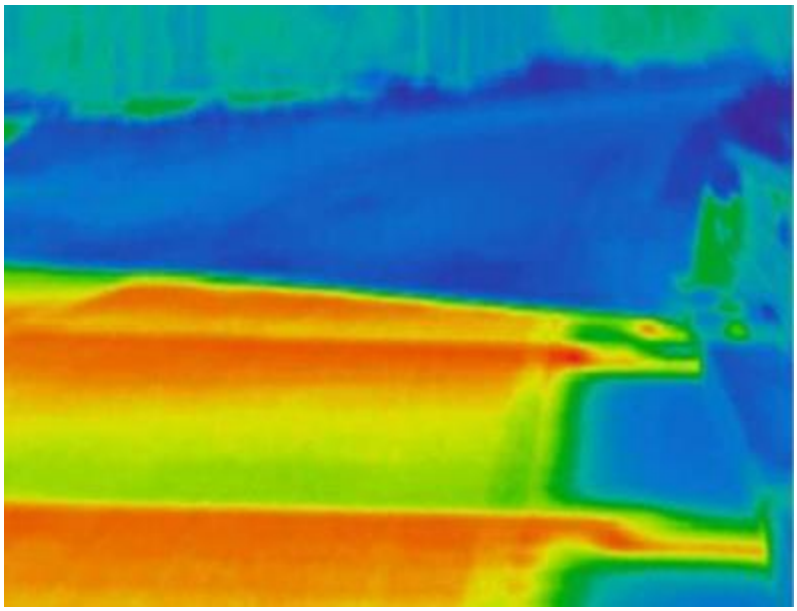

Figure 2- 14 Infrared photograph of the boundary of the heated and unheated roads (Yoshitake et al, 2011)

2.6.2. Gaia Geothermal System (Poland)

Heloasz and Ostaficzuk (2011) studied the use of geothermal energy and waste heat for the intended goal of de-icing in Poland. The Gaia system was employed as an environmentally friendly heating system that can maximize the use of geothermal reserved by indirect means. The thermal energy is initially collected at wells 150 m deep via a concentric pipe-heat exchanger (Morita and Tago, 2000). With the aid of a circulation pump, the heated fluid is transferred through the pipe network to a heating pump, which extends to sub-surface coils as shown in figure 2-15. Once the Winter season ends, both water loops are interconnected automatically such that solar energy can heat the flowing liquid re-directed towards the well. Figure 16 exemplifies the de-icing capabilities of the system after the installation process. To further enhance thermal reserves and minimize the heating capacity required via technological means, the use of waste heat was also introduced. The extra reserves greatly reduce the investment and maintenance cost over time. By extracting additional heat lost from municipal heated pipelines internally embedded within roads, the energy demands from the Gaia system can be reduced. Further, considerable heat can be extracted from coal mines via the ventilation and discharge waters, which can reach 20 ° C (Heloasz and Ostaficzuk, 2011). Combining the residual heat lost

from various sources coupled with technological advances such as heating coils and pillars prove to be a very innovative approach to save energy.

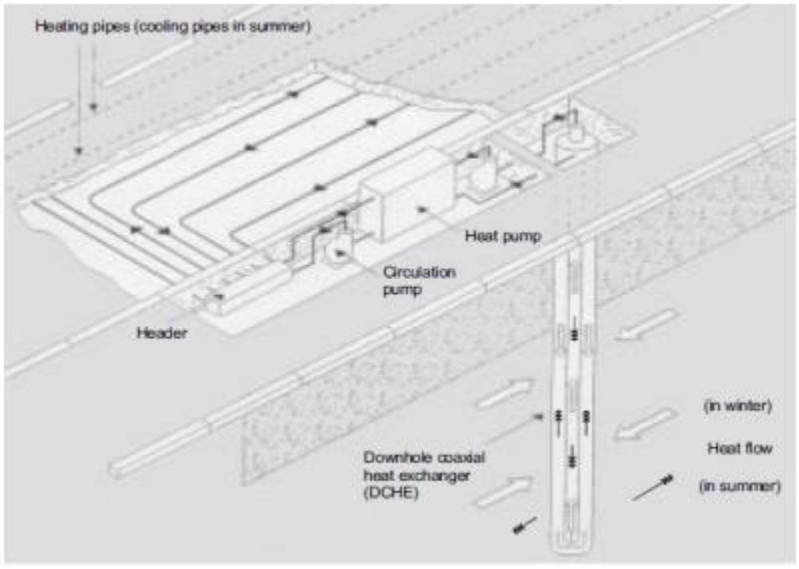

Figure 2- 15 Layout of the snow-melting system (Yu, et al, 2017)

Figure 2- 16 Result of deicing installation work on a part of road (Yu, et al, 2017)

2.6.3. SERSO Geothermal De-icing System (Switzerland)

This study presents the use of SERSO; an innovative solution for de-icing demands. The aim is to guarantee equivalent road conditions on the heated bridge element as the subsequent road sections. The system collects thermal energy from the summer period to store in an underground rock storage unit (Eugster, 2007). The heated area encompasses 1300 m^2 using a rock storage volume of 55,000 M^3. The tapped energy reserves are collected via 91 borehole heat exchangers with a depth of 65 m each. The energy is then translated via a pipeline network to surface of the roadway as indicated in figure 2-17. The system proved efficient at maintaining a surface temperature exceeding 0 °C, thus hindering ice formation (Eugster, 2007). The measured pavement temperature relative to the ambient conditions is illustrated in figure 2-18. The typical heat output of system was 100 W/m^2. This extensive thermal delivery system eliminates the need for high heat demands to effectively thaw sudden ice formation. Figure 2-19 proves that the operation system provides sufficient energy to maintain safe road conditions.

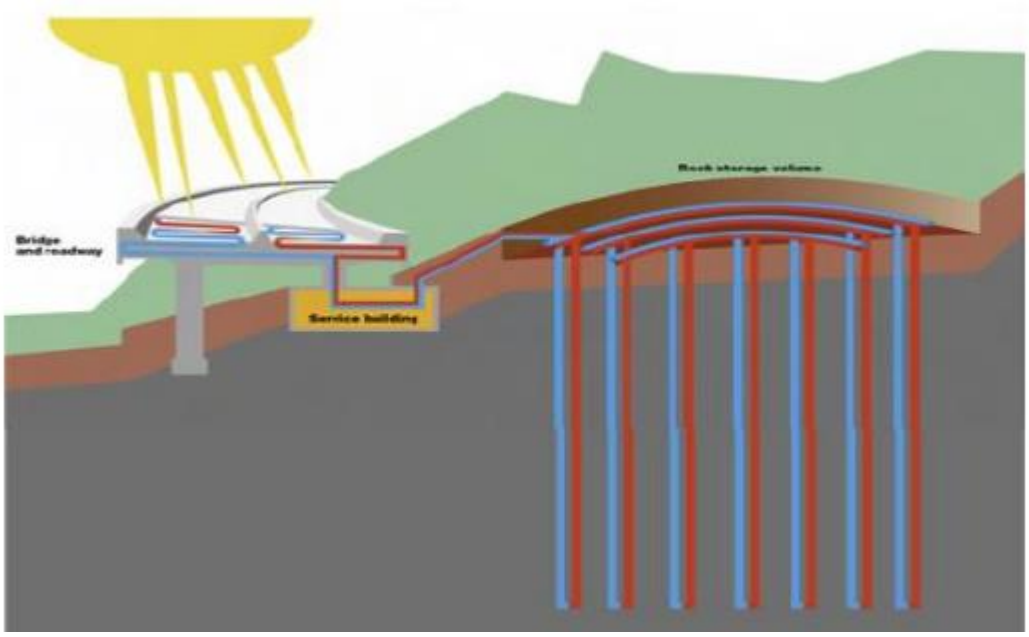

Figure 2- 17 SERSA solar system (Eugster, 2007)

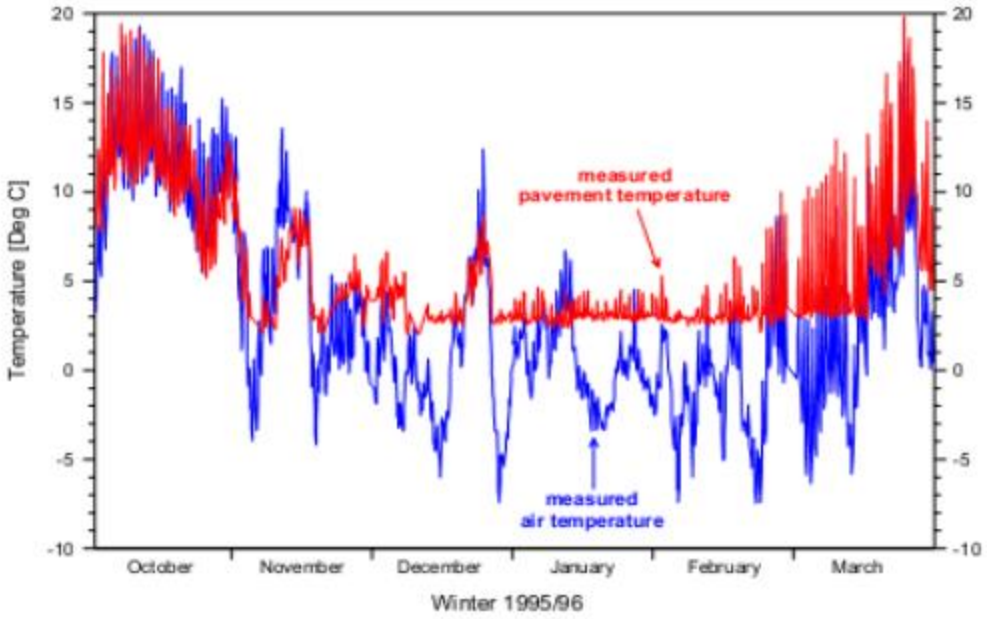

Figure 2- 18 Road surface temperature controlled by the SERSO system (Eugster, 2007)

Figure 2- 19 SERSO system in operation (Eugster, 2007)

2.7. Cost Benefit Analysis

2.7.1. Chemical Vs. Geothermal De-icing

The CSRS cost of de-icing a bridge deck is the relatively equivalent to de-icing pavements and includes the machinery, snow/ice control material, and labor. Numerous studies have estimated the cost of removing ice and snow from roads. Nixon (2001) reported that Oregon DOT reduced the cost of winter maintenance from $94 to $24 per lane mile in freezing rain conditions. Cuelho,

Harwood, Akin, & Adams (2010) estimated the cost of the winter operations implemented by the Colorado DOT to be $5,200 per lane mile using conventional methods, but reported that applying anti-icing techniques reduced the cost to $2,500 per mile lane. However, bridge decks require are more susceptible to ice formation and hence, require a higher threshold for de-icing to be permissible. Unfortunately, the literature lacks information pertaining to the cost of conventionally de-icing a bridge deck relative to de-icing pavement.

Every year, de-icing chemicals are applied to U.S. highways to mitigate ice development. The two most common types of de-icing chemicals are abrasives (e.g., sand) and chloride. Abrasives provide a temporary friction layer and improve skid resistance on icy road surfaces. They are applied to counter the reduction in friction due to ice formation. Table 2-2 summarizes the information on abrasives commonly used as de-icing materials. The Colorado DOT studies reveal that abrasives are the least expensive de-icing materials (Fischel, 2001). More recent research shows, however, that the overall cost of using abrasives is accelerated due to the implications regarding environmental clean-up (Fay, Volkening, Gallaway & Shi, 2008). Sodium chloride (NaCl) (rock salt) is the oldest and most popular de-icer in the chloride-based de-icer family; it is cheap, abundant, and has served many roads in the United States since the 1930s (Fischel, 2001). Table 2-2 also summarizes the information on chloride-based products used as a de-icing material.

Table 2- 2 Information on chloride-based and abrasives products used as a de-icing material. (Habibzadeh-Bigdarvish, et al, 2019)

Category	Product Type	Liquid/solid	Application rate	Cost
Abrasives	Sand	Solid	100-1000 lbs/l-m	$6-16/ton
	Cinder	Solid	100-500 lbs/l-m	$20/ton
	Crushed rock or gravel	Solid	100-500 lbs/l-m	$11-15/ton
	Pre-wet abrasives	Pre-wet solid	100-1000 lbs/l-m	$12-14/ton
Chlorides	NaCl	Solid	100-800 lbs/l-m	$30-100/ton
		Liquid	10-40 gal/l-m (anti-icing) 8-20 gal/l-m (pre-wetting)	0$0.04-0.09/gal
	MgCl2 and CaCl2	Solid	100-500 lbs/l-m	MgCl2: $100/ton
		Liquid	10-40 gal/l-m (anti-icing) 8-20 gal/l-m (pre-wetting)	MgCl2: $0.50-0.90/gal CaCl2: $120-300/ton

Table 2-3 shows the estimated annual cost of typical deicing operations for the Knik Arm Bridge. It is indicated that the total cost of the chemical method is substantially less than that of the thermal method (Yu, 2017). As expected, the equipment and installation costs for the thermal method is higher relative to the chemical method, however, the converse is true regarding the labor costs. Therefore, over the long run, the thermal method will eventually outpace the chemical method in terms of investment and return. Moreover, de-icing chemicals reduce the structural integrity of bridges and overpasses over time and degrades the environment, which further accelerates the costs.

Table 2- 3 Estimated annual cost of typical deicing operations on the Knik Arm Bridge (Zhang et al., 2007)

Cost		Chemical Method		Thermal Method
		Calcium Chloride	Potassium Acetate	
NPC	Equipment	20	20	300
	Installation	5	5	400
	Lifecycle	2	2	30
	Utility Incentive Payment	0	0	0
COO	Materials	60	120	100
	Labor	60	60	2
Total = NPC + COO)		147		832

Notes: NPC is the net participants cost; COO is the operation cost.

Chapter 3: METHODOLOGY

3.1. Scope and Motivation

This chapter provides a brief overview of the main methods utilized for the experimental model. The framework will be based on a prediction of the thermal energy required to de-ice under different environmental circumstances. The prediction will also relate to the overall efficiency of the system, which determines its feasibility to be safely translated to the field.

3.2. Externally Heated Slab

The Texas Department of Transportation (TxDOT) owns many overpass bridges that are in critical need of bridge deicing. Approximately 85 percent of the bridges in Texas were constructed using CIP-PCP bridge decks, which consist of precast, prestressed concrete panels (PCPs) and a cast-in-place (CIP) concrete deck (Merrill 2002). Therefore, the heated bridge deck design is intended to be used on the CIP-PCP bridge decks. Figure 3-1 presents a schematic of the attached hydronic heating loop design for a heated bridge deck, which consists of hydronic pipes and foam insulation materials. For bridges at service, the heating hydronic pipes are attached to the bottom of the bridge deck through metal fixtures. Insulation foam (polyurethane or geofoam) is installed to encapsulate the heat pipes and minimize the heat loss from the bottom. Warm water supplied from underground loops provides a heat source to warm the bridge deck surface above, due to the high thermal resistance of the underneath insulation.

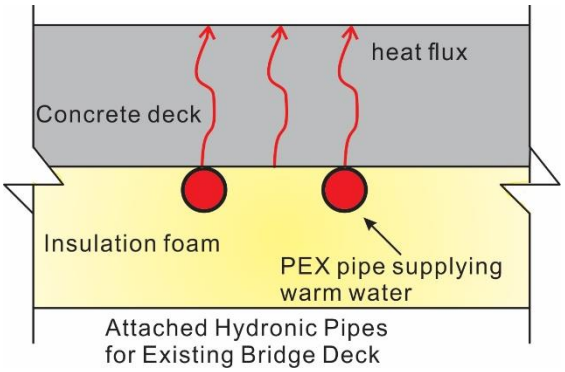

Figure 3- 1. Schematics of heated bridge decks for existing bridge

Deicing performance of the heated deck mainly relies on the supplied heat and heat transfer efficiency. In this study, a cross-linked polyethylene (PEX) tubing was selected as hydronic pipes to supply warm flow to the bridge deck. In this design, a 13-mm (0.5-in.) inner diameter PE pipe of circular cross-section, with approximately 152-mm (6-in.) spacing, was used for the hydronic loops. Concrete slabs of 4" and 8" thick were selected for heating test in freezer box or outdoor. The following schematic (figure 3-2) shows an example heated slab. Figure 3-3 shows the testing sequence that was utilized to attain the thermal response within the slab for all cases. Note that the initial ambient temperature set at 55 ° F differed from the desired ambient condition. Although there was deviance, the final steady-state condition within the slab is unchanged. This is because the final steady-state temperature is a function of the heat load (I-A), not the initial ambient conditions. Also, the initial spikes in temperature at the surface at the beginning of each test corresponded to the influx of heated air from the outdoor environment. The defrost cycles of the freezer box led to additional periodic spikes in ambient conditions for the duration of each test.

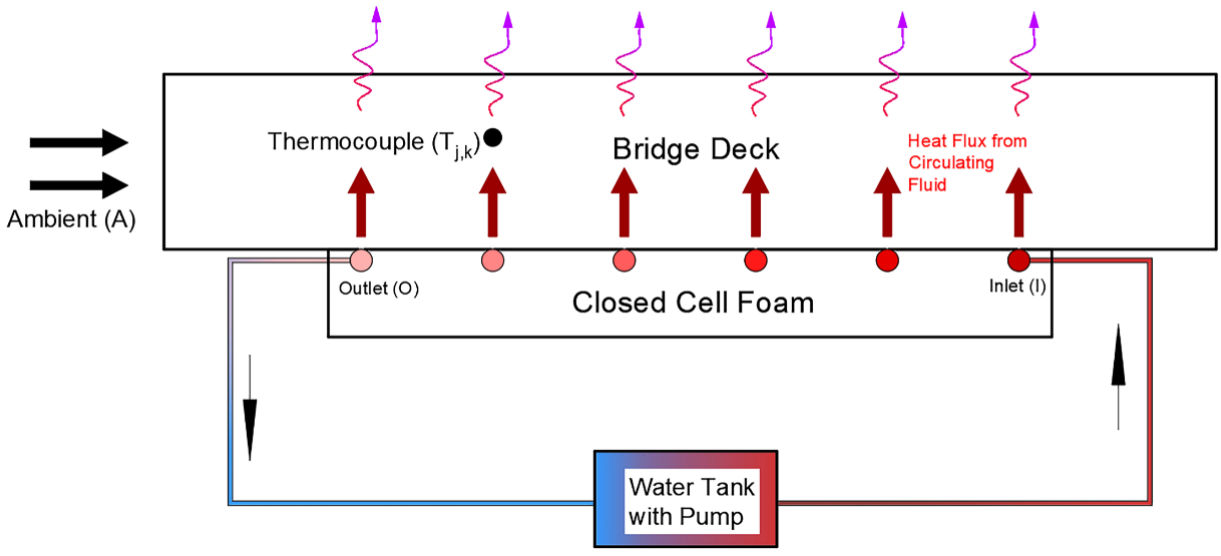

Figure 3- 2 Cross sectional view of thermocouple sets

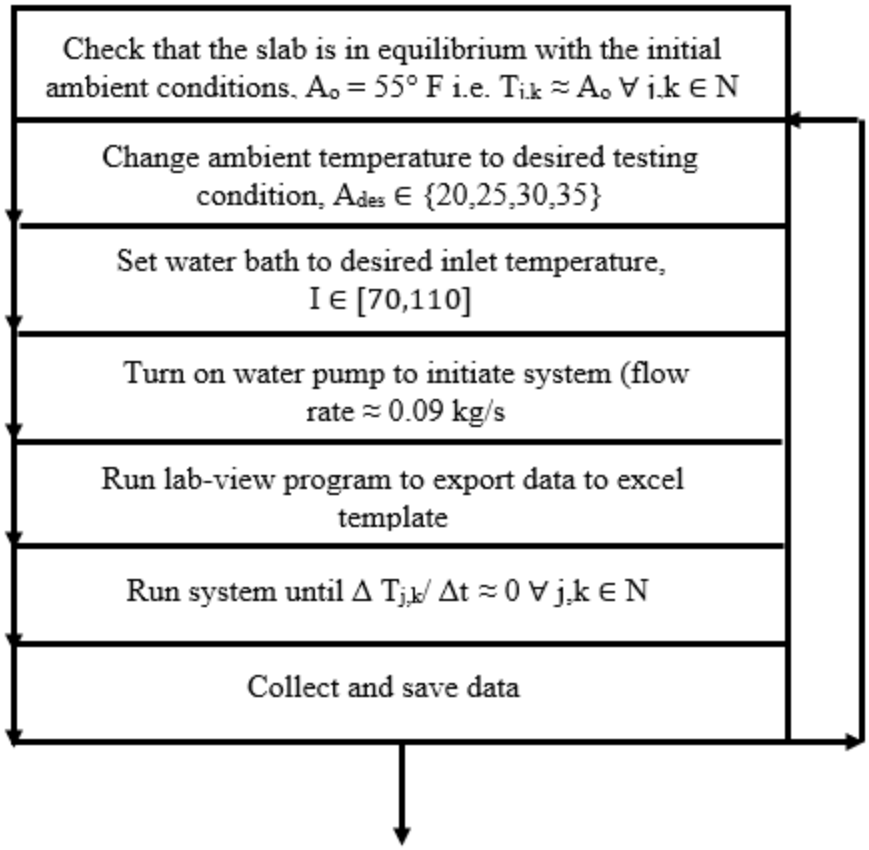

Figure 3- 3 Testing procedure for each sequence

Note: N denotes the set of natural numbers and R denotes set of real numbers.

3.3. Prediction of Thermal Demands

3.3.1. Defining the Proportion, *p*

To directly measure the efficiency of the system, a parameter denoted as the thermal gradient ratio, or the proportion, *p*, is utilized. Let the heating load be defined as the difference between the inlet and ambient temperatures (upper and lower bounds respectfully). The steady-state temperature exists between the upper and lower bounds and hence, represents a proportion of the heating load. For this study, we denote the cross-sectional depth of interest as k, where $k \leq 0$. The depth of interest, k is defined as zero at the surface and negative below the surface. The ratio of $(T_j - A)_k$ to $(W-A)$ is defined as the thermal gradient ratio or proportion, *p*, at thermocouple set j at depth k. The definition pertaining to the proportion is illustrated in figure 3-4. The temperature within the

slab at any defined set and depth of interest, $(T_{j,k})$ exists between the upper and lower thermal bounds (water and ambient temp) and therefore, can be equated as follows.

$$T_{j,k} = A + p_{j,k}(I - A) \quad (6)$$

where A = ambient temp. and $p_j(I - A)$ is the proportion of heating load $(I\text{-}A)$ transferred to depth, k.

If $p_{j,k} = 1$, then $T_{j,k}$ = I (inlet temp). Conversely, if $p_{j,k} = 0$, then $T_{j,k}$ = A (ambient temp). Therefore, the proportion exists within bounds such that $0 < p_{j,k} < 1$. Ideally, an efficient heating system would require a proportion that tends closer to 1 based on the possible range for the system. The proportion is, however, a function of the thermal conductivity and diffusivity of a heated material. Therefore, there will exists some constraint regarding the maximum proportion that can possibly be attained. The key is to minimize thermal losses due to boundary conditions or reduced surface area of heat transfer and maximize the thermal potential of the heating reserves. Using a 99% degree of confidence in relation to the average proportion across some plane of interest, p_{avg}, the following equations are derived to determine the upper and lower bounds corresponding to steady-state temperature.

$$T_{max} = A + (p_{max}) * (I - A) \quad (7)$$

$$T_{min} = A + (p_{min}) * (I - A) \quad (8)$$

Where A = ambient temp., I = Inlet temp., $p_{max} = p_{avg} + X(\sigma/(N\text{-}1))^{1/2}$, $p_{min} = p_{avg} - X(\sigma/(N\text{-}1))^{1/2}$, N = number of sub-tests, $X \in \{Z, t\}$, and σ denotes standard deviation.

For equations (7) and (8) to be valid, it must follow that the average proportion is approximately normally distributed for each depth, k. If the sample size is small (N < 30), then a t-test will be performed with parameter t inputted into equations (7) and (8). Otherwise, the Z-score (Z) will be utilized.

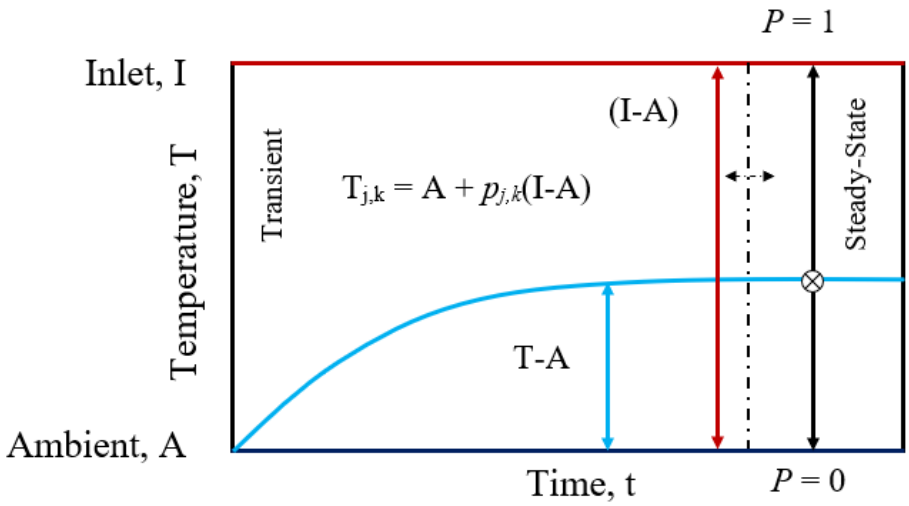

Figure 3- 4 (a) Schematic design of de-icing system, (b) Definition of the Proportion of heat transfer, p

3.3.2. Effect of Wind on the Performance of System

The efficiency of the system is inversely proportional to wind magnitude. That is, the proportion is reduced as a function of wind magnitude. Since $\tan^{-1}(p_{j,k}) = \phi$, it follows that progressively less thermal energy will be attained per incremented increase in the heating load *(I-A)*. This is assuming (6) follows a linear function. For the outdoor study (transient state), wind direction played a key role regarding convective heat transfer since the slab was positioned in a confined area blocked off to the North-South direction. A brief overview of the experimental set-up will be presented in papers A and B respectfully. A wind coordinate system was created to numerically relate the direction and magnitude simultaneously. Table 3-1 shows the wind coordinate system created to exemplify the transition in wind direction. The South direction was not recorded for the event and hence, was excluded from the coordinate system. For the indoor study, the effects of sustained wind on the heating efficiency of the system was determined. An additional thermal rebound and dissipation study was included to exemplify the effects of incremental decrease and increase in wind magnitude. The motivation behind the study was to create a method that could be useful to understand how thermal energy is recharged into the system (rebound cycle) relative to the case in which thermal energy is displaced (dissipation cycle). To attain a relation, a time frequency was defined according to a period of change in wind magnitude, denoted by W_x, where $x \in N$. For each of period of the cycle, the initial tangential

slope was attained over time frequency, F = 1 min^{-1}. For sustained wind, the dissipation rate follows a negative exponential function, yet this is not the actual case. Since wind naturally follows a random scattered function under very high frequency of change, linearization of the function is satisfied. The end objective of the study is to determine the tangential slope for each cyclic period to create a relationship between $\Delta T_{j,k}$ and Δw where w denotes wind magnitude in mph.

Table 3- 1 Wind Coordinate System

Wind Coordinates	Wind Direction
1	E
0.75	ENE
0.5	NE
0.25	NNE
0	N
-0.25	NNW
-0.5	NW
-0.75	WNW
-1	W

3.3.3. Thermal Requirements to Permit Snow Melting

Using a reference depth for all thermocouples, there exist a lower and upper bound in respect to the thermal gradient ratio, p for each thermocouple measurement, $T_{j,k}$. That is, the boundaries of the slab will exhibit less thermal energy than the central area of the slab. This follows from the 2nd law of thermal dynamics, which states that energy flows from a disordered state to an ordered state (hot to cold). Hence, more energy will dissipate towards the boundaries because the thermal gradient will increase drastically outside the geometric pipe area. By extending the bounds for each depth and applying a confidence interval, the slab base and surface temperature can be reasonably estimated. Some thermal energy will be lost along the outer perimeter and base of slab. Thus, predicting the heat flux at the surface of the slab will indicate how much energy was likely lost, which relates to the efficiency of the system. The heat flux for thermocouples $T_{j,k}$ can be estimated as follow:

$$q_{Tj,k} \approx -K * \left(\frac{\delta p}{\delta Z}\right)_{avg} * (I - A) \quad \text{.....(9)}$$

where K = thermal conductivity = 1.8 W/m^2*K, and $\alpha = \frac{\delta p}{\delta Z}$ is the gradient corresponding to the proportion (m^{-1}).

Therefore, the heat flux is a linear function where thermal load is the dependent variable. It is imperative to introduce enough thermal energy to the system such that the heat flux reaching slab surface exceeds the required heat flux to melt the ice/snow conditions. Equation (1) from the literature review section is utilized to estimate the heat flux for efficient snow melting whereas equation (2) is utilized to estimate the thermal energy due to hydronic heating. Table 3-2 shows the equation inputs and respected units. It is assumed that the snow melting process will initiate after precipitation, and hence, A_r is assumed to be zero. Equation (1) can be further reduced to the following: $q_{req} = q_s + q_m$ by taking $A_r = 0$ (assuming bridge slab is fully exposed to snow/ice conditions).

Table 3- 2 Equation Terms

Term	Unit	Parameters	Unit
Sensible heat flux, q_s	Watts/m^2	Density of water ρ_w	1000 kg/m^3
Latent heat flux, q_m	Watts/m^2	Specific heat of ice, cp_{ice}	2100 J/(kg*K)
Convective heat flux, q_h	Watts/m^2	Specific heat of water, cp_{water}	4200 J/(kg*K)
Radiative heat flux, q_e	Watts/m^2	Melting temperature, T_s	0° C
Snow free area, A_r	Dimensionless	Ambient temperature, T_a	-3° C
Heat of evaporation (film)	Watts	Heat of fusion of snow, hi_f	334,000 J/kg
Wind speed V	mph	Liquid film temperature, T_f	0.56 ° C
Vapor pressure	Watts*hr	Convective heat transfer coefficient, h	30
		Constant, c1	3.6*10^6

3.3.4. Prediction of Thermal Demands (Paper A)

To predict the steady-state temperature at any depth within the slab, it must follow that there exists minimal error between the predicted and actual results. By determining the alpha coefficient such that the error is minimized, the steady-state temperature can be reasonably

estimated. The following equation can be used to estimate a lower bound for steady-state temperature at any depth such that 0 < Z < 8:

$$T'_{j,k} = A + \left(P_{avg} - \alpha_{upper}\sum_{i=1}^{3}|Z_i|\right) * (I - A) \quad \text{.....(10)}$$

Where p_{avg} is the initial average reference point corresponding to the proportion at the base plane, α_{upper} is the upper bound for α, $|Z_i|$ is the modulus corresponding to depth intervals 1-3, and "$T'_{j,k}$ " denotes the predicted value.

To predict the thermal demands required for de-icing, there must exists a degree of separation between the actual and predicted result such that $T'_{j,k} = T_{j,k}$ - C where C is a separation factor. This will ensure any error bound will not overlap with the predicted results, which is exemplified in figure 3-5. Therefore, to ensure a reasonable degree of separation, a hypothesis test will be performed to determine a lower and upper bound in respect to *p and α* respectively. It is important that the alpha coefficient has marginal variation per depth interval. Otherwise, the results would be skewed. Applying a confidence interval relative to the mean gives a probable zone of possible values. If there is too much divergence between the bounds for each depth interval, then the prediction is not valid. That is, the most probable range for the mean must coexist in similar range for all planes of interest. The following equations can be derived to determine the upper bound for α.

$$\alpha_{upper} = \{x \in R \mid \forall n \in R, \nexists j,k \in N \text{ s.t.} \left(x - \alpha_{j,k}\right) * \sum_{i=1}^{n}|Z_i| < 0\} \quad \text{.....(11)}$$

where $\alpha_{j,k}$ denotes the alpha coefficient at set j at depth k, and $|Z_i| = abs(\Delta Z_i)$ is the depth modulus corresponding to interval i, and n denotes test sample. The depth intervals in respect to α are defined in table 3-3. Using a design threshold at $T_{design} = A_o + \Delta T_{design}$ and inputting into equation (10), the following equation can be derived to determine the required heat input to effectively eliminate snow/ice accumulation for any environmental condition.

$$(I - A)' = \Delta T_{design} / \left[\left(p_{avg,-6} - x * \sum_{i=1}^{3}|Zi|\right]\right. \quad \text{.....(12)}$$

where $T_{design} > 32$ ° F, $p_{avg,-6}$ is the average proportion at a depth of 6 inches below the slab surface for sets 1-4, and x = α_{upper} (m^{-1}). By inputting the adjusted variables into (12), it will be certain under high degree of confidence, that the thermal energy demands will not be under-estimated. By combing equations (9) and (12) and using the average alpha coefficient, the following equation can be derived to solve the required inlet demands to permit de-icing:

$$q' = (\Delta T_{design} * K * \alpha_{avg})/p_{lower} \quad \text{.....(13)}$$

where p_{lower} is the lower bound proportion corresponding to the thermal minimum across the slab length (outlet-end), ΔT_{design} (° C) = ($T_{design} - A_o$) *(5/9), K is the thermal conductivity (W/m^2K), and $\alpha_{avg} = \left(\frac{\delta p}{\delta z}\right)_{avg}$ (m^{-1}).

Therefore, the thermal demands can be reasonably estimated if the thermal conductivity and design threshold (T_{design}) are known. The aim is to validate that the proportion is relatively fixed for each depth interval so that the estimation is precise. There must exists a degree of divergence from the critical freezing boundary to satisfy efficient de-icing of snow/ice. For this study, the design threshold, T_{design} will be set at 34° F so that enough energy will be translated for de-icing. To satisfy the de-icing demands, it must follow that $q' > q_{req}$ where the required thermal demands obtained from equation (1) are sensitive to environmental conditions, wind, and snowfall or ice accumulation rate. Figure 3-6 shows the direct relationships between inclination angle, Φ and the proportion, *p.* The lower bound in respect to the proportion attained for all sets at the slab surface is denoted as p_{lower} whereas the average proportion across sets 1-4 is denoted as p_{avg}. The relationship shows that a higher heat flux is required via equation (13) to permit steady-state equivalence between the average and lower bound cases.

Table 3- 3 Depth intervals for sets 1-5 (Paper A)

Depth Interval, i	Depth Range, Z_i
1	$Z_1 \in [-2, 0]$
2	$Z_2 \in [-4, -2]$
3	$Z_3 \in [-6, -4]$

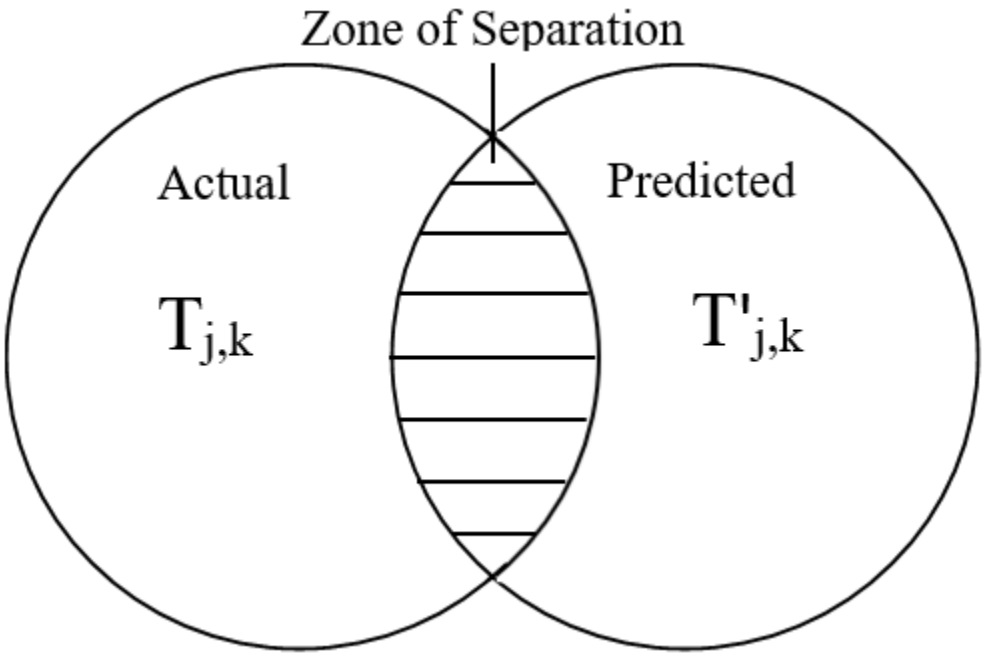

Figure 3- 5 Venn diagram showing zone of separation to account for Variance and possible error

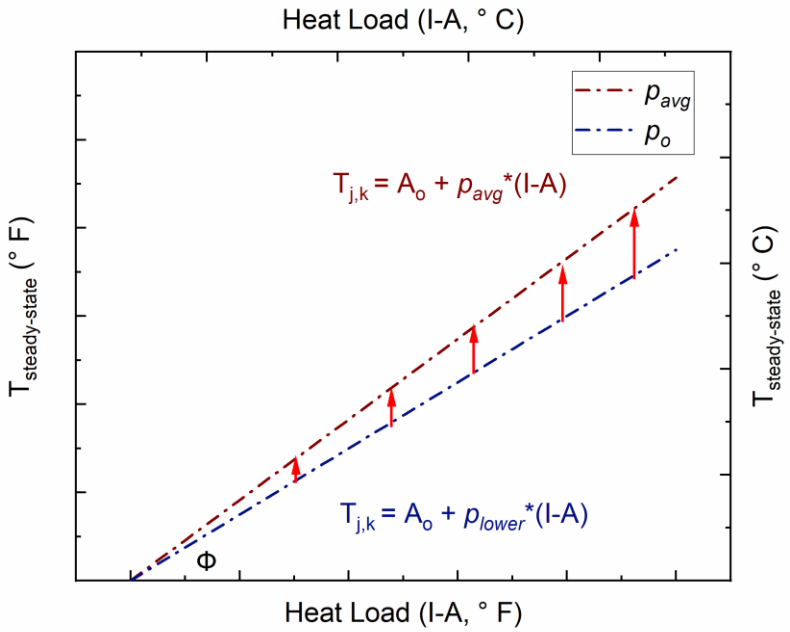

Figure 3- 6 Relationship between p and inclination angle Φ

3.3.5 Heat Flux Deviation

Measuring the temperature variation across a pipe section is useful for determine heat flux as a function of lateral distance from the midpoint of the pipe section. If the variation is marginal per loop section, then the average heat flux can be reasonably estimated across the slab area. Yet, the uniformity in temperature is a function of the pipe spacing. If the spacing is increased, then the uniformity will decrease and vice versa. According to the thermocouple layout illustrated in figure 3-6, sets 2 and 5 will be utilized for this study. Note that although set 2 is not orientated transversely in respect to set 5, the temperature will be roughly equivalent for the same loop section because the supplied water temperature will marginally change. Since less thermal energy will be directed towards the midpoint of a pipe section relative to the boundaries, there will exist a lateral thermal gradient. By attaining the temperature gradient for a loop section, the deviation in respect to heat flux can be attained per depth interval. As the surface of the slab is approached, there exists more points of coincidence in respect to heat flow. Therefore, the temperature distribution should be more uniform towards the surface relative to the base. Figure 3-7 shows a schematic that illustrates the lateral variation from the midpoint to the pipe

boundary, which corresponds to sets 2 and 5 respectfully. If $T_{5,Z}$ is defined as $T_{2,Z} + \Delta T$, then the deviation in heat flux per depth interval can be calculated as follows.

$$q_{dev} = \left(\frac{K}{|Z_i|}\right) * (\Delta T_k - \Delta T_{k+1}) \quad \text{.....(14)}$$

Where ΔT_k is the change in temperature at depth k, K is the thermal conductivity (w/m^2 K), and $|Z_i|$ is the depth modulus in meters.

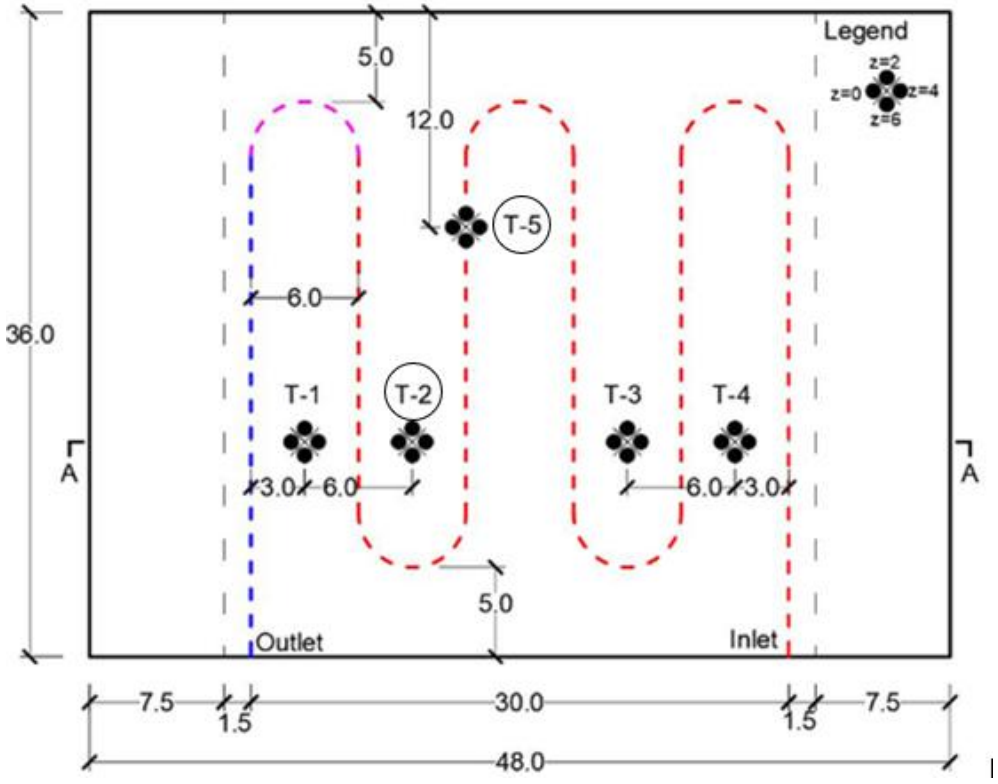

Figure 3- 7 Thermocouple Layout for sets 1-5

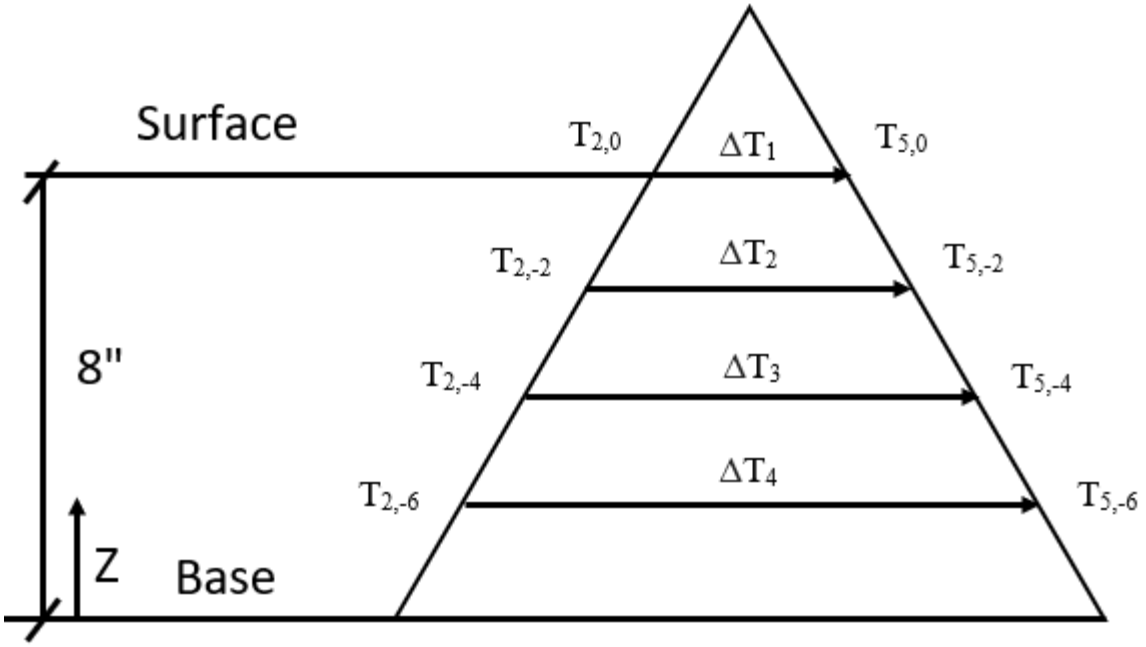

Figure 3- 8 Schematic of relation to measure heat flux deviation

3.3.6 Prediction of Thermal Demands (Paper B)

For transient conditions (paper B), there exists a high degree of variance in respect to the proportion because environmental conditions are continually changing. For this reason, the proportion cannot be averaged because the bounds are widely spread, however, the proportion is a function of wind magnitude. Thus, wind is a major contributing factor to the high degree of variation. Because wind influences the slab surface more prominently than the base, the alpha coefficient should decrease as a function of wind. A wind sensor was not utilized for the analysis, so data from the weather underground database was extracted. Ideally, a wind sensor should be utilized to obtain an accurate representation of wind magnitude over time. To minimize the variance, the following equation can be utilized to predict the thermal demands with reasonable accuracy. A limitation for the analysis is that the slab wasn't fully exposed to wind conditions (slab blocked off in the N-S direction).

$$P'_{j,k} = \left(P_o - \alpha'_{j,k} \sum_{i=1}^{3} |\mathrm{Zi}|\right) \quad (15)$$

Where $\alpha'_{j,k} = \{x' \in R \,|(P'_{j,k} - P_{j,k}) \to 0\}$, P_o is the reference proportion at the base of slab as a function of wind, and Z is slab depth in meters.

Table 3- 4 Depth intervals for thermocouple plan (Paper B)

Depth Interval, i	Depth Range, Z_i
1	$Z_1 \in$ [-.8, 0]
2	$Z_2 \in$ [-1.6, -0.8]
3	$Z_3 \in$ [-2.4, -1.6]

To estimate P_o, it is assumed that the proportion follows a negative exponential function for increasing wind magnitude. This relationship was verified in paper C (conference proceeding), which analyzed the negative effect of wind on the heating performance of slab in controlled static environment. Therefore, the following equation can be utilized to solve P_o:

$$P_o = e^{-\lambda w} \quad \text{.....(16)}$$

where λ denotes the exponential factor, and w is wind magnitude in mph. Equation (15) will be utilized in paper (A) to predict the thermal demands under sustained wind conditions.

3.4. Hypothesis Testing

3.4.1. Introduction

A hypothesis is a theory or proposition set in place to explain the recurrence of some observed phenomenon, asserted based on a conjecture called a working hypothesis, or accepted as highly probably according to established facts. A scientific hypothesis can eventually transition to a theory if there exist continual validation via experiments. Hypothesis testing is a common method in the realm of statistics to strengthen the likelihood of a case. That is, testing a hypothesis will ascertain whether an observation is likely to have occurred based on statistics and hence, strengthen the case (Sirah Dubois, 2019).

The p-value approach consists of the formulation of an initial hypothesis (H_o), which is assumed true until proven otherwise via the alternative/null hypothesis (H_a). The likelihood of the initial hypothesis being true is dictated by the probability a more extreme test statistic hold- assuming the null hypothesis were true. If the P-value is small, say less than or equal to α_z, then the null hypothesis is unlikely. Otherwise, the null hypothesis is likely and hence, the result is statistically indeterminant (Penn-State University, 2019). The following case is utilized to determine test hypothesis is standard deviation is known and sample size is greater than 30. For a dataset to be assumed normally distributed, the following relations must hold:

- Approx. 68% of data falls between 1 standard deviation of the mean
- Approx. 95% of data falls between 2 standard deviations of the mean
- Approx. 99.7% of data falls between 3 standard deviations of the mean

Tests of the true value of an unknown population mean can be one of the following: one-tailed (left-tailed or right-tailed) or two-tailed. The rejection region represents the area under a normal distribution such that the probability of attaining a measurement within it is less than α_z. There are three typical scenarios for determining the test statistic (Z) using a known mean and standard deviation (Penn-State University, 2019):

1. Two-tailed (non-directional) H0: $\mu = \mu_o \leftarrow$ a possibility you want to test (null hypothesis) Ha: $\mu \neq \mu_o \leftarrow$ what the sample evidence suggests (alternative hypothesis). Reject H_o if $(Z) > (Z_{\alpha/2})$ or $(Z) < (-Z_{\alpha/2})$

2. Left-tailed H0: $\mu \geq \mu_o\}$ Reject H_o if $(Z) < (-Z_{\alpha})$

3. Right-tailed H0: $\mu \leq \mu_o\}$ Reject H_o if $(Z) > (Z_{\alpha})$

where $Z = (\bar{x} - \mu)/(\sigma / n)$……(17)

Figure 3-3 shows the possible regions of rejection according to the three aforementioned cases. If the population sample size is greater than 30, and the relation is satisfied for normal distribution, then a Z score hypothesis test may be proposed according to a one-sample test. Otherwise, a t-test score hypothesis can be proposed. The objective for the proposed hypothesis test is to determine an upper bound for α such that the relation in (11) is satisfied for the entire population, N.

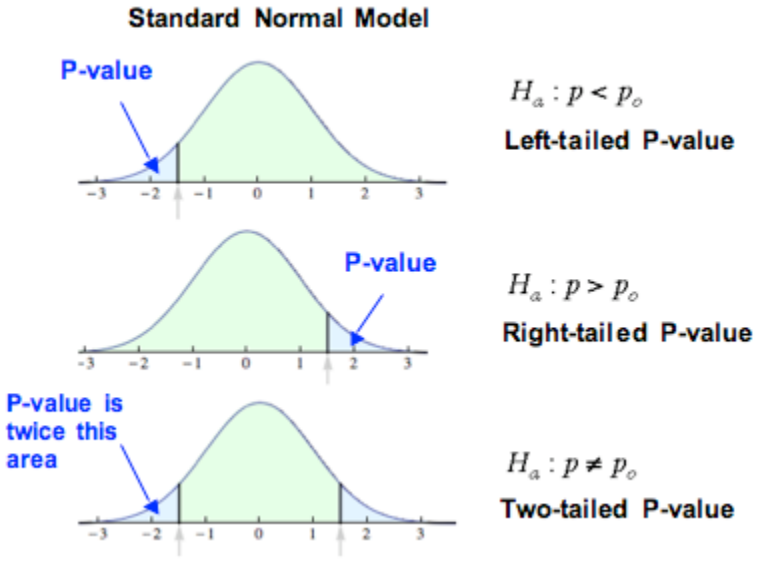

Figure 3- 9 Hypothesis Testing Scenarios

3.4.1. Shapiro Wilk Test for Normality

The following test is conducted on relatively small sample sizes (N < 30) to verify whether the dataset follows a normally distributed function. The Shapiro Wilks test uses the following hypothesis assumptions to determine whether a sample satisfies normality. Typically, the chosen level of confidence is 95% or $\alpha = 0.05$.

1) H_o: The sample data are not significantly different than a normal population.
2) H_a: The sample data are significantly different than a normal population.

The main objective is to accept the null hypothesis, meaning that there is enough evidence to conclude that the sample follows a normal distributed function. To perform the analysis, W-statistic is calculated, which tests whether a random sample, $x_1, x_2, \ldots, x_n$ comes from a normal distribution. The W-statistic, obtained via monte carlo simulations, were reproduced by Pearson and Hartley (1972). It is measured against α at a 95% level of confidence to determine the threshold for rejection. If $W < \alpha$, then there is a high degree of divergence from normality to permit a rejection of the null hypothesis. The W-statistic is calculated as follows.

$$W = \left(\sum_{i=1}^{n} a_i x_{(i)}\right)^2 / \sum_{i=1}^{n}(x_i - \bar{x})^2 \quad \text{.....(18)}$$

where $x_{(i)}$ is the ith component of an ordered sample of size n (n_1 being the smallest), and a_i are constants generated from the means, variances and covariances of the order statistics of a sample of size n from a normal distribution (Pearson and Hartley, 1972).

3.4.2. Variance of the Proportion, *p*

It is important to test the variance of a dataset prior to the construction of an error bound estimate to ensure convergence. If a sample population is normally distributed, yet the sample size is relatively small (N < 30), then a t-distribution function will be utilized to determine the confidence bounds. To verify whether the sample population corresponding to the proportion is confined within narrow bounds and isn't widely skewed from the mean, the following relations will be utilized.

1) $n(S_1/N) = n(\{s_s \in R | -1 < (p_n - p_{avg})/\sigma < 1\})/N$
2) $n(S_2)/N = (\{s_s \in R | 0 < -2 < (p_n - p_{avg})/\sigma < 2\})/N$

Where N = population size = $n\{s_1, s_2, \ldots, s_n\}$, σ is the standard deviation, and $n(S_i)$ is the number of elements per set for i = 1,2.

That is, if most elements of each set are confined between -i and i, then the distribution is convergent towards the mean. Otherwise, there's a high degree of scatter for the sample population. Figure 4-4 shows the generalized relation to verify normal distribution.

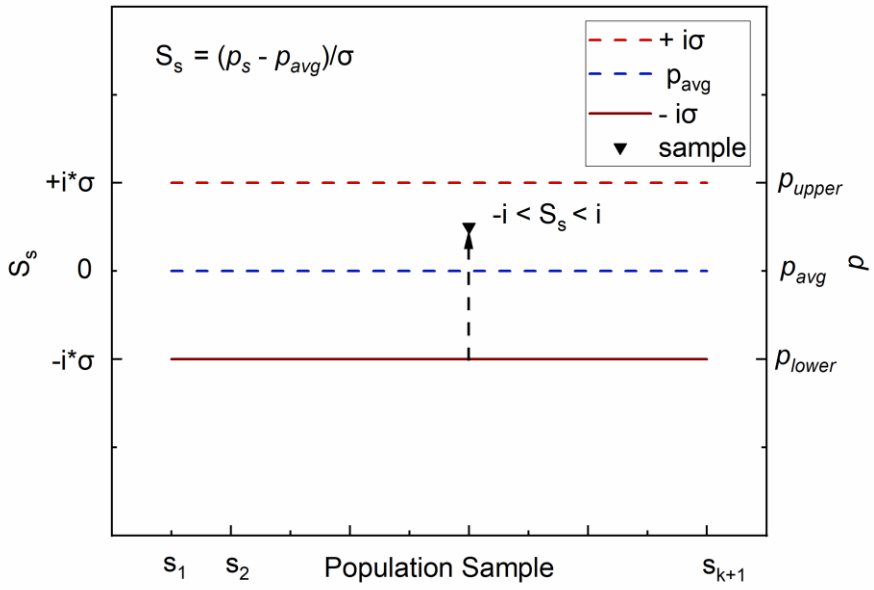

(a)

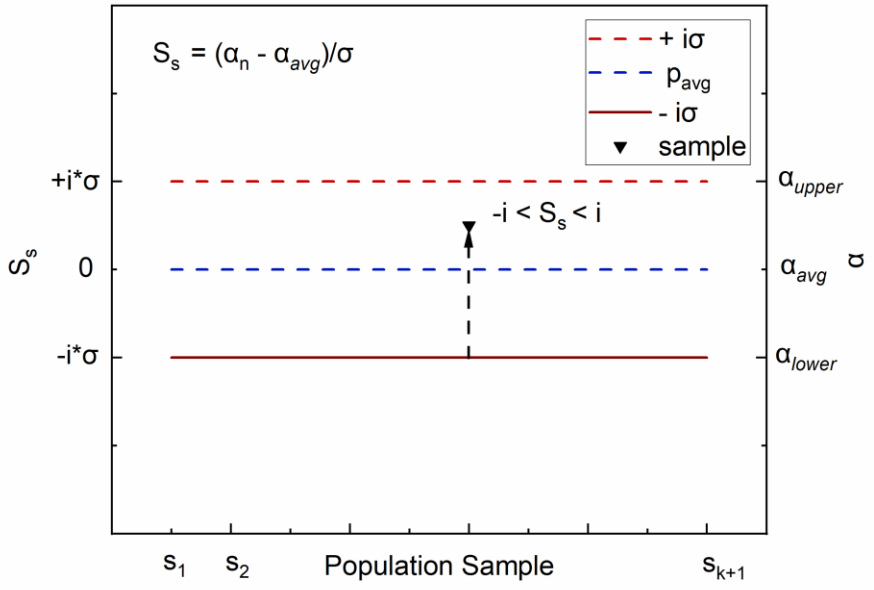

(b)

Figure 3- 10 Population Spread from the mean: (a) Proportion, (b) Alpha coefficient

3.5. Data Collection

In order to record temperature changes within the concrete panel, thermocouples have been installed at different locations within the panel. A compact data logger from National Instruments (NI) cDAQ 9178 with a thermocouple module NI 9213 were utilized to extract data for testing and analysis. Once the data logger is connected to a power source and a USB channel, the software NI Max (Measurement Automated Explorer) ensures the device is connected properly and allows you to perform the following:

- Configure your National Instruments hardware and software
- Back up or replicate configuration data
- Create and edit channels, tasks, interfaces, scales, and virtual instruments
- Execute system diagnostics and run test panels
- View devices and instruments connected to your system
- Update your National Instruments software.

Once the data logger is configured properly, the thermocouple module NI 9213 is inserted into one of the module slots. Each module has 16 channels that pick-up thermocouple signals and the data logger calibrates the signal and records the corresponding temperature in degrees Celsius or Fahrenheit. The module and data logger from National Instruments are shown in Figure 3-4 (a) and (b) respectfully.

Figure 3- 11 (a) NI 9213 Chassis and (b) NI cDaq 9178 unit (National Instruments)

The data acquisition device utilized for our project was created by National Instruments for the purpose of creating virtual instrumentation via lab-view, a data flow programming language. Lab-view allows the user to tabulate, plot, or alter the input signals directed from the data acquisition device to satisfy a problem. Type-T thermocouples are selected due to their broad temperature range, and high accuracy. Once the thermocouple module is assembled in the cDAQ chassis, type-T thermocouples were installed in the bridge deck. Each thermocouple is composed of two separate wires composed of copper and copper-nickel alloy which pick up a different voltage depending on the temperature. The temperature input at the coupled end is interpreted from the difference between the currents of the two metals. Thermocouples made for instrumentation use metals of high purity for an accurate temperature/voltage relationship (as linear and as predictable as possible).

Chapter 4. Laboratory Study of Externally Heated Geothermal Bridge Deck System in Controlled Sub-Freezing Environment

4.1. Scope and Motivation

Based on the results attained from paper A, the thermal demands required for de-icing could be reasonably estimated. A variable, denoted as the thermal gradient ratio or proportion, *p*, directly relates to the performance of the system. Therefore, the slab was subjected to multiple thermal loads (I-A) and wind conditions to determine the proportion of thermal energy reaching the slab surface.

Abstract

The following study presents an experimental model of a geothermal bridge de-icing system subjected to sub-freezing controlled conditions. The vertical and lateral temperature profiles were investigated to gauge the overall heating efficiency of the system. Various winter scenarios were applied to the system to determine its performance, and how feasible it will be for the system to be transferred to the field. A prediction equation was developed to estimate the total energy reserves required to permit de-icing, and statistical analysis was provided to for validation. The negative influence of sustained wind on the thermal response of the slab is investigated. A thermal rebound study is included to emphasize the potential transient effects of wind following cyclic wind loading and unloading periods.

4.2. Introduction

Texas is especially prone to freezing rain conditions which can lead to black ice, an invisible threat to bridges and overpasses. The probability black ice will accumulate is higher for bridges due to lack of insulation and thermal energy output from the sub-surface. The treacherous conditions have led to multiple fatalities that could have been prevented if de-icing measures were improved. Therefore, devising an innovative solution to prevent any recurrences of these

problematic events is imperative for the future. Currently, TX-DOT has supported our research endeavors to create and implement the design of a geothermal de-icing system utilizing a hydronic heating system. The field testing has been conducted contemporaneously with the laboratory testing. The goal of the laboratory tests is to gauge the performance of the proposed deign, which is to be constructed on an actual bridge. A geothermal bridge de-icing experimental model is necessary to predict the quantity of heat that must be generated to counteract freezing conditions. To replicate Winter scenarios in the Texas area, a concrete slab was emplaced within a freezer box to simulate the geothermal heating system.

4.2.1. Installation of De-icing System

Prior testing the heating performance of the slab, PEX pipes were attached in a series of loops spaced six inches apart at the underside of the slab. A 5-inch-thick wooden framework was attached to outer boundary of the slab base to confine the pipes prior to the application of spray foam. Once the pipes were attached to the base, closed cell spray foam was utilized to ensure the base was properly insulated. The following figures display the events preceding the initiation of the heating system. Once the freezer box was secured in place, concrete blocks were placed such that it could support the dimensions of the slab. The distance between the blocks and height was roughly 3.5 and 4 feet, which is displayed in figure 4-1 (a). Figure 4-1 (b) shows the PEX pipe network attached to the base of the slab. It consists of five total loops that span approximately 4 feet along the slab length. To apply the pipes, compression fittings and copper pipe connectors were utilized along each loop and pipe segment to prevent tension from developing after the spray foam was to be applied, and to maximize the surface area of contact at the interface between pipe and base of slab.

Figure 4-2 (a) shows the wooden framework that was utilized to conceal the spray foam for a maximum thickness of 5 inches. Semi circles were drilled on the opposite side of the slab to conform to the inlet and outlet sections of the pipe. Figure 4-2 (b) shows the spray foam during the curing process. It’s quite difficult to achieve uniformity, hence, there will exists troughs and peaks. Thus, achieving a greater thickness than what is typically required decreases the

likelihood that the minimum thickness (trough) will be at an insufficient thickness. The maximum and minimum thickness was roughly 5 and 3 inches respectively.

(a) (b)

Figure 4- 1 (a) Concrete block support for 4” by 3” slab, (b) PEX Pipe network secured to base of slab

(a) (b)

Figure 4- 2 (a) Wooden framework utilized to Conceal Spray Foam, (b) Closed cell foam curing process

4.2.2 Thermocouple Layout

Figure 4-3 (a) shows the thermocouple map (planar view) utilized for testing the performance of the slab. Five sets of four thermocouples were installed within the slab at depths of 0, -2, -4, and -6 inches respectively. The left outermost thermocouple of each set was applied to the surface of the slab (Z ~ 0”), and the remaining depths in ascending order, were applied in a counterclockwise pattern. There are five sets of thermocouples defined by two index numbers: the first and second index correspond to the set number and depth respectfully. The depth index of each thermocouple applied to the surface is defined as 0. Also, the inlet and outlet portion of the pipe is labeled according to the first letter (I & O). Sets 1-4 show the lateral and vertical change in temperature across the slab length, whereas set 5 shows the vertical change in temperature at a specific location along the pipe centerline. The thermocouples corresponding to set 5 malfunctioned for most of the testing sequence and hence, was excluded from the analysis. Figure 4-3 (b) shows a cross section view of the thermocouple layout corresponding to sets 1-4.

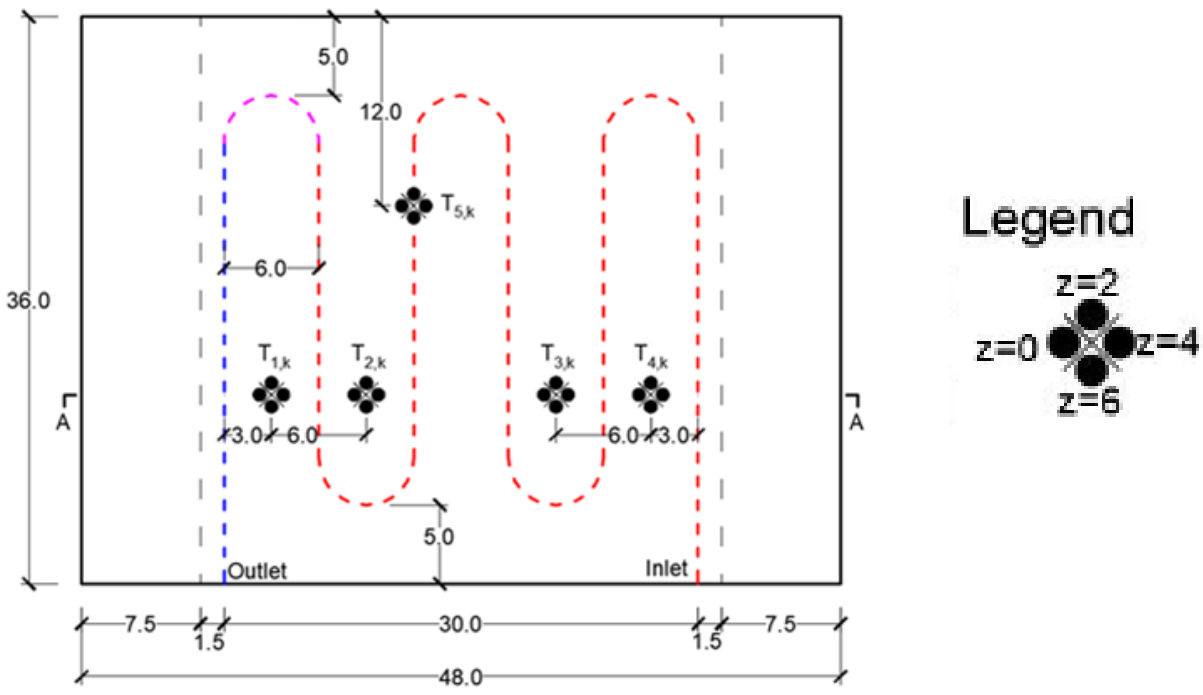

(a)

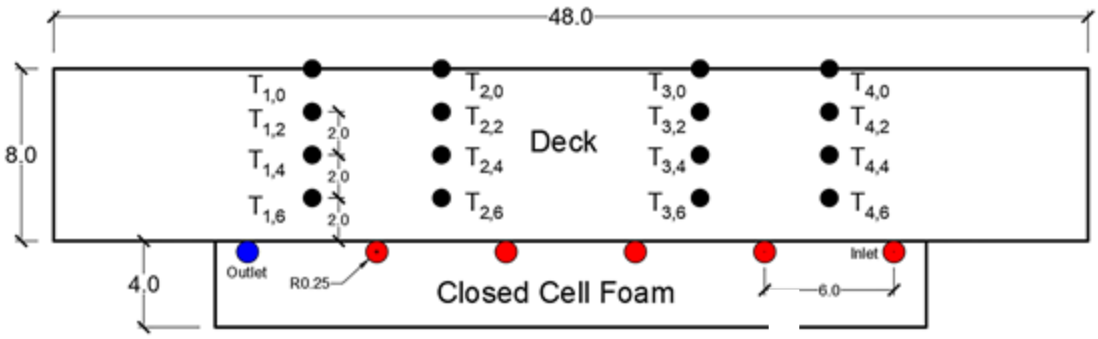

(b)

Figure 4- 3 (a) Thermocouple Mapping (Planar View), (b) Slab Cross Section

Results and Discussion

4.3. Vertical Temperature Variation ($S_{1,2}$)

4.3.1 Introduction

The following section presents the vertical temperature response within the slab in respect to sets 1-5. It is important to determine the vertical profile of the slab to conduct heat flux analysis to ensure that de-icing will be fulfilled. Table 4-1 displays each test sequence, which comprise of one or more sub-tests corresponding to altered inlet (water) temperatures. Sub-test y of sequence x will be denoted as $S_{x,y}$ such that the first and second indices represent the sequence and sub-test numbers respectively where $x \in \{1,2,3,4\}$ and $y \in \{1,2,3,4,5\}$. Let X and Y be denoted as the sets where indices x and y reside. Each test was run for sufficient time to ensure steady-state conditions were approximately met. That is, $\Delta T/\Delta t \approx 0$ $\forall j,k \in N$ (set of natural numbers). Prior to the initiation of each sub-test, the ambient temperature was initially set to 55 ° F to ensure the water bath doesn't run continuously. Once the slab was approximately in equilibrium with the initial ambient condition, the water bath and freezer box were set to the desired temperature. The water pump and testing program were turned on contemporaneously. Once the slab attained steady-state conditions at the surface for each set, the data was collected, and the proceeding sub-test was initiated. The average steady-state temperature for sets 1-4 at each depth interval was provided in respect to each sub-test as indicated in table 4-1. Sub-test 3 of test sequence 1 ($S_{1,3}$)

was conducted as a verification case to show that the average proportion across sets 1-4 can be utilized to predict the inlet temperature to reach the freezing point. Thus, the proportion was averaged for sub-tests corresponding to set J – {3} to estimate the required inlet temperature to cross the freezing boundary, defined at 32 ° F. The thermal gradient ratio or proportion, p, was calculated emphasize an approximate linear relationship between steady-state temperature and depth, which is exemplified via the mean and standard deviation (table 4-1).

Table 4- 1 Testing Sequence

Test Sequence	Sub-Test	Ambient Temp (° F)	Inlet Temp. (° F)	Set Ambient Temp (° F)	Flow Velocity (gpm)	Average Steady-State Temp. (° F)			
						Z0	Z2	Z4	Z6
1	1	26	77.3	25	2	30.9	33.6	35.3	36.8
	2	26.1	86.7			31.8	34.9	36.7	38.3
	3 (*)	25.7	93.4			31.9	34.9	37	38.7
	4	26.2	100.1			32.8	36.1	38.5	40.6
	5	26.4	109.8			34	38.1	40.9	43
2	1	20.8	101.1	20		28.1	31.8	34.3	36.4
	2	20.4	110.8			28.3	31.6	34.3	36.8
3	1	31.0	109.4	30		37.9	41.7	44.2	46.5
	2	30.9	100.0			37.2	40.4	42.5	44.4
	3	31.0	90.1			36.4	39.0	40.8	42.2
	4	30.5	70.0			34.1	36.0	37.3	38.2
4	1	35.6	70.0	35		38.8	40.4	41.4	42.2
	2	35.6	80.1			39.9	41.6	42.9	44.1
				ρ_{avg}		.092	.138	.168	.195
				S.D., σ		.003	.005	.006	.007

(*): Verification case
$S_{x,y}$ denotes the test sequence x and subtest y.

4.3.2. Test Procedure Definitions and Conditions

For section 4.3-4.5, a total of four test sequences were conducted according to ambient temperature, which was incrementally altered such that Δ A = 5° F. Additionally, each sequence included 2-5 sub-tests defined according to different heating loads (I-A) where I ∈ [70,110]. The ratio between the thermal gradient of the slab and heating load, or proportion *p*, was included to relate with the system efficiency for each testing sequence. Prior to conducting each test, the freezer box was set to 55 ° F. Once equilibrium conditions were satisfied, the water tank and

freezer box were set to the desired temperature, and the water pump was turned on to initiate the sub-tests. Each sub-test was terminated once steady-state conditions were satisfied at the surface of the slab. The average time to reach steady state was approximately 20 hours. The definitions corresponding to the following sections are shown in table 4-2.

Table 4- 2 Testing Definitions

Term	Definition
Proportion, *p*	$(T_{j,k} – A)/(I-A)$
Heating Load	(I-A); Difference between inlet and ambient temperature
Alpha coefficient	$\delta p/\delta Z$; Change in proportion per unit depth
W_x	Period corresponding to rebound or dissipating wind cycles where $x \in N$
Time frequency, (F, min^{-1})	$1/ (t_n – t_{n-1})$
T_o	Initial steady-state temperature at Z = 0.
T_f	Final steady-state temperature at Z = 0.

4.3.2. Test for Normality in respect to the Proportion, *P*

Before proceeding to define the error bounds for the verification case, the proportion must follow a normally distributed function. The Shapiro-Wilks method is utilized for this purpose. SS is denoted as the sum of the squared variances relative to the mean and b is the weighted co-variance relative to a standardized normal distribution function. The null hypothesis states that the data follows a normal distributed function. Thus, the objective is to not reject the null hypothesis to satisfy normality. The W-statistic is a measure of the convergence of a dataset to a normally distributed function, meaning the co-variance is positive. The level of significance is assumed to be 0.05. Therefore, to accept the null hypothesis, it must follow that P > 0.05. The closer P tends to 1, the stronger the normality of the sampled function. Table 4-3 verifies that the proportion is normalized and hence, confidence bounds can be reasonably applied.

Table 4- 3 Shapira Wilk method to verify normality of *p* for N < 50

Depth (Z, inch)	SS	b	$W=b^2/SS$	$W_{p=0.05}$	p
0	0.00008	0.009	0.9475	0.866	0.54
-2	0.00032	0.02	0.9479		0.54
-4	0.0004	0.02	0.95		0.58
-6	0.0006	0.023	0.946		0.51

4.3.3. Verification Case ($S_{1,3}$)

To attain a prediction of the required inlet temperature to cross the freezing boundary, the proportion was averaged for sets 1-4 of test sequence $S_{1,\ J-\{3\}}$ where $J - \{3\} = \{1,2,4,5\}$. Equations (7) and (8) were utilized to determine the upper and lower confidence bounds at a level of significance of 0.01. The objective was to estimate of the required thermal input (inlet temperature) to cross the critical zone. The critical zone is synonymous with the defined freezing boundary set at 32 ° F, which was laterally projected to attain the estimate. According to figure 4-4 (a), the estimated inlet temperature to induce de-icing along the slab surface is 93.4 º F for an ambient temperature sustained at 25 º F. The average thermal gradient ratio, p_{avg}, was calculated at 0.092 for depth Z_0 (Z= 0). The inlet temperature can be estimated with reasonable confidence since the standard deviation, σ, in respect to the proportion at the surface level is 0.003. The upper and lower bounds are applied to emphasize the degree of error that could be associated with the estimation. According to the bounds, the required inlet temperature will very likely exist in a range from 30.48º C to 37.8 º C for a 99% degree of confidence. Equations (7) and (8) were utilized for the upper and lower bounds. Figure 4-4 (b) shows the test results conducted at the predicted inlet temperature. There was a 0.12 ° F difference between the actual and estimated measurements, implying that the average proportion, p_{avg}, is a good approximation.

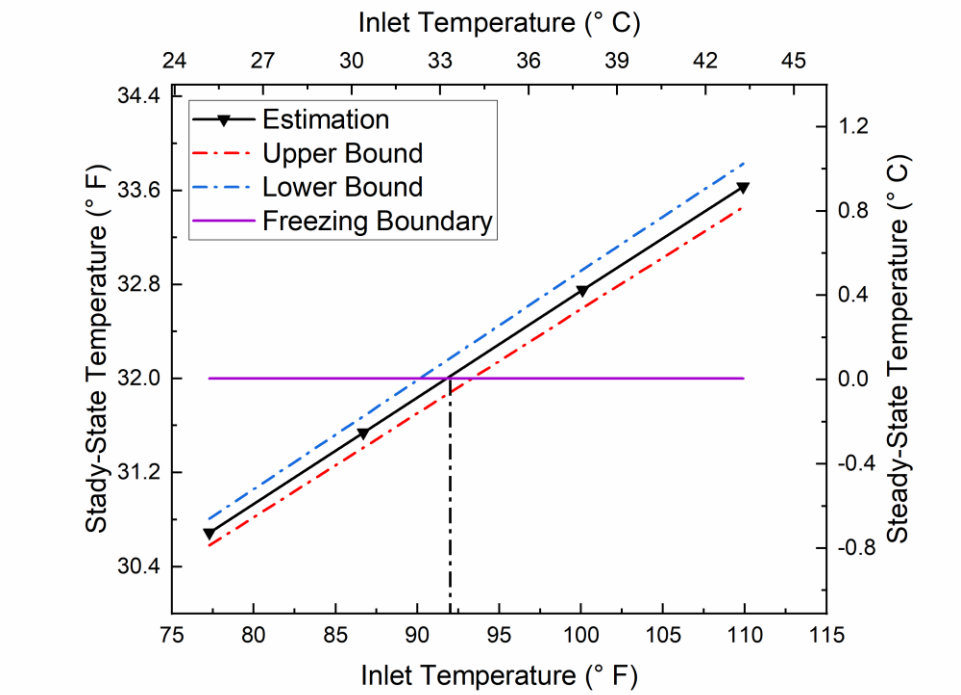
Inlet Temperature (° C)
24
27
30
33
36
39
42
45
34.4
33.6
32.8
32.0
31.2
30.4
Stady-State Temperature (° F)
Estimation
Upper Bound
Lower Bound
Freezing Boundary
1.2
0.8
0.4
0.0
-0.4
-0.8
Steady-State Temperature (° C)
75
80
85
90
95
100
105
110
115
Inlet Temperature (° F)

(a)

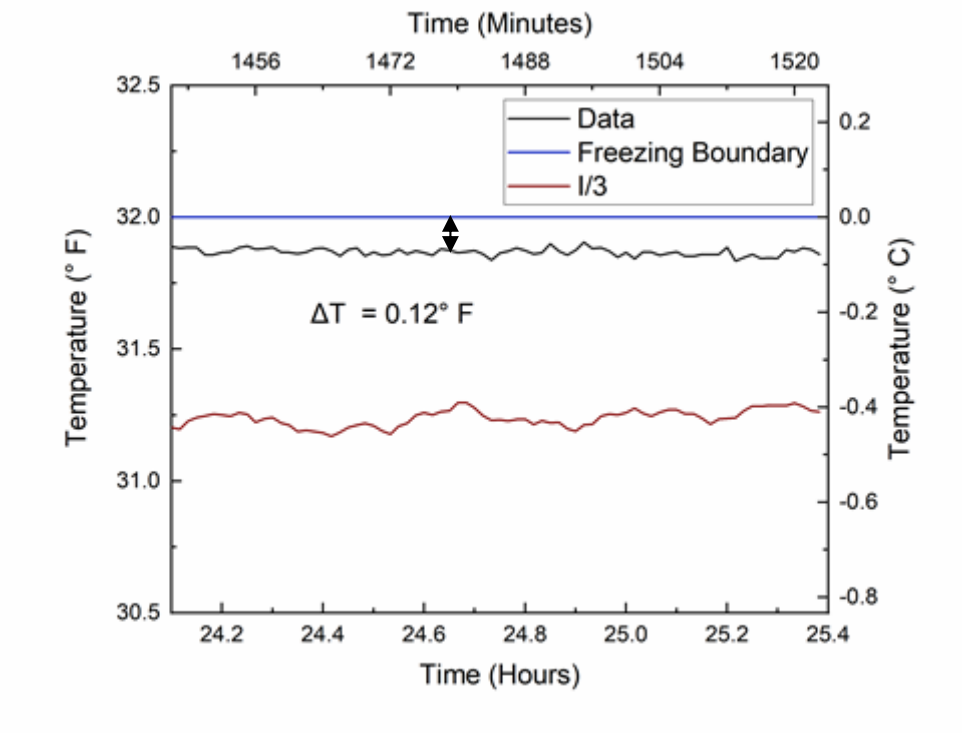

(b)

Figure 4- 4 (a) *Test Conducted at Predicted Inlet Temp. (b)* Prediction of required inlet temperature to cross freezing boundary

4.1.4. Maximum Thermal Variation along Pipe Loop Section ($S_{1,1}$)

The objective of this section is to determine the maximum lateral temperature variation corresponding to $T_{5,k}$ and $T_{2,k}$, where k ∈ {0, -2, -4, -6}. Set 5 is located along the pipe network in terms of geometry whereas set 2 is located at the midpoint of a loop section. Test sequence $S_{1,1}$ was chosen to construct the relationship because set 5 malfunctioned for the proceeding sub-tests. Figure 4-5 (a) shows the temperature variation as a function of depth below the slab surface. There is a direct relationship between temperature deviance and depth from the surface and therefore, the temperature is more uniform towards the surface. Hence, the surface temperature can be averaged with higher precision relative to the base. Figure 4-5 (b) shows the heat flux deviation by taking the summation of the depth modulus per interval starting with the base depth (Z = -6). So, $\sum_{i=1}^{n} |Z_i|$ = (2*n) in inches where i is the depth index shown in table 3-3. Equation (14) was utilized to calculate the deviation in heat flux between sets 2 and 5. The

results indicate that heat flux is divergent per depth interval in respect to sets 2 and 5 respectfully. The maximum deviation was determined to be 3 W/m^2K for case $S_{1,1}$.

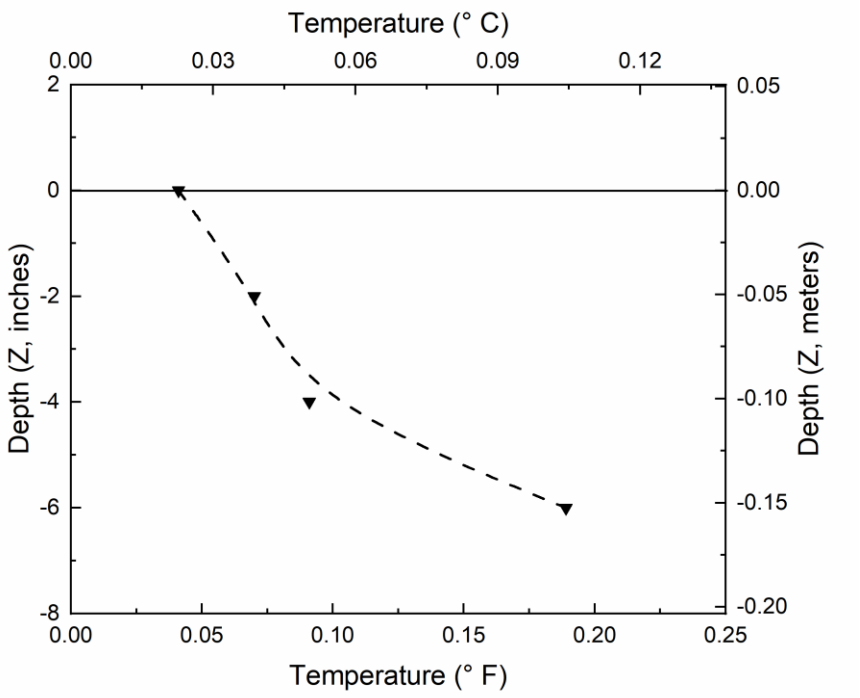

(a)

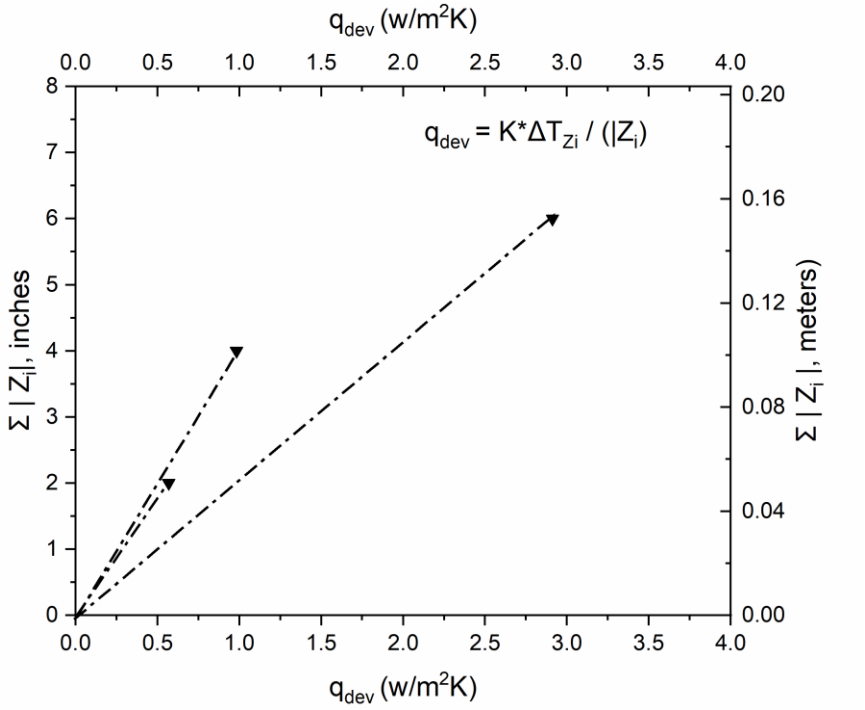

(b)

Figure 4- 5 (a) Temperature Variation between Sets 2 and 5, (b) Heat flux variation between sets 2 and 5 ($S_{1,1}$)

4.1.5. Vertical Temperature Profile of Slab

Figure 4-6 (a) and (b) correspond to test sequence $S_{1,2}$ and thermocouples $T_{4,k}$ where $k \in \{0,-2,-4,-6\}$. According to figures 4-6 (a), the temperature corresponding to the indices k, is consistent. That is, the temperature increases as the depth increases. The temperature inputted into the system via a heated water bath was sustained at 30.5 ° C (87 ° F) whereas the ambient temperature was sustained at -3.3 ° C (26 ° F). The rapid spikes in ambient temperature are caused by the defrost cycles within the freezer box. It takes roughly 20 hours to attain an approximation of steady-state conditions. There is a strong linear relationship corresponding to the steady-state temperature per unit depth within the slab at set 4, which is exemplified in figure 4-6 (b). This signifies that that thermal demands can be estimated with marginal error in vicinity of set 4, however, the global thermal demands must be equated to ensure the entire slab can safely eliminate all snow/ice. By using equation (1) from the literature review section and utilizing the thermal gradient to measure the heat flux at the slab surface level, the thermal demands for snow/ice melting can be determined. By creating an upper bound in respect to the

thermal gradient, the certainty that de-icing will be permissible increases. Since the change in proportion per unit depth, denoted by α, is synonymous with the thermal gradient within the slab, a relationship can be developed to determine the approximate upper bound for α. This ensures that under all scenarios, the heating demands will not be under-estimated. The temperature of thermocouple, $T_{4,0}$ coincided with the freezing boundary once steady state was attained, implying that the minimum thermal input such that $T_{4,0} \geq 32°$ F is approximately 87 ° F. Figure 4-7 shows the vertical profile for sub-tests 1-5 using the average temperature across all sets. The divergence from the ambient temperature (A = 25° F) is included as a point of reference. The required thermal input to permit a phase change is estimated at 94° F.

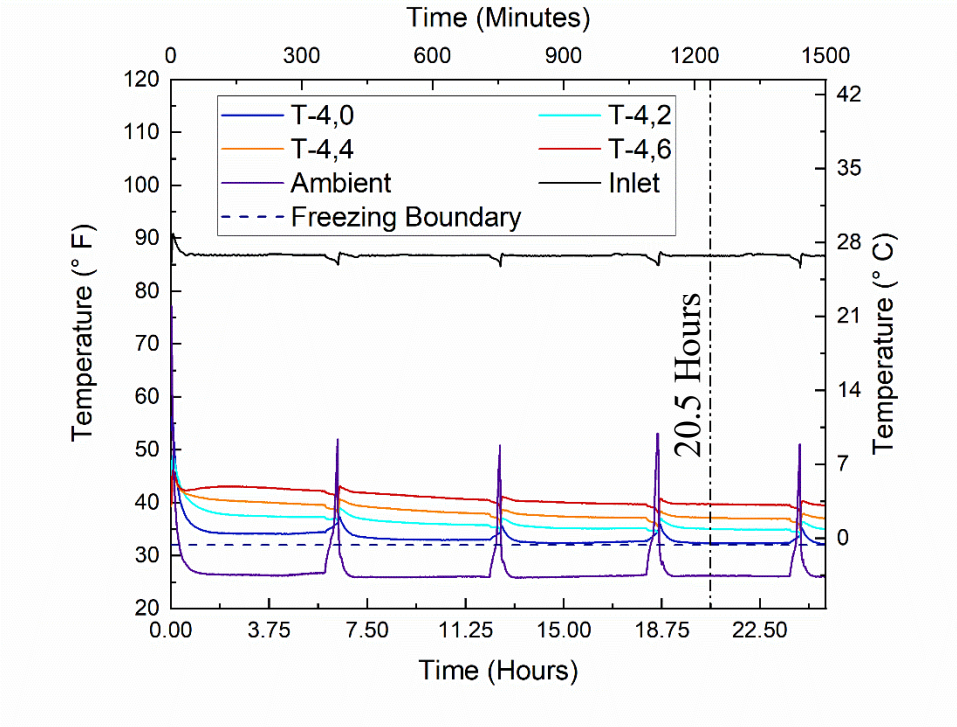

(a)

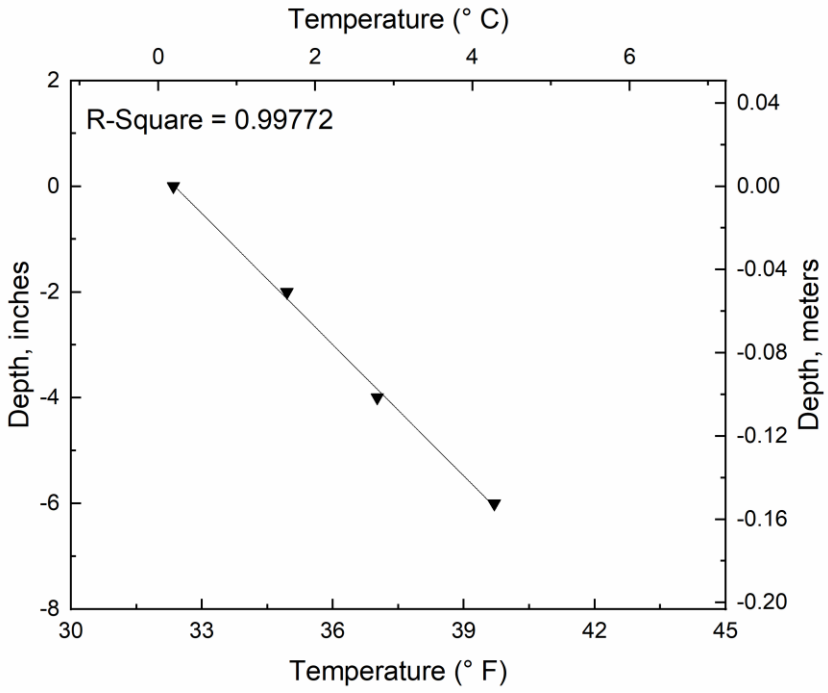

(b)

Figure 4- 6 (a) Temperature Response at set #4 ($S_{1,2}$), (b) Vertical Profile for set #4 ($S_{1,2}$)

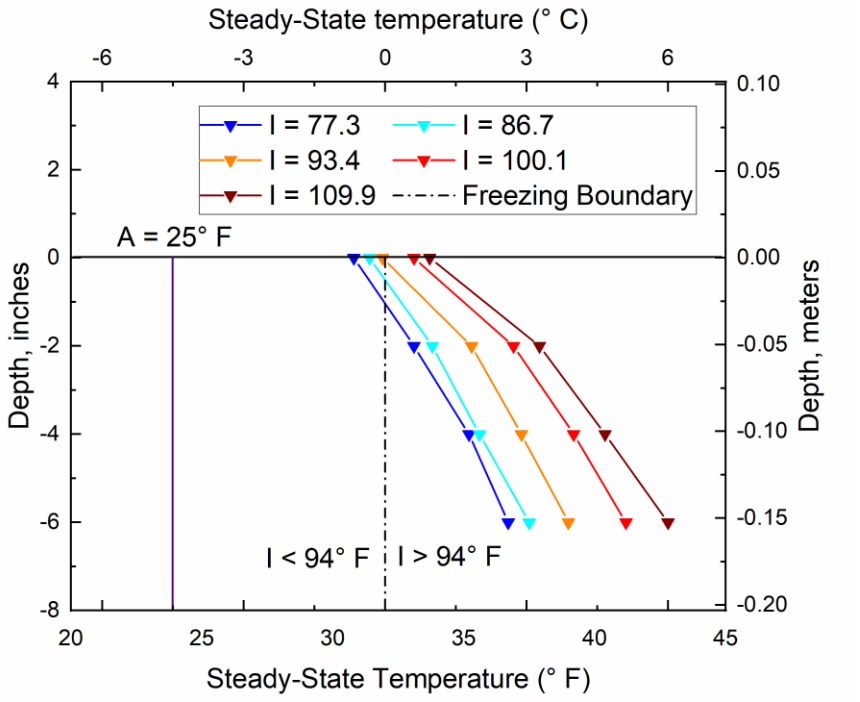

Figure 4- 7 Vertical Temperature Profile in Respect to Test Sequences 1

4.2. Lateral Temperature Variation

4.2.1. Introduction

The following section presents the lateral temperature variation across the slab length for sets 1-4. It is imperative to obtain a lateral temperature profile so that the required inlet demands for de-icing can properly be adjusted. That is, $I_{required} \geq \max \{x \in R | \forall j, T\text{-}j_{,0} > 32\}$ where $j \in \{1,2,3,4\}$. Since the outlet end of the pipe network exhibits the minimum temperature, it will follow that j = 1 (set 1). Table 4-4 (a) and (b) show the lateral change in temperature for depths Z = 0 and Z > 0 respectively.

Table 4- 4 (a) Lateral Temp. Response (D = 0); (b) Lateral Temp. Response (D > 0)

Test Sequence	Sub-Test	Inlet Temp. (° F)	Ambient temp. (° F)	Average Steady-State Temp. (D = 0, ° F)			
				Set #1	Set #2	Set #3	Set #4
1	1	77.9	25	30.4	31.82	31.15	31.00
	2	86.9		30.46	32.54	32.31	32.34
	3	93.4		30.51	32.56	32.38	32.8
	4	100.9		31.4	33.36	32.58	32.54

(a)

Test Sequence	Sub-Test	Inlet Temp. (° F)	Ambient temp. (° F)	Average Steady-State Temp. (D > 0, ° F)			
				Set #1	Set #2	Set #3	Set #4
1	1	77.9	25	34.54	35.26	35.67	35.46
	2	86.9		35.34	36.57	37.35	37.17
	3	93.4		35.62	36.90	37.92	37.64
	4	100.9		37.30	38.38	39.14	38.72
	5	109.8		38.75	40.55	41.85	41.52

(b)

4.2.2. Parabolic Lateral Temperature Profile

Figure 4-8 (a) shows the average temperature variation in respect to sets 1-4 for test sequence $S_{1,2}$. The thermocouple measurements were attained below the slab surface ($Z < 0$). Figure 4-8 (b) shows that there exists a parabolic temperature profile corresponding to the results from (a). Due to the boundary effect, the temperature will converge to the ambient along the outer perimeter of the slab because heat escapes at a faster rate. The thermal differential is maximized at the outer boundaries, and for this reason, more heat will be lost beyond the geometric pipe layout. The thermal differential is minimized toward the center of the slab where the heat distribution is more uniform. Figure 4-9 (a) shows the parabolic temperature profile in respect to surface conditions ($Z = 0$) for sub-tests 1-5. The thermal minimum and maximum occurred at set 1 and 2 respectfully. Figure 4-9 (b) shows that the variance in temperature increases toward the inlet section of the slab. The minimum proportion attained at set 1 was approximately 0.067. Therefore, the possibility for ice accumulation for this region of the slab is high since roughly 7% of the heat load may be transferred. Figure 4-10 shows that the thermal minimum and

maximum occurred at sets 1 and 3 respectfully (Z < 0). One possible reason for the inconsistency regarding the thermal maximum is due to the vertical offset among thermocouples or the environmental interference towards the surface of the slab. That is, some thermocouples may be offset to account for a discrepancy in measurements, and there may exists some influx of air which effects the thermocouple readings at surface.

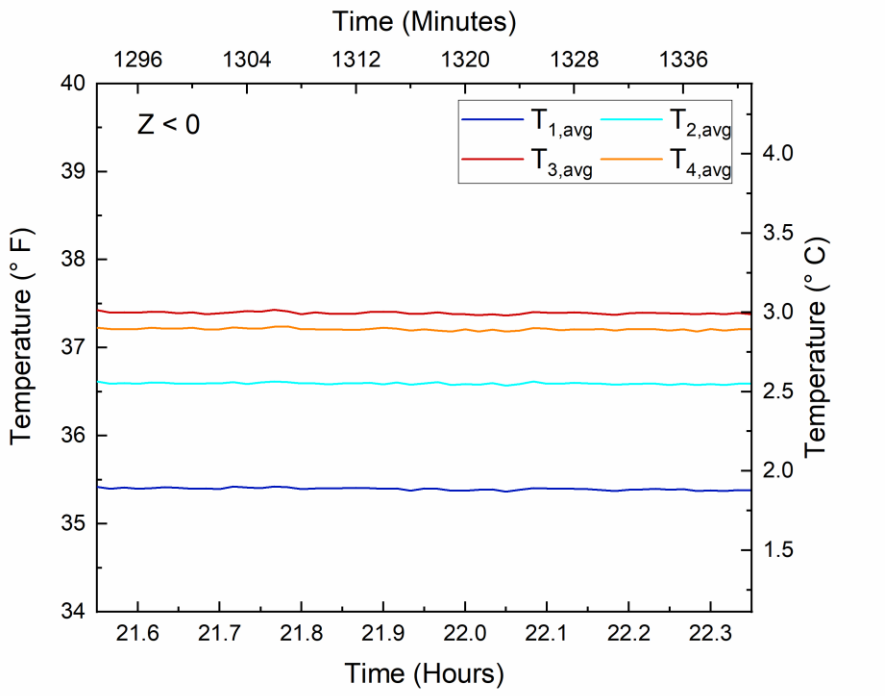

(a)

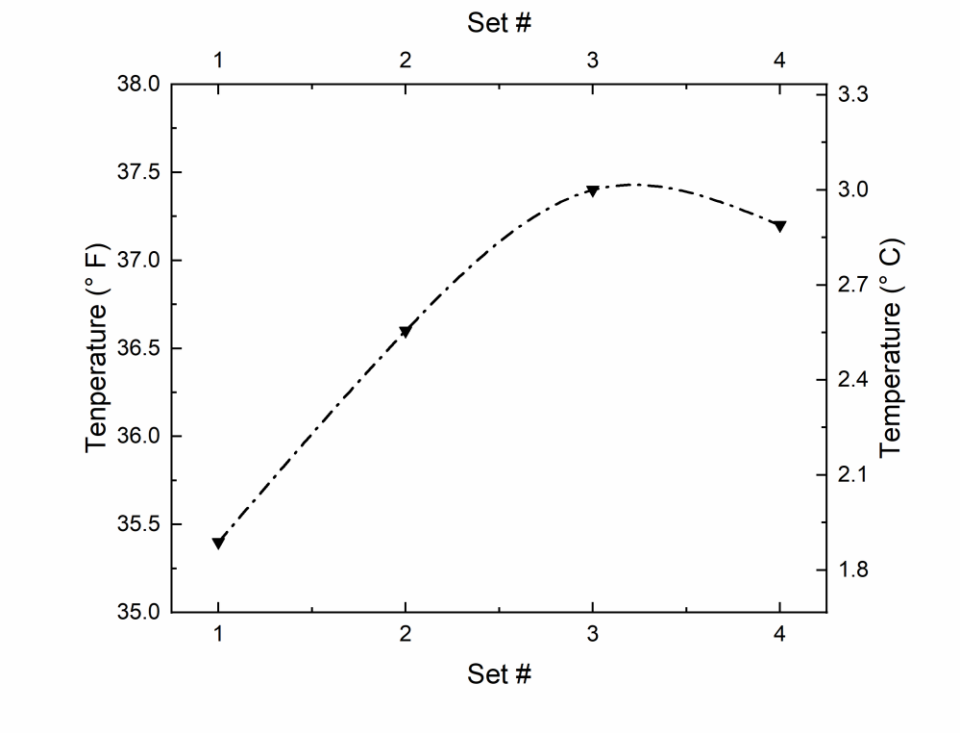

(b)

Figure 4- 8 (a) Average Temperature Response in respect to each Set for D >=0 # ($S_{1,2}$), (b) Parabolic Relationship in respect to Average Slab Temperature across Slab Length, D>=0

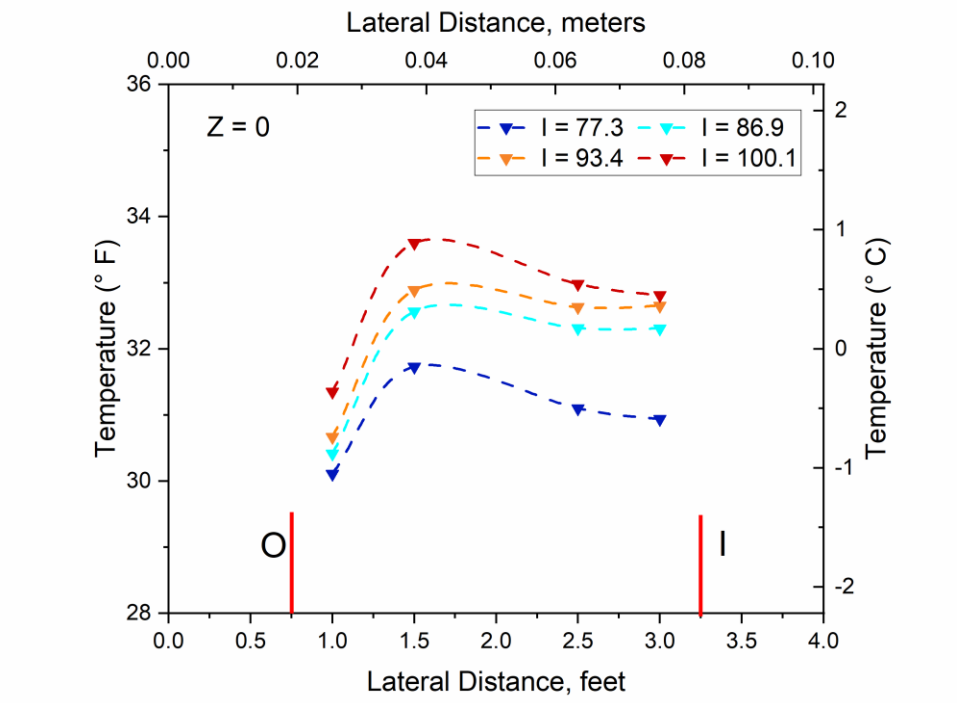

(a)

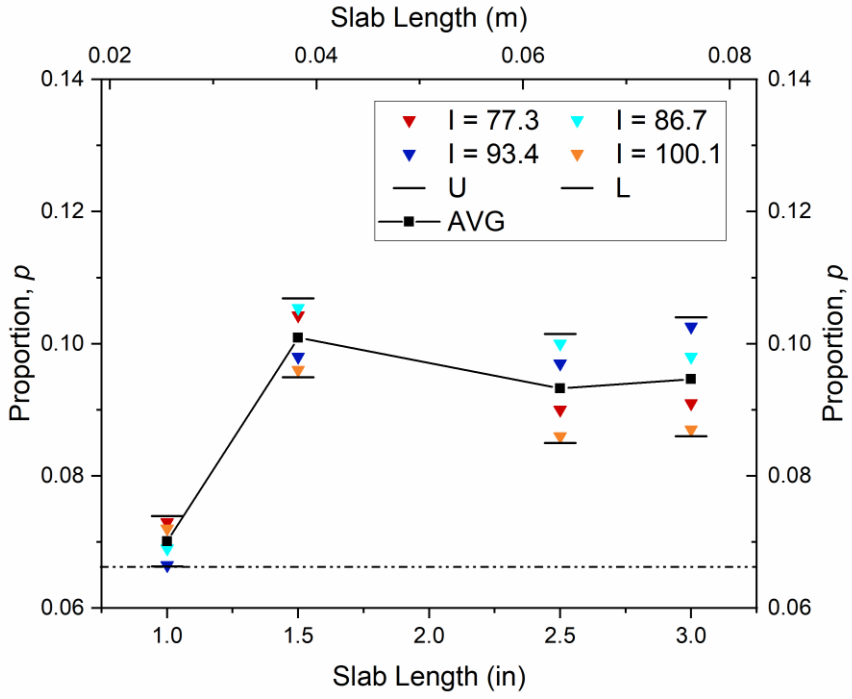

(b)

Figure 4- 9 (a) Lateral Temperature Variation for D = 0, (b) Variance in respect to the proportion for sets 1-4

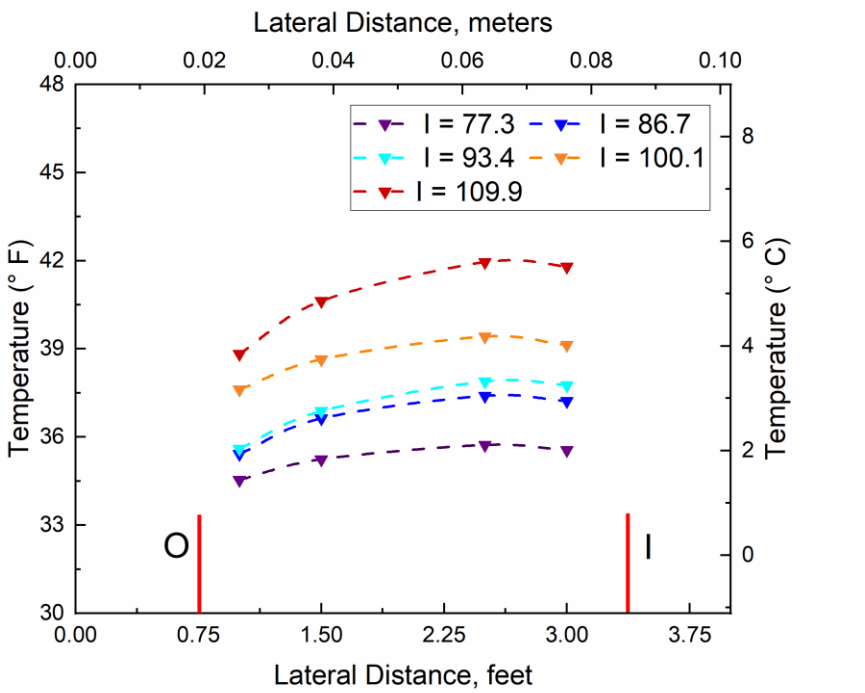

Figure 4- 10 (a) Lateral Temperature Profile for D > 0

4.2.3 Thermal Minimum

It is imperative to adjust the thermal demands according to the region of the slab that exhibits the highest potential for developing ice. As expected, the minimum thermal energy was produced toward the pipe outlet and hence, the thermal demands should be adjusted accordingly. The aim is to ensure the entire surface area of the slab is free from ice. By finding the minimum proportion of heat transfer constrained within a confidence bound, the probability that de-icing will occur along the entire slab surface is very high. Figure 4-11 (a) shows that 76% of the sample population corresponding to the proportion at set 1 is confined within the bounds within 1 standard deviation. Roughly 85% and 93% of the sample population falls between 1 S.D and 2 S.D respectfully. Moreover, 92% is confined within 2 standard deviations from the mean as shown in figure 4-11 (b). The mean and standard deviation is 0.0794 and 0.00506 respectively. A 99% confidence region was utilized for this study to increase the accuracy of the estimated thermal demands. Figure 4-11 (c) shows the proportion for each sub-test in respect to set 1. There is a high probability that the average proportion at set 1 will be constrained to the following bounds: $P_{1,0} \in [0.075, 0.0835]$, which were obtained using a t-test for a sample population of 13. It is worth noting that the proportion is very sensitive to fluctuating

environmental conditions because it takes time to adjust. The freezer box internal temperature was sensitive to the outdoor conditions, which lead to fluctuating temperatures at times. This is the reason it is of high importance to take an error bound to account for such changes. There will exist outliers as a consequence, which will skew results in both directions. Thus, it is not advisable to consider the minimum proportion for the analysis and instead take the lower bound estimate. For this case, $P_{\text{lower}} = 0.075$.

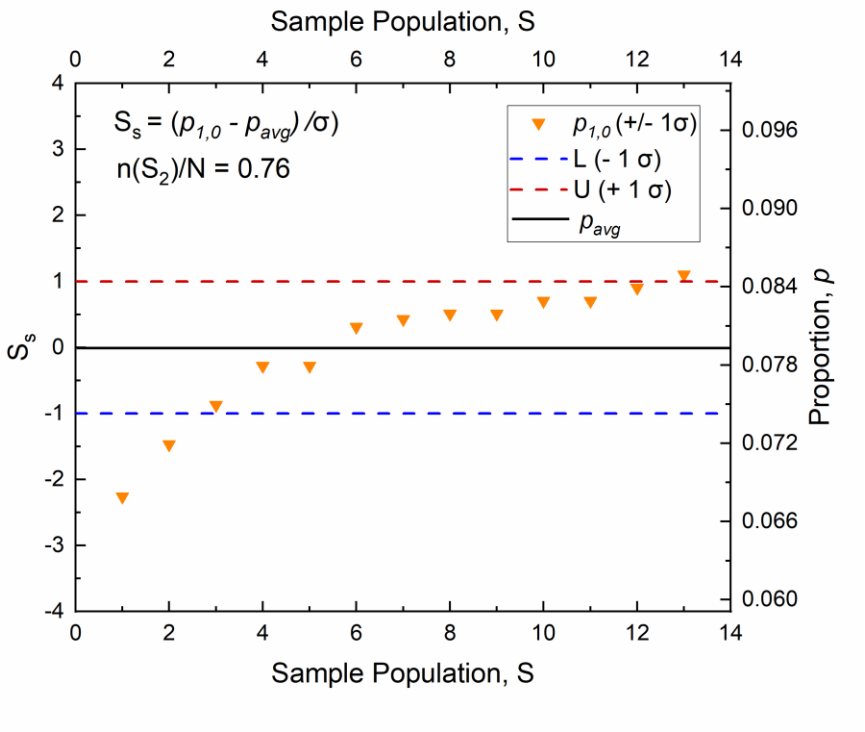

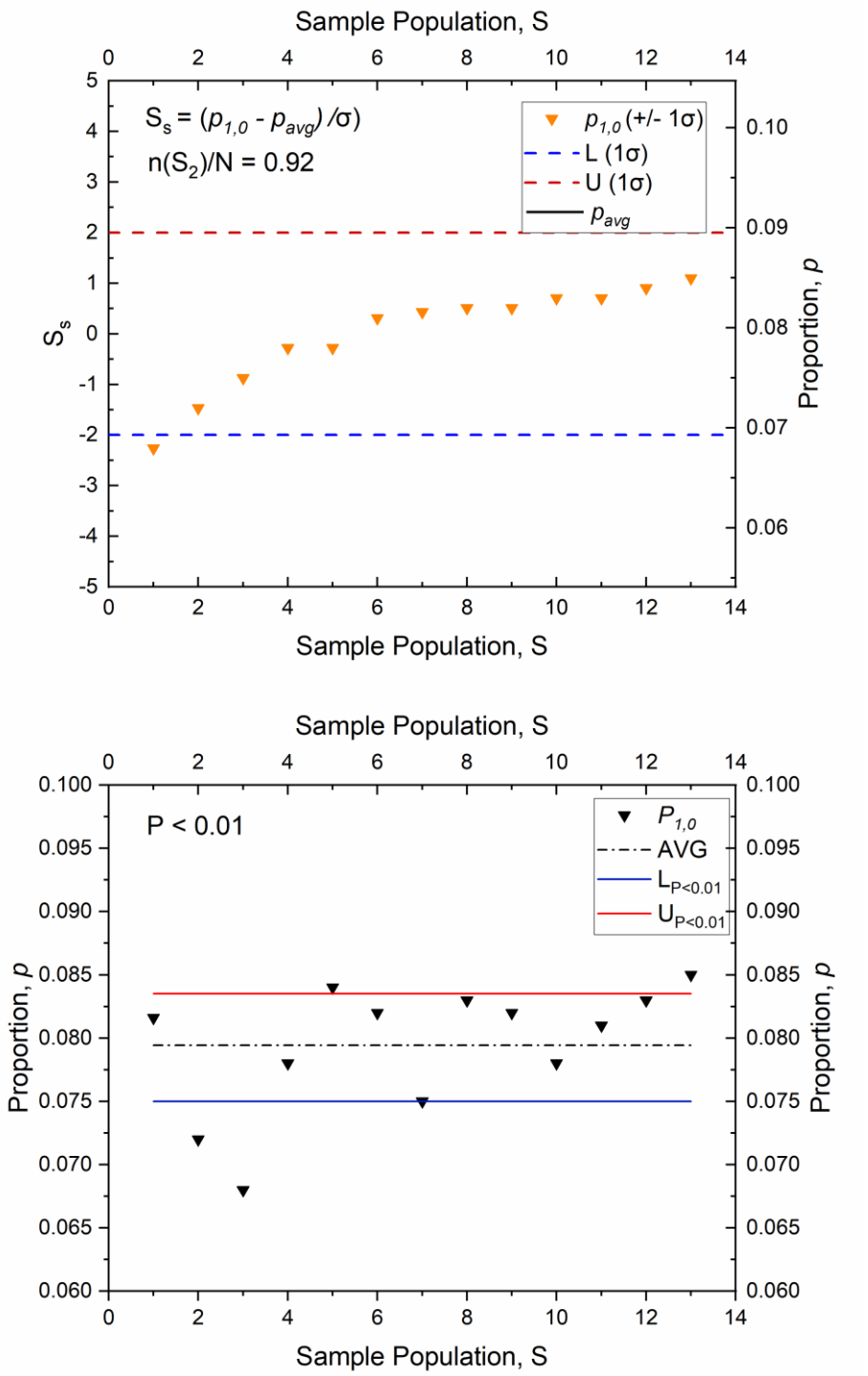

Figure 4- 11 (a) Normal Distribution Verification, (b) Proportion in respect to set #1

4.3. Foam and Ambient Temperature Variation

4.3.1 Introduction

It is imperative that the quantity of heat generated at the slab base is conserved to minimize the energy needed for de-icing. Closed cell spray foam as opposed to open cell, is a more densely packed synthetic material with very high R values to ensure increased efficiency (ECOMECH, 2019). The structural lattice of the spray foam material helps inhibit the mobility of vibrational energy and hence, greatly restricts the flow of heat. Therefore, thermal energy can be retained and stored at the base of the slab to maximize the thermal reserves for de-icing. The following study is conducted to prove the usefulness of closed cell foam at the base of the slab to minimize heat loss.

4.3.2. Experimental Set-up

To measure the vertical profile of the spray foam, thermocouples were secured to a plastic rod at 1-inch increments and inserted within the foam to ensure the tip was positioned at the interface between concrete base and foam. The rod was positioned to be aligned directly below set #4. The ambient temperature profile was measured at 2-inch increments directly above set 4. Utilizing the temperature distributions within the foam and ambient air, the complete vertical temperature profile could be obtained. A schematic of the set-up for each case is shown in figure 4-12.

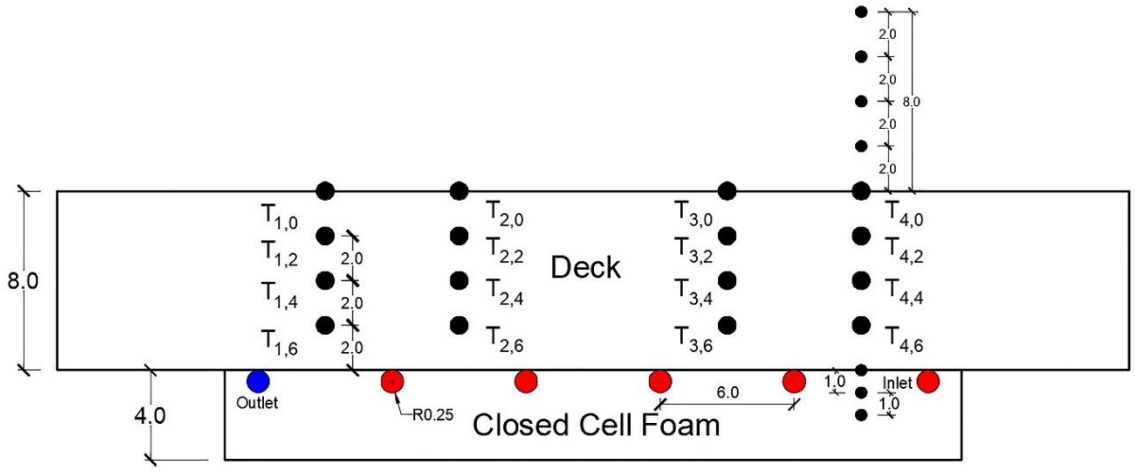

Figure 4- 12 Thermocouple set-up for complete temperature profile at set # 4

4.3.3. Complete Vertical Temperature Profile

Figure 4-13 (a) shows the temperature change at one-inch increments below slab base within the spray foam. Figure 4-13 (b) shows the relationship between the vertical changes in temperature in respect to depth, Z_i. The slab base corresponds to a depth of 6 inches below the surface Therefore, the foam and ambient measurements are taken at negative and positive depths respectively from the surface reference plane (Z = 0). The ambient profile was transposed using figure 4-13 (c). There exist a significant change in temperature within the foam relative to the slab, which is a consequence of the very low thermal conductivity of the foam. That is, the spray foam converges towards the ambient temperature (26 ° F) to a higher degree relative to the slab. One issue is that the thermocouples were secured on a plastic rod and inserted within the foam such that the tip touched the base, however, unnecessary tension can displace it from the interface zone. The tension developed may have exceeded thermocouples resistance to vertical movement, which would cause a slight offset. The rod was pulled out a few times to ensure minimal movement, if at all.

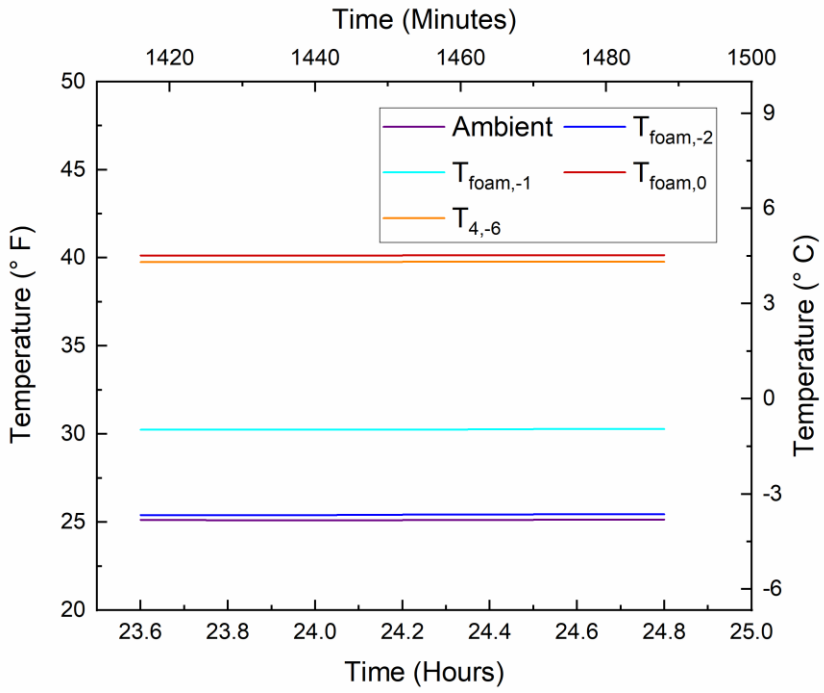

(a)

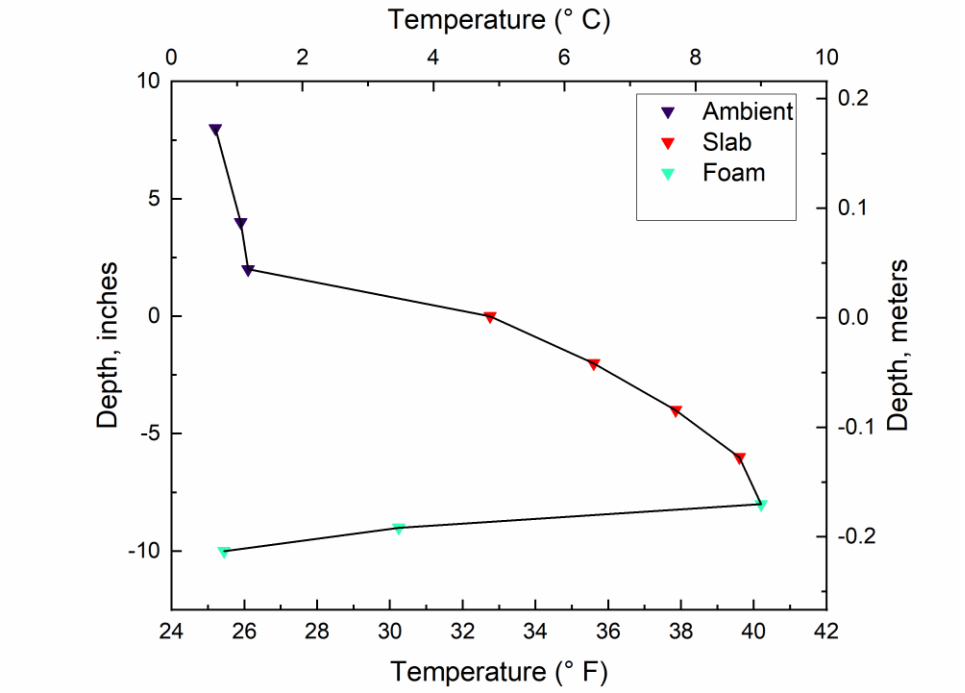
Temperature (° C)
0
2
4
6
8
10
Ambient
Slab
Foam
Depth, inches
Depth, meters
10
5
0
-5
-10
0.2
0.1
0.0
-0.1
-0.2
24
26
28
30
32
34
36
38
40
42
Temperature (° F)

(b)

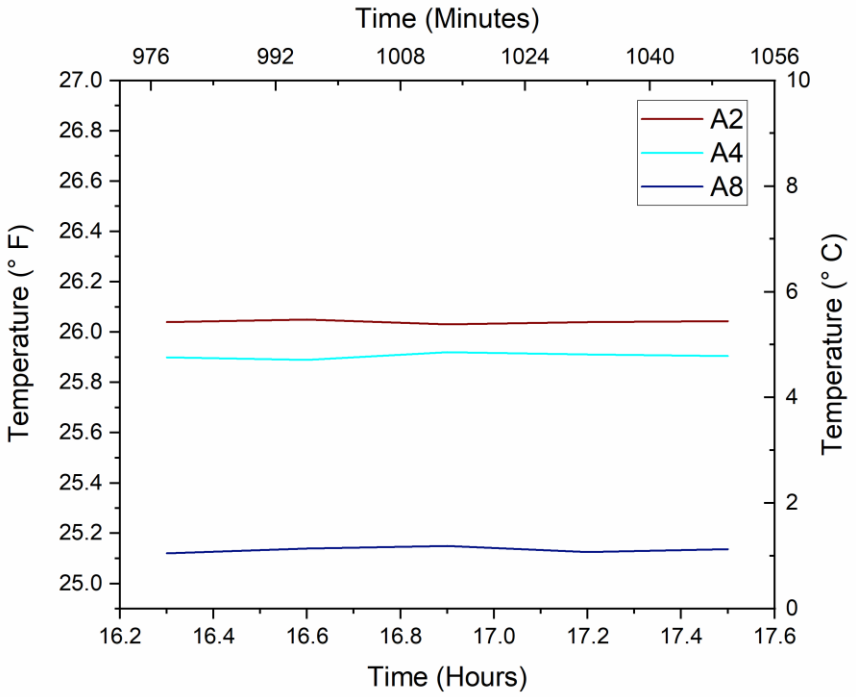
Time (Minutes)
976
992
1008
1024
1040
1056
A2
A4
A8
Temperature (° F)
Temperature (° C)
27.0
26.8
26.6
26.4
26.2
26.0
25.8
25.6
25.4
25.2
25.0
10
8
6
4
2
0
16.2
16.4
16.6
16.8
17.0
17.2
17.4
17.6
Time (Hours)

(c)

Figure 4- 13 (a) Temperature Distribution of Spray Foam, (b) Vertical Temperature Profile in Respect to set #4, (c) Ambient Temp. Response

4.4 Steady-State Analysis and Prediction

4.4.1 Introduction

It is of high importance to understand the steady-state relationship because for some Winter weather scenario, the transient state within the slab will exceed the final steady-state temperature for some ambient condition. Thus, the steady-state reading determines the least likelihood for de-icing. To obtain such a relationship and measure the overall efficiency of the system, the proportion is utilized in the analysis. The objective is to determine whether the proportion and alpha coefficient are consistent for each plane. Therefore, the mean and standard deviation is taken into consideration to provide validity when formulating a method to predict the steady-state temperature at different depths. Before proceeding to perform a hypothesis test, it must initially be verified that the dataset follows a normal distribution function. Otherwise, the null hypothesis cannot be rejected to an accurate degree. By applying a hypothesis test for the corresponding variables, the prediction can be confirmed for validity.

4.4.2. Alpha Coefficient Follows a Normally Distributed Function

Table 4-5 shows the calculated parameters associated with verification cases (1) and (2) in the methodology section (section 3.4.1). According to table 4-4, the alpha coefficient follows a normally distributed function for all depth intervals. Therefore, a hypothesis test can be conducted to determine the upper bound for α, and confidence intervals can be applied for the dataset.

Table 4- 5 Shapira Wilk method to verify normality of α for N < 50

Depth interval	SS	b	$W=b^2/SS$	$W_{p=0.05}$	p
1	0.00005	0.0069	0.965	0.866	0.784
2	0.000008	0.0027	0.937		0.561
3	0.000014	0.0036	0.957		0.664

4.4.3. Hypothesis Test

The following hypothesis tests are created to ensure the alpha coefficient used for the prediction is valid, and to determine the best-fit upper bound. Each test corresponds to depth interval, Z_i from table 3-3. Instead of taking a separate value for α per depth interval, the average will be taken at a level of significance of 0.01. According to table 4-6, the null hypothesis was rejected at the selected population mean (μ). The mean, standard deviation and corresponding p-value for each hypothesis case are included. Hypothesis 1 is defined at depth interval Z_1 and so forth. Therefore, it is very unlikely that the null hypothesis holds true, implying that an upper bound can reasonably selected as μ for each depth interval. To satisfy the relation in equation (11), the following upper bound estimate can be determined as follows.

$$\alpha_{upper} = \sum_{i=1}^{3} u_i + C = 0.721\ m^{-1} + C \geq \alpha_{max}$$

Where C is a constant added to ensure that α_{upper} is an upper limit for the entire sample population, S. Figure 4-14 shows the variation in α from table 4-1 (cases 1-13). Using $\alpha_{max} = 0.754\ m^{-1}$, it follows that $C \geq 0.033\ m^{-1}$ satisfies the relation. For convenience, α_{upper} is set to 76 m^{-1}.

Table 4- 6 Hypothesis Test results for Alpha Coefficient

Hypothesis test	$\bar{x}(m^{-1})$	σ	h_o	h_a	$t_{0.01}$	t	p < 0.01
1	0.910	0.002	$\mu_1 >= 0.976\ m^{-1}$	$\mu < 0.976\ m^{-1}$	-2.68	-3.08	0.0046
2	0.611	0.001	$\mu_2 >= 0.637\ m^{-1}$	$\mu < 0.637\ m^{-1}$		-2.97	0.0057
3	0.513	0.001	$\mu_3 >= 0.550\ m^{-1}$	$\mu < 0.550\ m^{-1}$		-3.18	0.0039

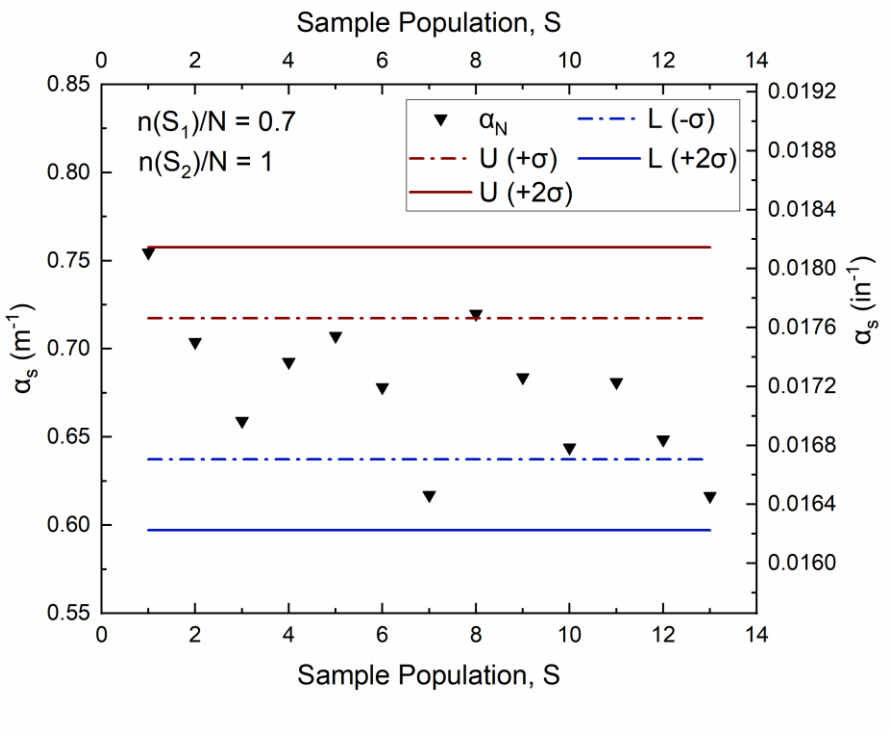

Figure 4- 14 Variation in respect to α (sub-tests 1-13)

According to table 4-7, approximately 70% of the measured results corresponding to the alpha coefficient is confined within 1 standard deviation from the mean whereas 100% is confined within 2 standard deviations. This correlates well with a normally distributed function being that 68% of a random sample should be fall between -1 σ and +1 σ relative to the mean. Thus, the sample population is not overly skewed.

Table 4- 7 Normal Distribution Spread for Alpha

Depth Interval	N	$n(S_n)/N$		Mean ($\bar{x}$)	S.D. (σ)
		+/- 1 σ	+/- 1 σ		
-6 < Z < 0	13	0.59	0.97	0.677 m^{-1}	0.00452

4.4.4. Steady-State Gridline

Figure 4-15 (a) shows the vertical profile of the average proportion in respect to cases 1-4 of test sequence 1. As shown, there is a near linear relationship per each depth interval. The alpha coefficient increases slightly along interval 1 ($Z \in [0, -2]$), most likely due to disturbance from ambient conditions, such as air void infiltration through the mortar paste securing the thermocouples at the surface. Another possible reason could be the depth at which the

thermocouples were installed at the surface exhibit more variation relative to depth intervals 2-3. This will introduce some error in respect to the measurements. Figure 4-15 (b) displays a steady-state gridline, which gives an accurate approximation of the steady-state temperature at any depth according to the constrained environmental conditions from each testing sequence. The results were compiled using table 4-1 and taking the average proportion corresponding to all sub-tests (1-13).

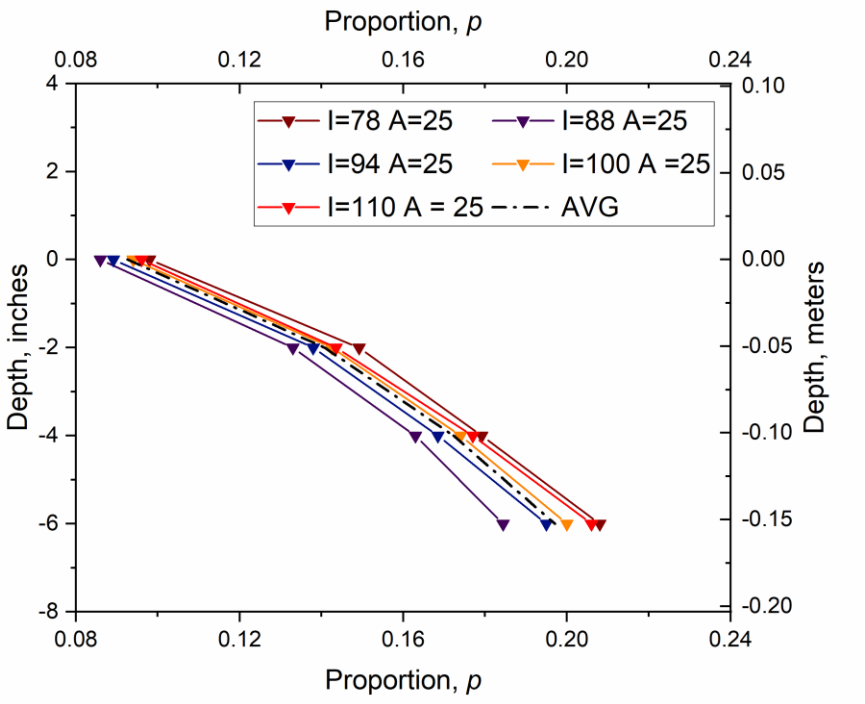

(a)

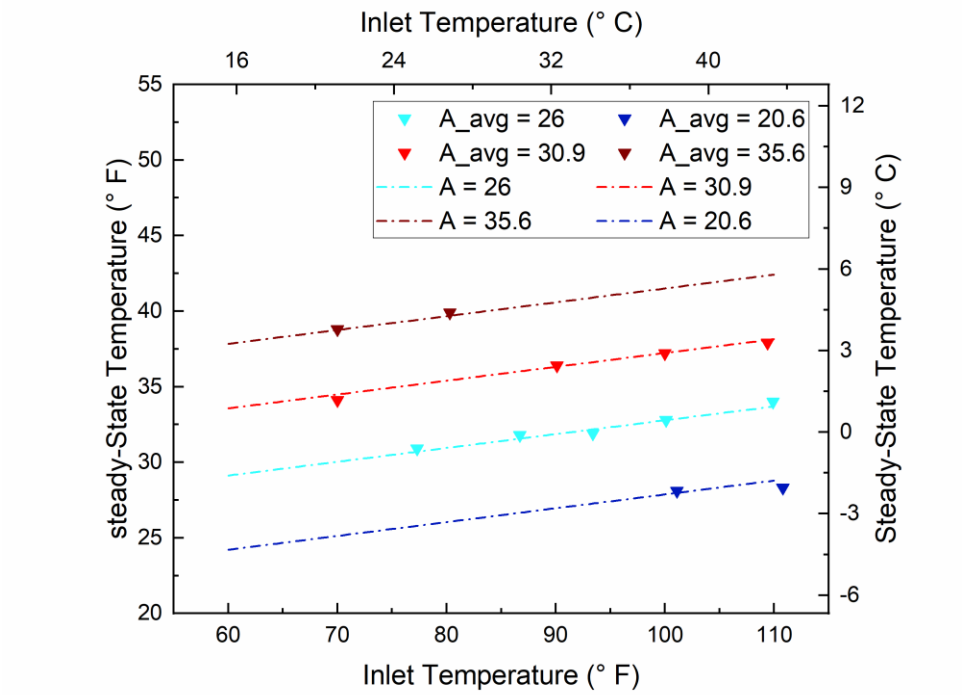

(b)

Figure 4- 15 (a) Vertical Profile in respect to the average proportion, p_{avg}, (b) Steady-state gridline in respect to sets 1-5

4.4.5. Proportion and Alpha Coefficient as a Function of Depth

Figure 4-16 (a) shows the average proportion for sets 1-5. The proportion ranges from 0.086 (surface) to 0.208 (Depth = 6″). Based on the trends, the change in proportion is relatively constant up to a depth of 2 ″ from the surface, then gradually increases. The average standard deviation in respect to the proportion for each layer is 0.005, which is insignificant. Figure 4-16 (b) shows the variance of the proportion for each plane. There is a marginal increase in variance at the base of the slab relative to the surface, perhaps due to the boundary effect near the base. Figure 4-17 (a) displays the alpha coefficient per depth interval using a 99% confidence range. The upper bound yielded from the hypothesis test is included along with the p-value. Figure 4-17 (b) exemplifies that the variance increases toward the surface of the slab, however, the divergence is marginal. By using the upper bound via the hypothesis test, a lower bound can be attained in respect to the average steady-state temperature. Thus, the likelihood the steady-state temperature will fall within the range constrained by the bounds is very high.

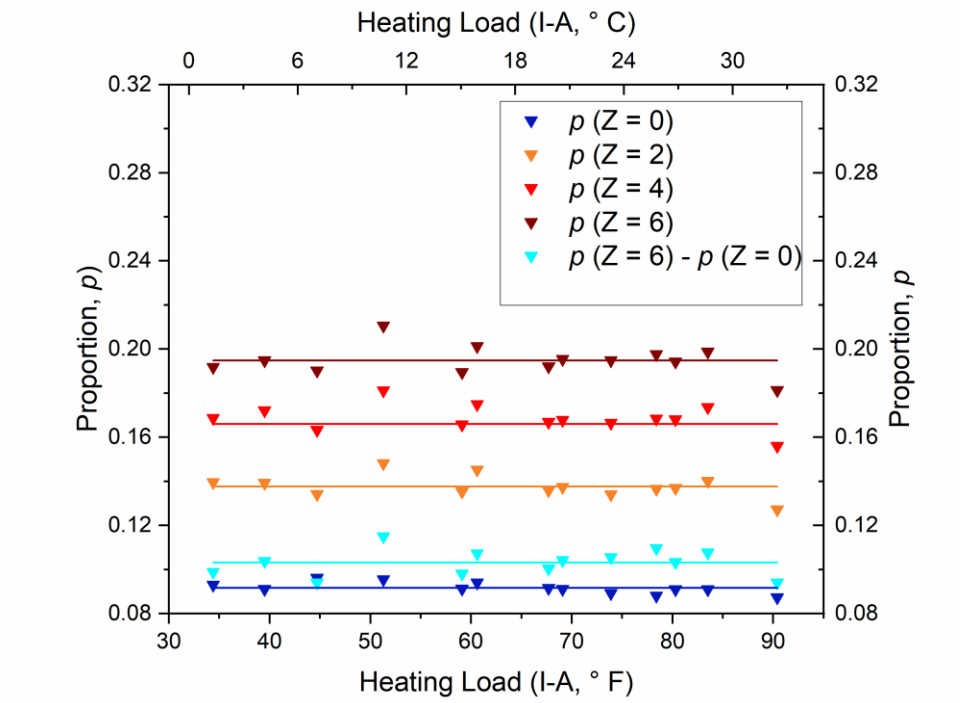

(a)

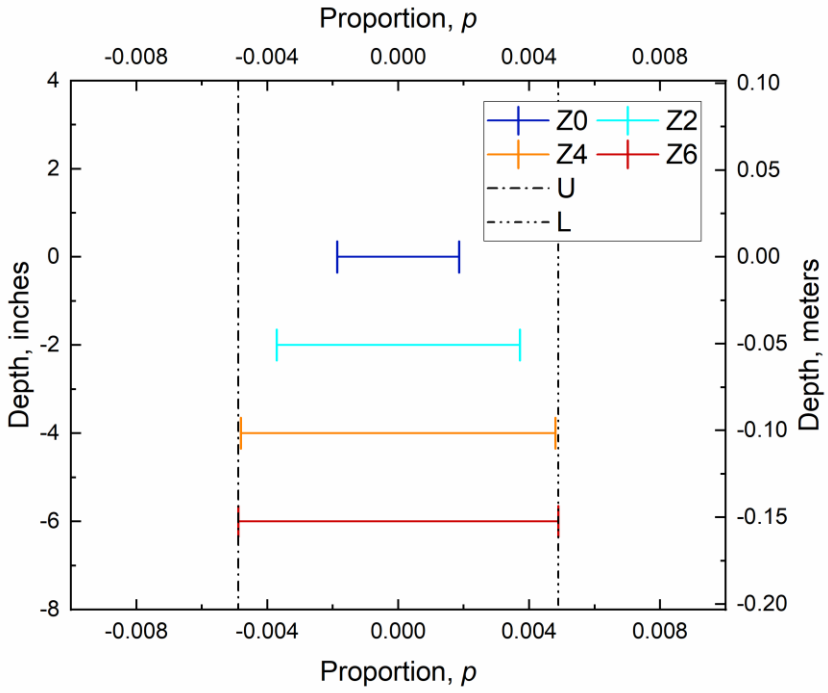

(b)

Figure 4- 16 (a) Proportion, p, as a function of Heating Load (I-A), (b) Confidence Intervals as a Function of Depth

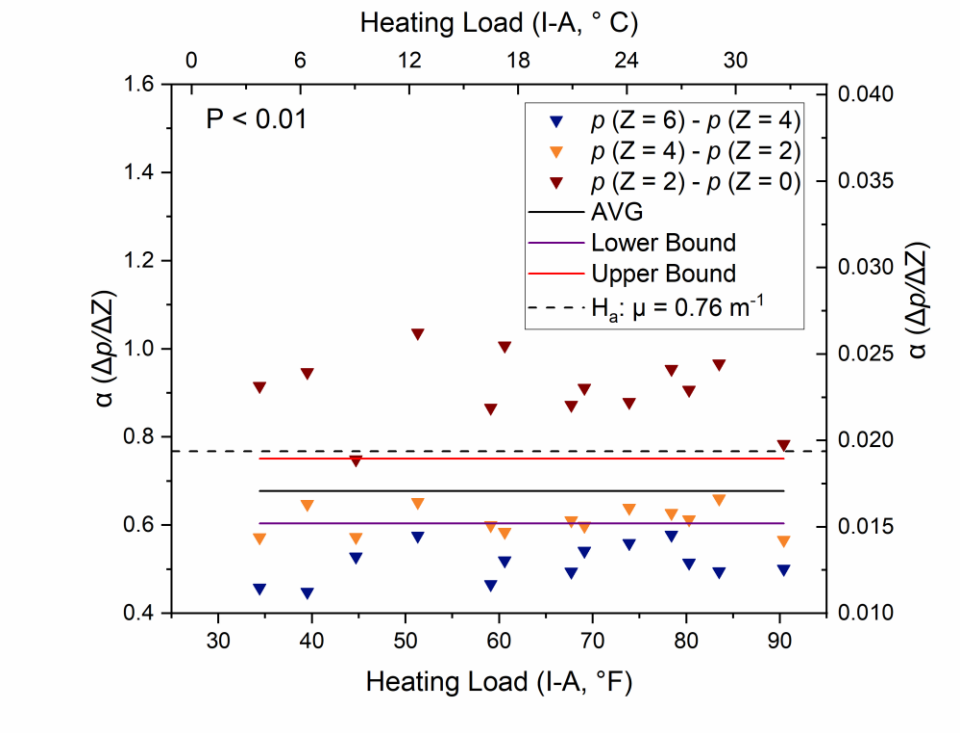
Heating Load (I-A, ° C)
0
6
12
18
24
30
P < 0.01
p (Z = 6) - p (Z = 4)
p (Z = 4) - p (Z = 2)
p (Z = 2) - p (Z = 0)
AVG
Lower Bound
Upper Bound
Ha: μ = 0.76 m-1
α (Δp/ΔZ)
α (Δp/ΔZ)
1.6
1.4
1.2
1.0
0.8
0.6
0.4
0.040
0.035
0.030
0.025
0.020
0.015
0.010
30
40
50
60
70
80
90
Heating Load (I-A, °F)

(a)

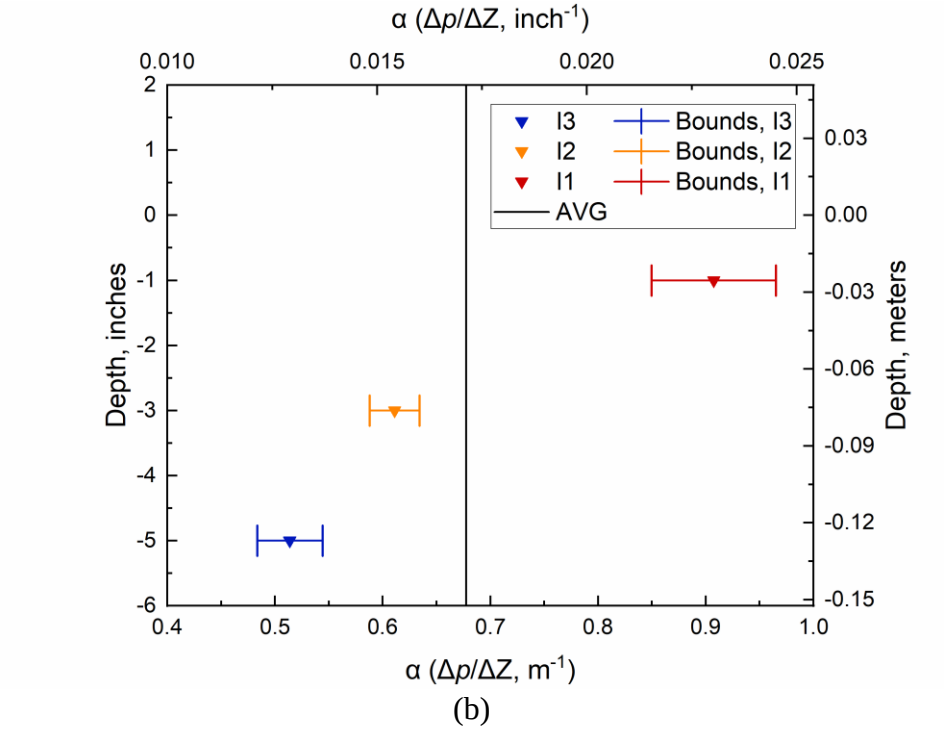

(b)

Figure 4- 17 (a) Alpha Coefficient, α (Δp/ Δz) as a Function of Heating Load, (b) Confidence Intervals as a function of Depth

4.4.6. Development of Thermal Demand Estimate

Figure 4-18 (a) displays the upper and lower bound trend-lines using a 99% confidence interval, in respect to steady-state temperature as a function of depth. The measured data compiled from table 4-1 is confined within the bounds, which is the possible range of variance relative to the mean proportion. The minimum steady-state temperature denoted as T_{min} is also within the bounds, which implies the likelihood of de-icing is high. T_{min} was attained using the minimum proportion at set 4, P_{min}. If the entire slab is ensured to be ice free, the minimum proportion must be considered. The upper bound alpha coefficient, α' is a close approximation of the upper confidence bound, which is expected at a level of significance of 0.01. At the surface level of the slab, T_{min} passes the freezing boundary for A <= 25 F, implying that the heat demand would exceed 100° F. According to figure 4-18 (b), the minimum and maximum change in proportion from the slab base to surface level falls between the upper and lower confidence bounds. Thus, the spread between all cases is confined within a marginal limit, which is required to accurately predict the thermal demands of the system. The alpha coefficient corresponding to the testing

hypothesis exceeds all testing cases, which is exemplified in figure 4-18 (c). Ideally, an upper bound estimate is needed to ensure that de-icing is permissible under all scenarios

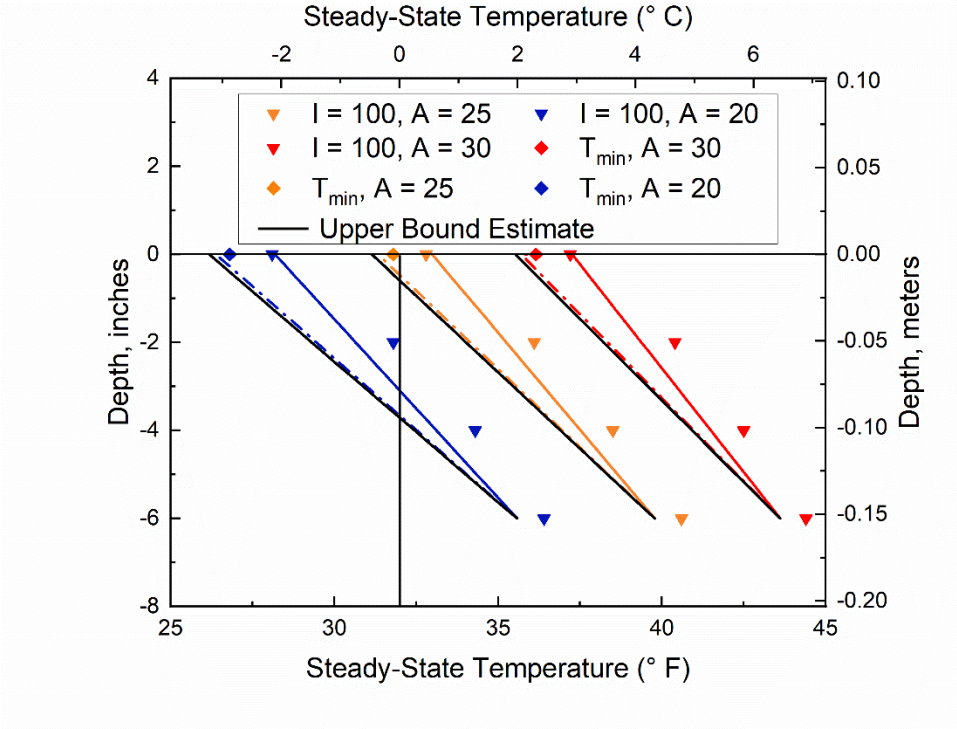

(a)

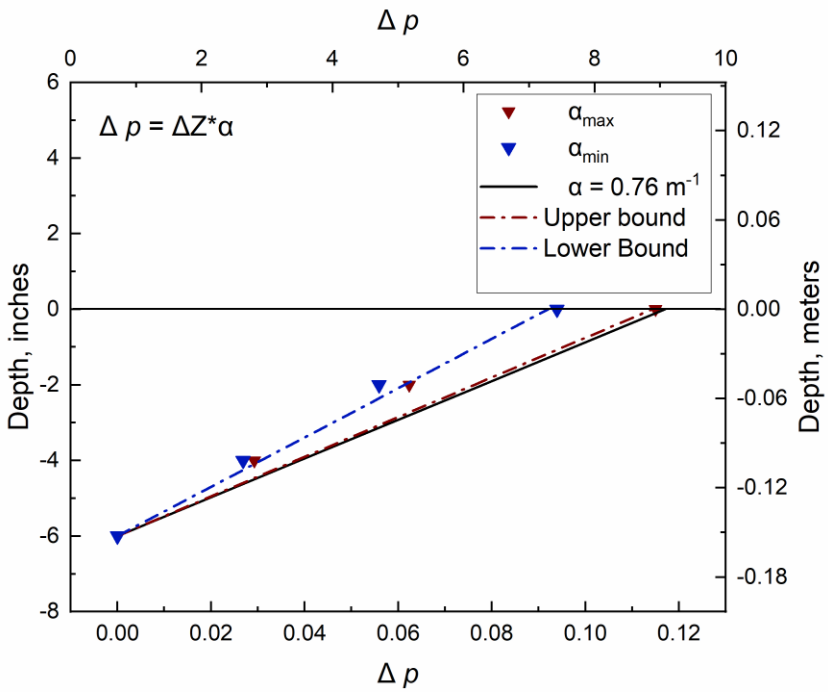

(b)

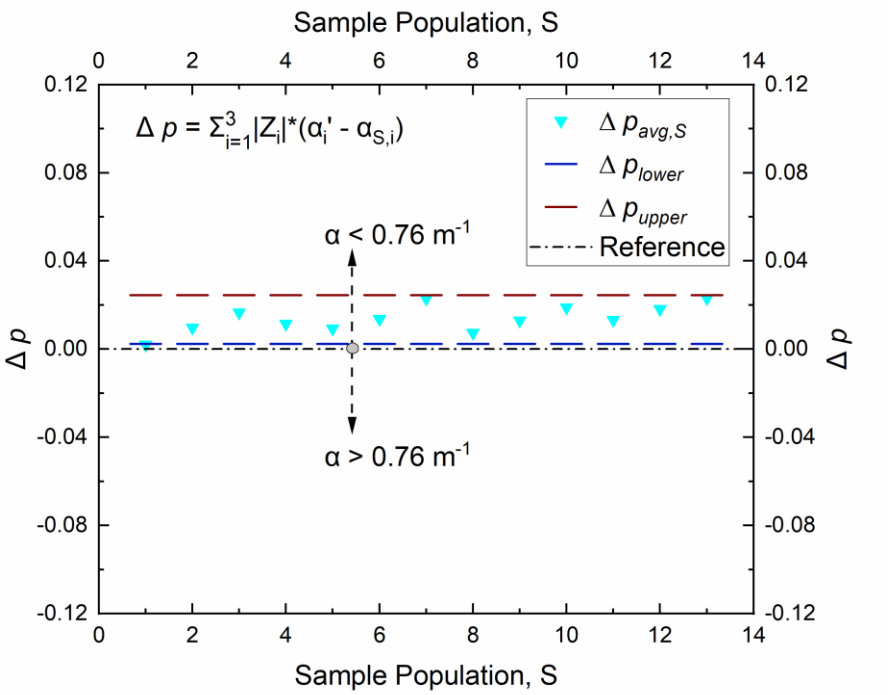

(c)

Figure 4- 18 (a) Probable Zones for Steady-state temperature at Differing Environmental Condition, (b) Δp as a function of depth, (c) Variance in Δp from the predicted value

4.4.7. Upper Bound Estimate of Thermal Demand

Figure 4-19 (a) shows the required inlet temperature to satisfy de-icing using equation (9), (12), and (13) respectively. The local estimate, I_{max} is equated using lower bound estimate for set 1 whereas the global estimate, I' takes into consideration the average proportion across sets 1-4. By taking the average proportion for set 1, I_{avg} was determined. The results indicate that the thermal demand is significantly sensitive to changes in respect to the proportion. The design threshold set at 34 ° F (ΔT_{design} = 9) was sufficient at countering the heating demands for a snowfall rate of s = 1 mm/hr, assuming A_r = 0, w = 0 mph, and A_o = 25 ° F. Figure 4-19 (b) shows that the required thermal demands are highly sensitive to an incremental change in the proportion, so it's imperative to idealize the system to minimize the input requirements. That is, refine the system such that the proportion of heat transfer tends closer to 1, which will exponentially minimize the thermal demand.

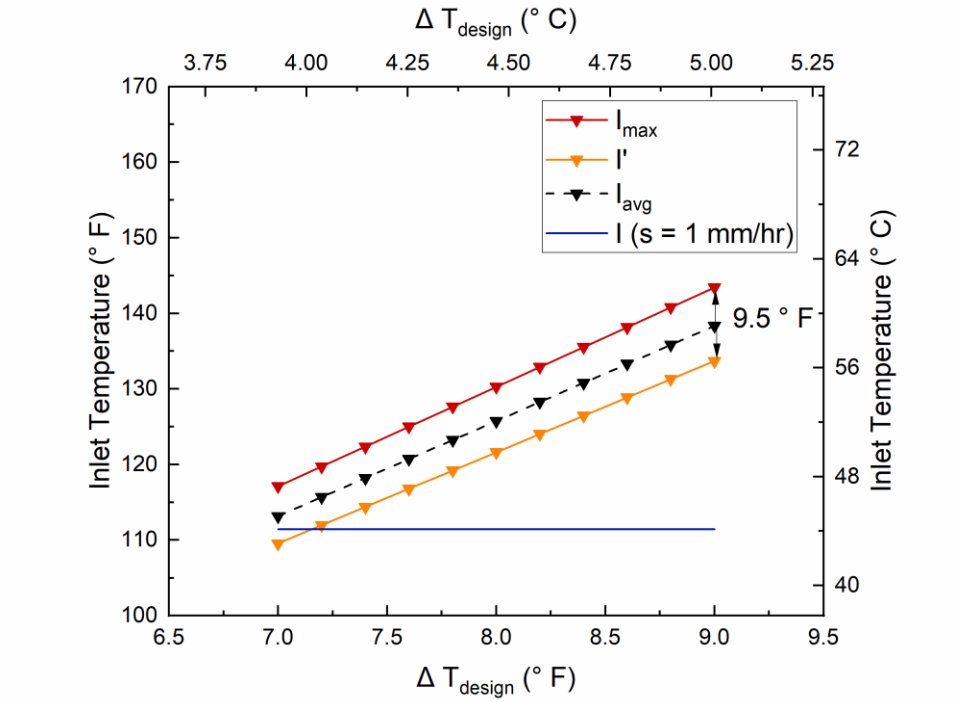

(a)

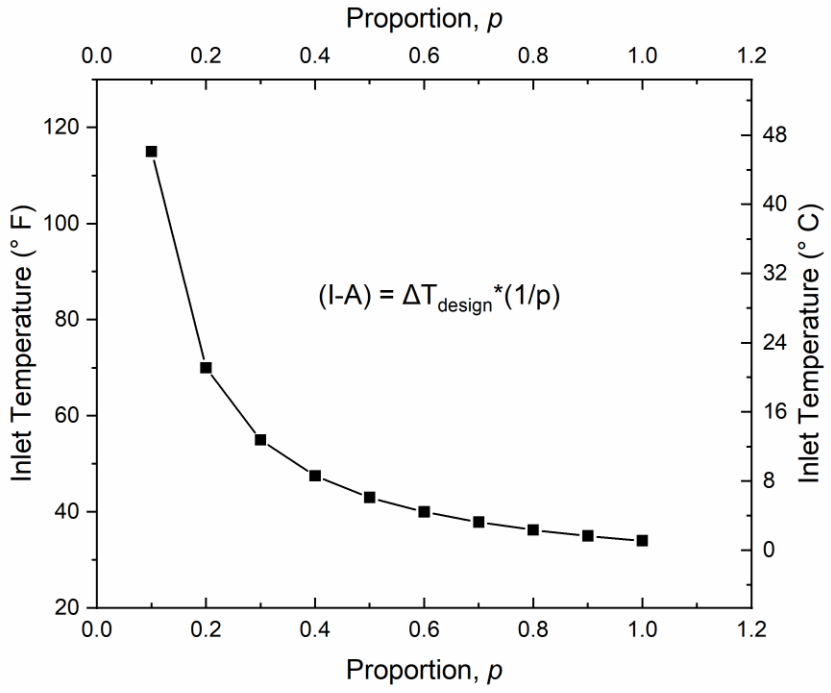

(b)

Figure 4- 19 (a) Required inlet temperature to permit de-icing (A = 25, w = 0), (b) Required inlet temperature as a function of proportion (A_o = 25, Δ A = 9)

4.5. Heat Transfer Study

4.5.1. Introduction

The following study was conducted to approximate the heat flux through the slab based on the thermal energy transferred throughout the pipe network. Heat flux is proportional to the vibrational energy of atoms throughout an area. There are three factors involved in heat transfer, which include conduction, convection, and radiation. For this study, heat transfer is limited to convection via fluid flow and conduction via metallic bonds. A total of 5 sub-tests were run such that the ambient temperature was held constant at 25 ° F and the water temperature was altered in 4 ° F increments. Each test had a duration of 24 hours or greater to ensure equilibrium conditions were satisfied. Two thermocouples were inserted within the inlet and outlet section of the pipe network and sealed accordingly. Table 4-8 shows the variables attained from the conduction of each sub-test.

4.5.2. Heat Flux Analysis

Using equation (9) from the methodology section, the following relation can be attained to predict the required heat flux at the surface of the slab:

$$q_{(slab)} = 1.22*(I-A) \quad \text{.....(15)}$$

where the thermal conductivity, K, was assumed to be approximately 1.8 W/m^2K based on previous measurements from a different slab of similar thickness using a KD-2 pro thermal property analyzer, and $\alpha_{avg} = 0.677\ m^{-1}$.

Table 4-8 shows the difference in temperature between the inlet and outlet sections of the pipe, which spans a total of 6.14 feet. There is a near linear change in temperature among each sub-test. Figure 4-20 (a) displays the temperature differential over the entire pipe span. The best fit line is projected toward the origin to emphasize consistency in respect to the heat load and temperature difference (I-O). That is, a zero-heat load implies that no heat will be transferred throughout the slab (i.e: (I-O) = 0). Figure 4-20 (b) shows the heat flux transferred to the slab via the pipe network using equation (2) whereas figure 4-20 (c) shows the heat flux within the slab

using equation (9) in respect to sets 1-3 for test sequence 1 (cases 1-5). There is a steady increase in the amount of heat transferred from sets 1 to 3, which is consistent with the orientation of the sets relative to the inlet and outlet sections. That is, more heat is transferred closer to the inlet end of the slab. Lastly, figure 4-21 shows the predicted and upper bound estimate for surface heat flux in respect to all test cases using equations (9) and (13) respectively. There is a marginal deviation between the actual and predicted results, which is exemplified via an R^2 value close to 1 (0.956). The upper bound estimate corresponds to the thermal input (energy demand) necessary to attain an equivalent match with the actual results. That is, the heat flux demands will increase as a function of the change in inclination angle required to achieve static equivalence.

Table 4- 8 Pipe Network Thermal Differential

Test #	$T_{ambient}$ (° F)	T_{inlet} (° F)	T_{outlet} (° F)	$T_{inlet} - T_{outlet}$ (° F)
1	25	72.4	70.8	1.6
2		76.6	74.8	1.8
3		80.7	78.8	1.9
4		84.5	82.4	2.1
5		88.4	86.1	2.3

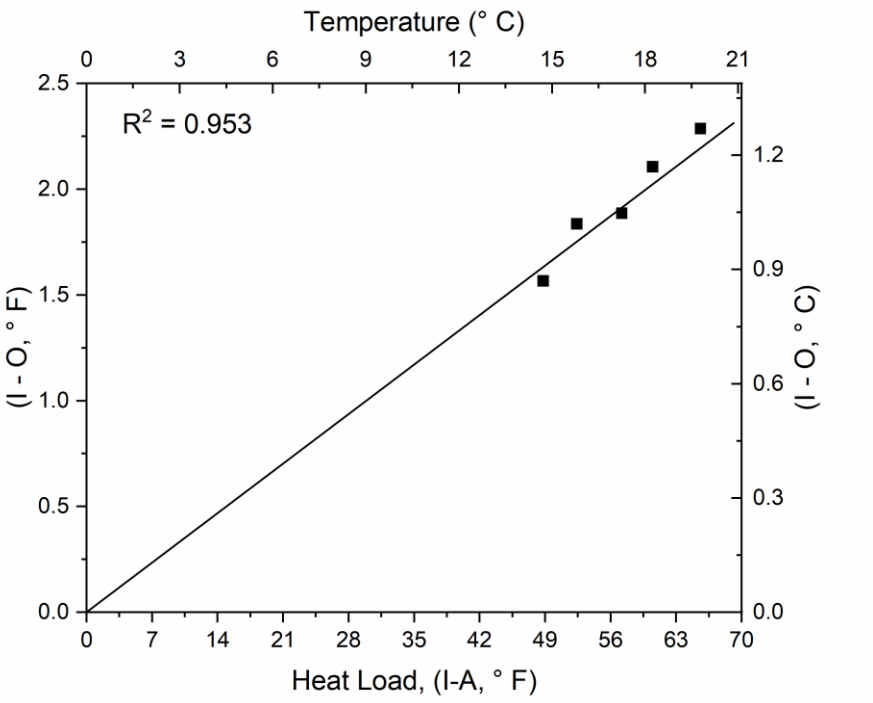

(a)

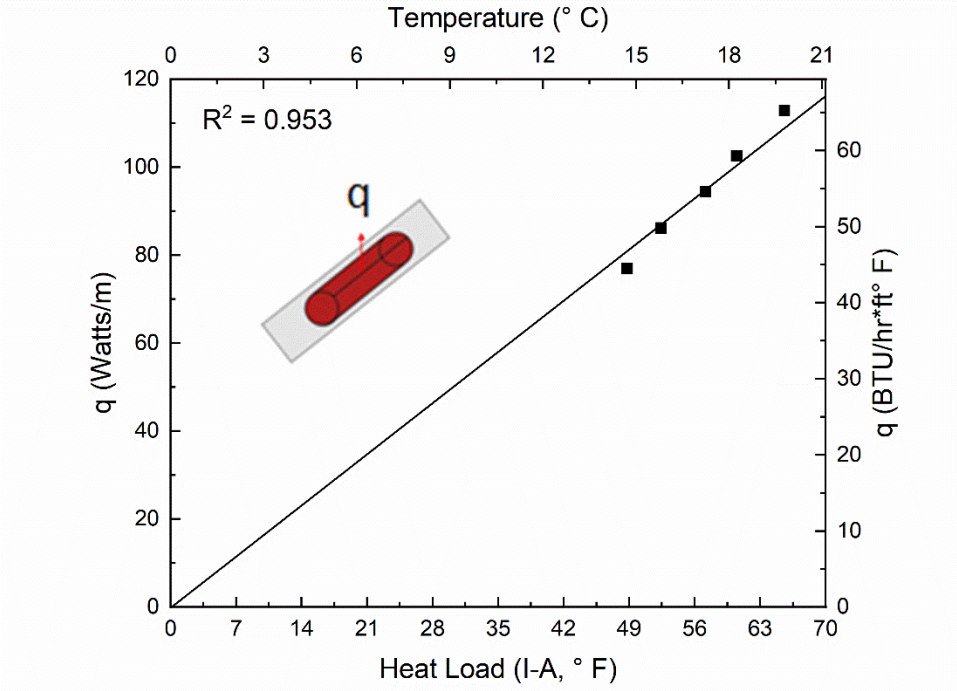

(b)

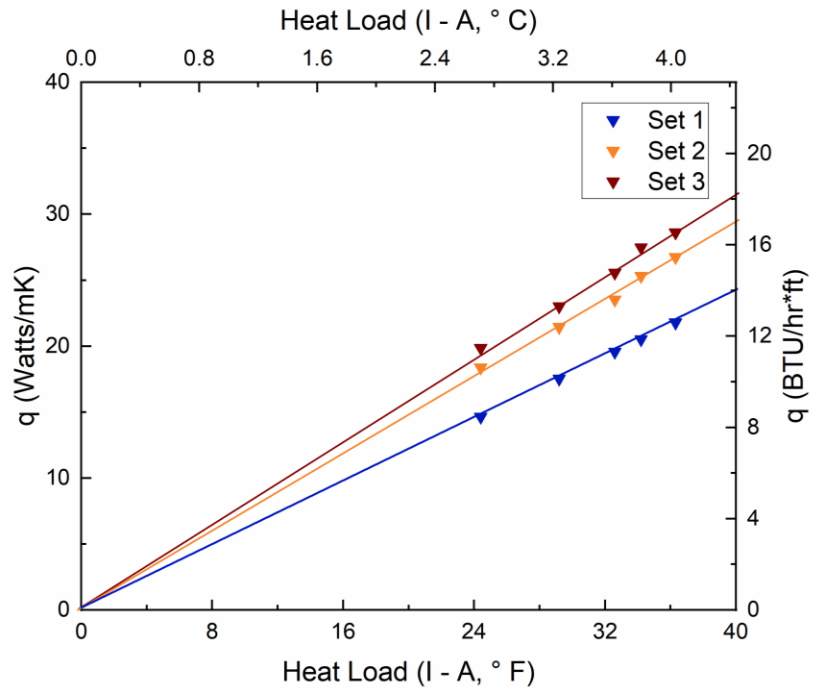

(c)

Figure 4- 20 (a) Temp. Difference between Inlet and Outlet Sections, (b) Heat Energy Transferred to Slab via Pipes, (c) Heat Energy Transferred to Slab Surface ($S_{1,1} - S_{1,5}$)

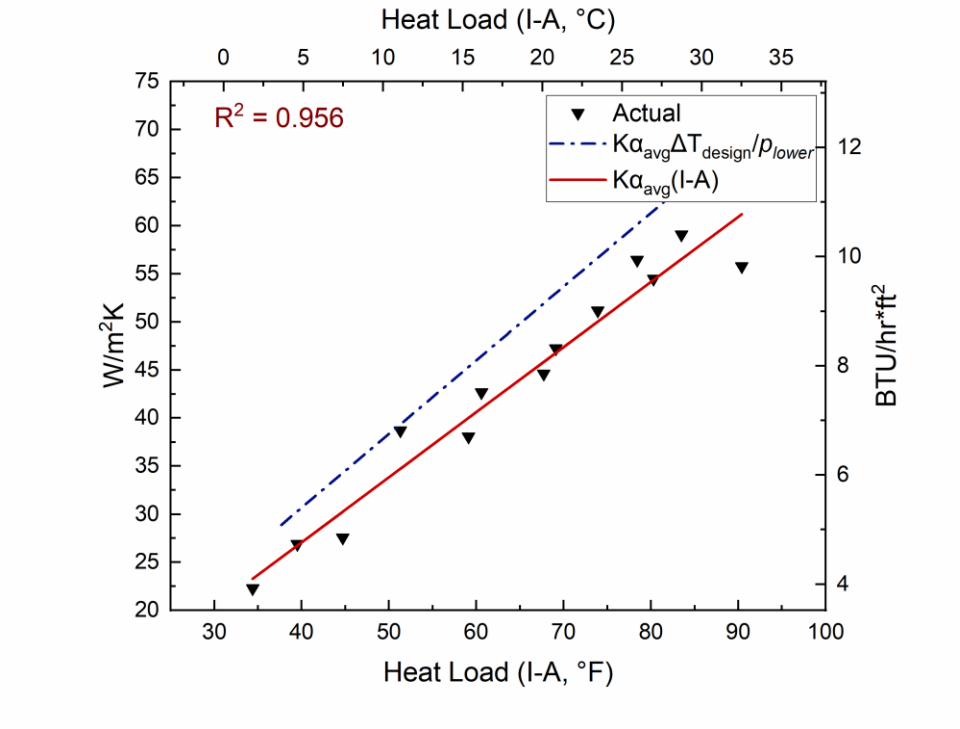

Figure 4- 21 Heat Flux at Surface; Prediction Versus Actual

4.6. Thermal Dissipation due to Sustained Wind

4.6.1. Introduction

The possibility that a de-icing system will function properly to melt snow/ice along bridge overpasses is heavily dictated by the wind conditions. Wind readily displaces the thermal gradient that exists above a heated surface due to convection, which causes an increase in heat transfer away from the surface via the 2nd law of thermodynamics. The issue arising regarding wind, is that there is no exact function to define transient wind conditions. That is, wind is a scattered function that exists between an upper and lower bound for some daily cycle and hence, a thermal rebound effect will be initiated. The following section shows the deleterious effects of sustained wind conditions on the heating performance of the system as well as a thermal rebound study using alternating wind cycles. Let T_o be denoted as the initial steady-state temperature at the surface of the slab. Figure 4-22 shows the translation of the initial thermal energy (T_o) as a function of wind magnitude. So long the wind is sustained, there will be a minimum depth at

which the initial energy is translated. If wind conditions change, the displacement depth will adjust accordingly. Figure 4-23 displays the fan orientation for the testing process.

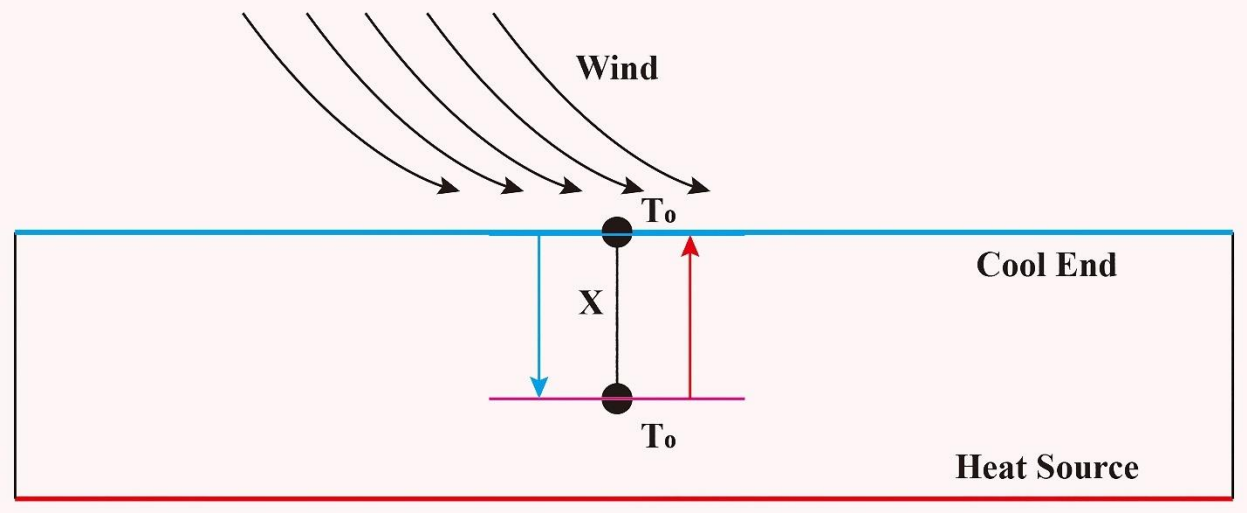

Figure 4- 22 Translation of Thermal Energy due to Sustained Wind Conditions

Figure 4- 23 Fan set-up

4.6.2. Experimental Test Conditions, Set-up and Procedure

A low powered fan was projected at set #3 at a 45-degree angle to induce the convective process. Four sub-tests were conducted at varying wind magnitudes for two test-sequences defined according to inlet temperature. The ambient conditions were set 25 ° F for the duration of each sequence. The inlet temperatures were set at 70 ° F and 80 ° F respectfully. A string of

thermocouples was positioned above set #3 at 1-inch increments to measure the ambient profile due to varying wind conditions. Table 4-10 shows the test results based on the template provided from table 4-9 where index, i = 1,2. The ambient profile above the slab was excluded for sequence 1 due to fluctuation caused by a higher temperature differential between the freezer box interior and exterior (outdoors).

Table 4- 9 Testing Template

Test Sequence	Sub-test	Fan Mode	Wind Speed (mph)
i	1	V. low	0.8
	2	Low	3
	3	Medium	4.8
	4	High	6.2

Table 4- 10 Tabulated Results for Sustained Wind Test

w (mph)	A_{min} (° F)	I (° F)	To (° F)	T_f (° F)	P_o	P_f	$T_{ambient}$ (° F)			
							Z2	Z3	Z4	Z5
0.8	25.09	67.7	29.1	27.9	0.094	0.066				
3	25.42	67.17	29.3	27.6		0.052				
4.8	25.39	67.42	29.3	27.2		0.044				
6.2	24.84	67.5	28.9	26.6		0.040				
0.8	26.31	79.86	31.3	29.8		0.064	27.66	27.10	27.07	27.02
3	24.88	78.72	29.9	27.6		0.050	25.72	25.44	25.40	25.37
4.8	24.67	79.12	29.8	26.9		0.041	25.34	25.14	25.12	25.07
6.2	24.75	79.32	29.9	26.8		0.037	25.24	25.08	25.06	25.02

4.6.2. Steady-State Response

Figure 4-24 (a) shows the thermal response corresponding to the following environmental conditions: A = 25° F, I = 80 ° F, and w = 4.8 mph. There is a large reduction in temperature directly above the slab, due to the displacement of heat. Figure 4-24 (b) shows the proportion as a function of wind speed from the compilation of each test case. There is a strong linear relation for the tested wind range (0 < W (mph) < 6), however, convergence would eventually be eminent for very high speeds. This effect is exemplified in figure 4-25 (a) and (b), wherein the ambient temperature above the slab rapidly converges to the thermal minimum within the freezer box denoted as A_{min}. Thus, there exists a limit regarding the amount of heat that could be displaced above the slab surface. To obtain the proportion above the slab, the minimum ambient temperature was utilized, which was positioned at a depth of 2' above the surface.

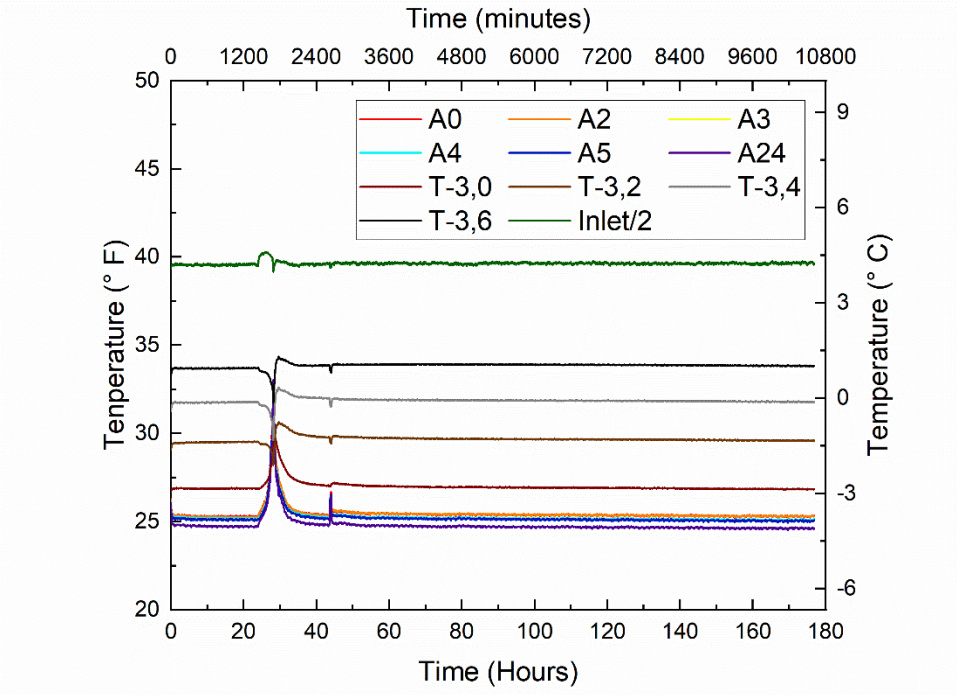

(a)

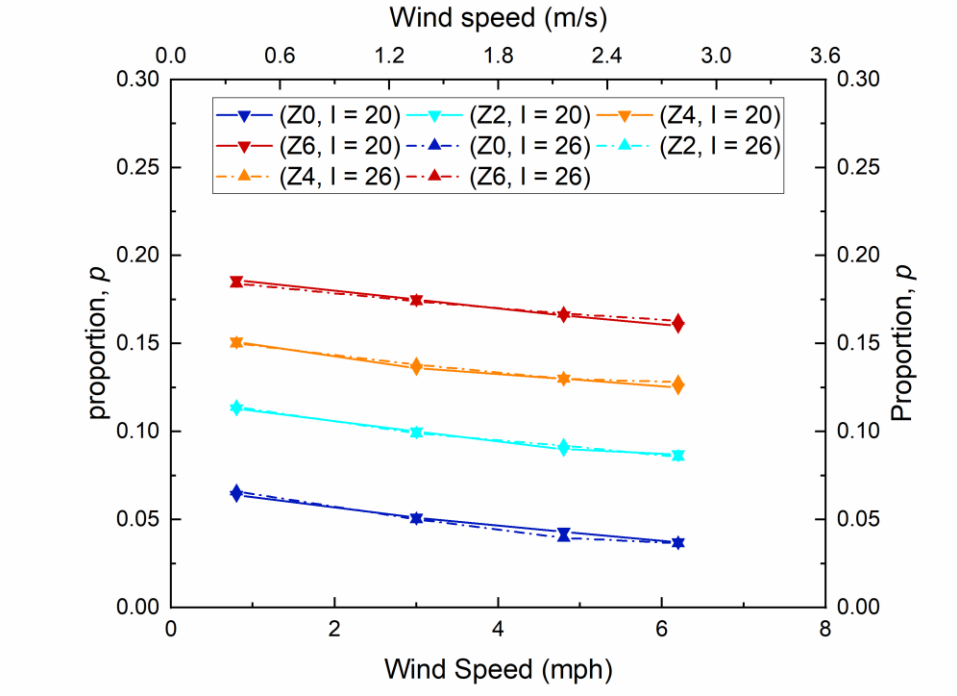

(b)

Figure 4- 24 (a) Thermal Response to Sustained Winds at 4.8 mph, (b) Proportion, p, as a function of wind

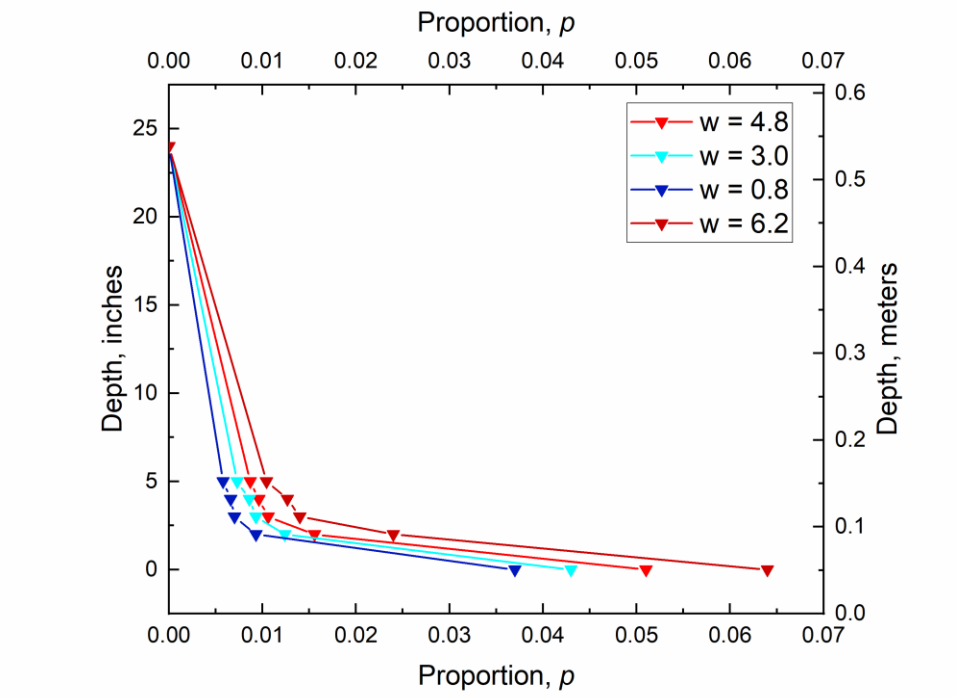

(a)

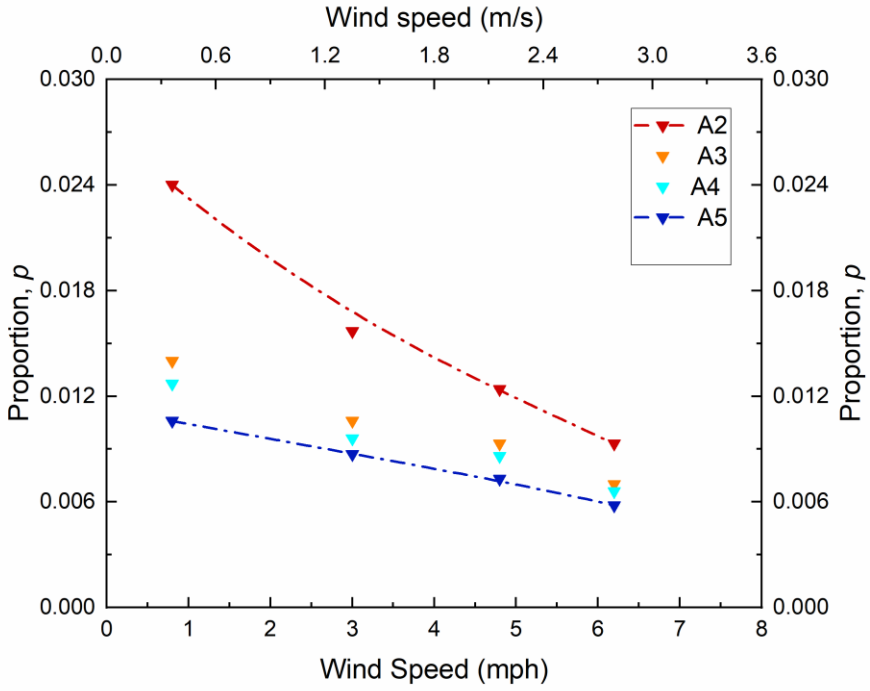

(b)

Figure 4- 25 (a) Vertical profile of Proportion above Slab Surface, (b) Proportion above Slab Surface as a Function of Wind Speed

4.6.3. Proportion as a Function of Wind

To estimate the thermal demands for sustained wind conditions, equation (16) was utilized to solve the exponential factor, λ. By inputting the known variables, the exponential factor was determined to follow a powered function with marginal error, as shown in figure 4-26 (a). Equation (6) can then be used to solve the estimated inlet temperature such that $T_{j,k} > 32$ ° F, which is exemplified in figure 4-26 (b). There is a large degree of divergence for low wind magnitudes, however, the negative effect will taper as wind progressively increases. This is because the proportion will eventually converge within a limit, and there will exists a marginal decrease once the wind reaches an upper threshold. The results show that wind significantly compromises the performance of the system under sustained conditions. Therefore, careful consideration must be taken to ensure the thermal demands account for the negative influence of wind.

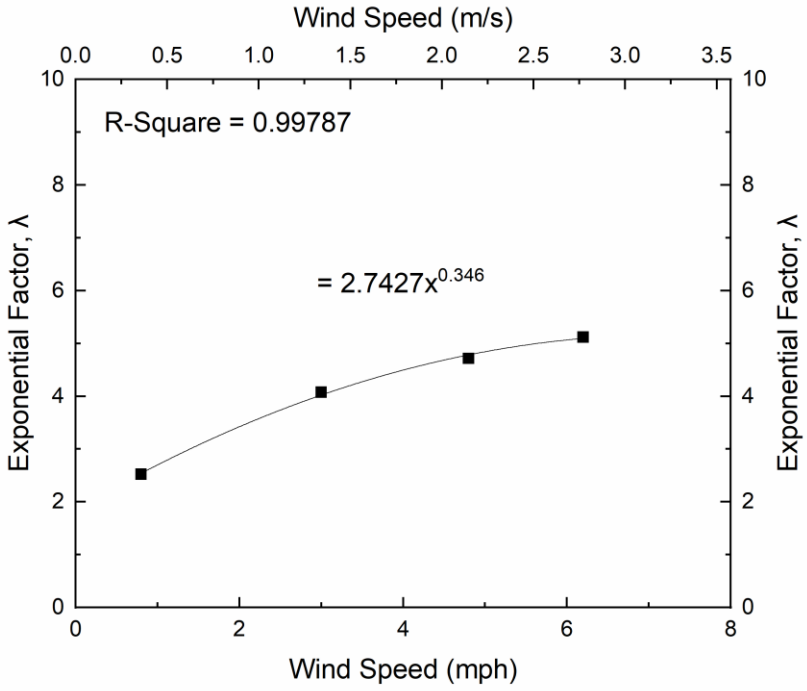

(a)

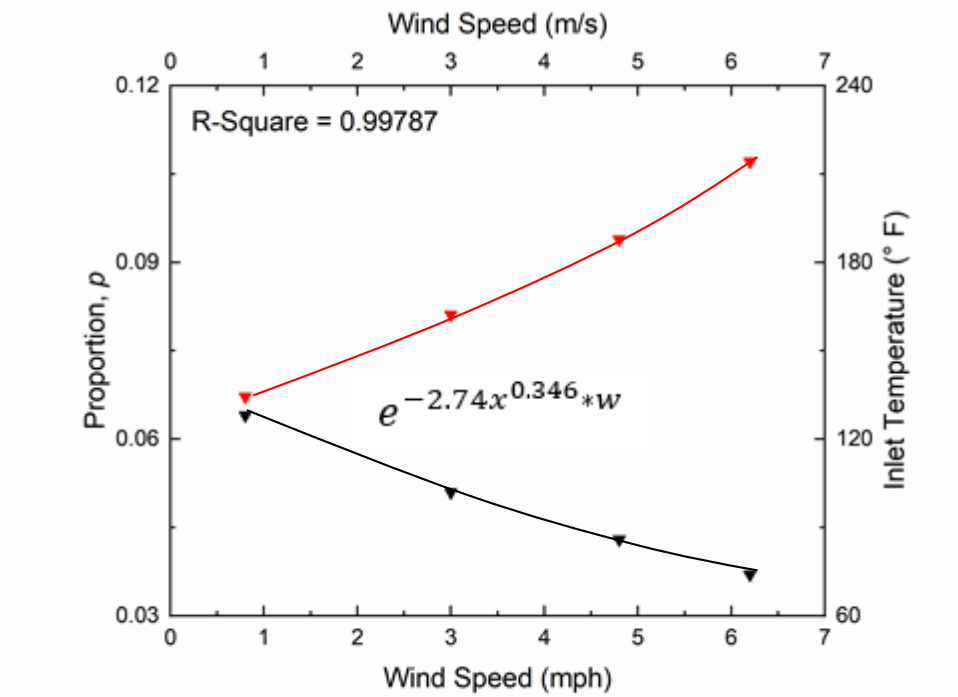

(b)

Figure 4- 26 (a) Exponential factor as a function of wind, (b) Proportion as a function of wind

4.6.4. Vertical Translation of Thermal Energy

Figure 4-27 (a) shows the vertical profile of the proportion for each case. There is a rather significant reduction in the heating efficiency of the system for very low wind magnitudes (w_{min} = 0.8 mph). In fact, there is a 3 ° reduction in the inclination angle Φ, as the wind magnitude increased from 0 to 6 mph. By taking the average slope of the four cases and projecting the trendline at the origin, the minimum depth at which the initial steady-state temperature (T_o) is translated was estimated at 4.7 inches. The relation between the minimum depth of thermal translation as a function of wind magnitude is exemplified further in figure 4-27 (b). This indicates that the time to recover initial conditions will be less than the time to attain it. Therefore, a possible relationship can be made in terms of time lag as a function of wind magnitude where time lag represents the time to satisfy a full recovery of thermal energy.

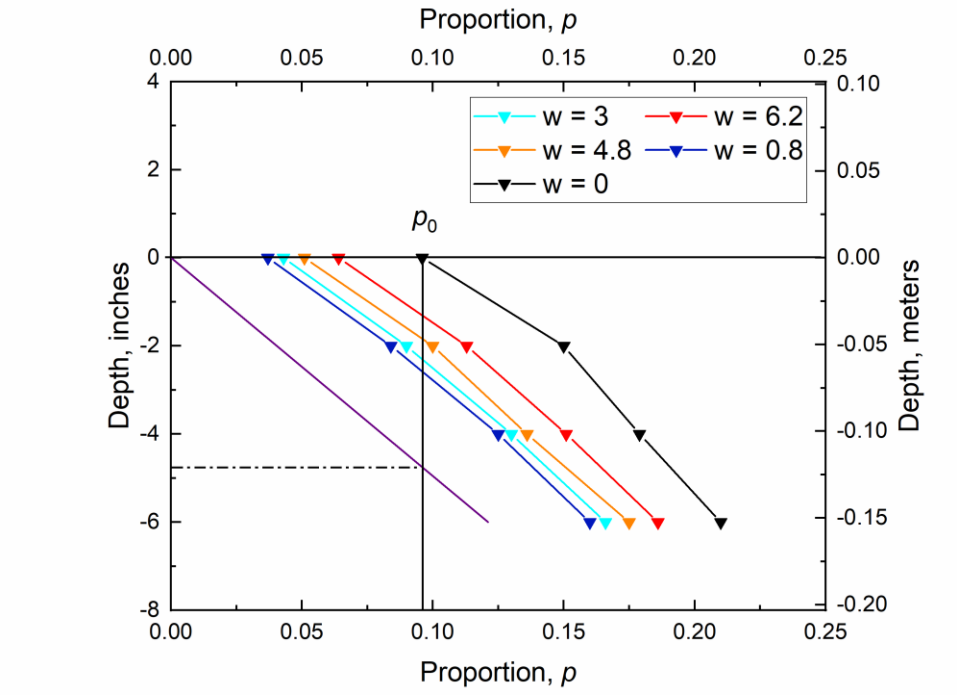

(a)

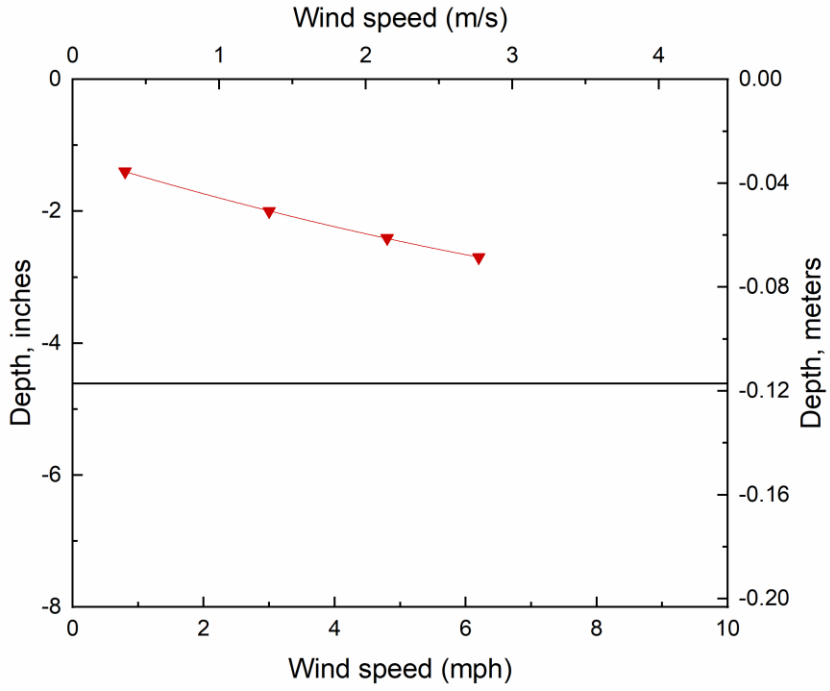

(b)

Figure 4- 27 (a) Vertical profile corresponding to proportion as a function of wind, (b) Vertical translation of thermal energy in response to varying wind conditions

4.7. Wind Rebound Effect

4.7.1. Introduction

The following study is presented to determine the rebound effect of wind cessation induced by some change in wind magnitude. According to previous research, the focus was predominately confined to finding the convective heat transfer coefficient by experimental means using sustained wind conditions. The limitation for our study is that the negative effect of wind could only be analyzed locally rather than globally across the slab. Therefore, the heat transfer coefficient would likely be over-estimated due to influx of heat outside the local region. Also, it can be assumed that wind follows some random scattered function, which implies that there will exist thermal rebound. Since the frequency at which wind changes magnitude is high, the initial tangent slopes are a reasonable approximation of the energy lost and gained due to the cycles. If tangent slops are attained over a wide range in respect to change in wind magnitude, then a model can be created to predict the thermal demands under transient wind conditions. The objective of this study is to determine the magnitude of thermal rebound and dissipation due to multiple cycle defined as follows. Let t_o be the initial time for which wind is projected at the slab at some point x. Define $F = 1/(t_n - t_{n-1})$ as the frequency of alternating upper/lower bound cycles in respect to wind speed where W_0, W_1, W_2,….,W_n represent alternating upper and lower bound cycles. For this study, the time frequency for each upper/lower bound cycle was set at 1 minute whereas the time frequency to satisfy initial steady-state conditions after each period was doubled at 2 minutes. The goal is to measure the net change in temperature at the surface of the slab in respect to a net change in wind magnitude. Figures 4-28 (a) and (b) display the step functions created to represent each cycle period corresponding to thermal rebound and thermal dissipation. Ideally, the frequency should be increased so that initial equilibrium conditions are satisfied for each step period, however, the testing process was not automated which leads to time constraints.

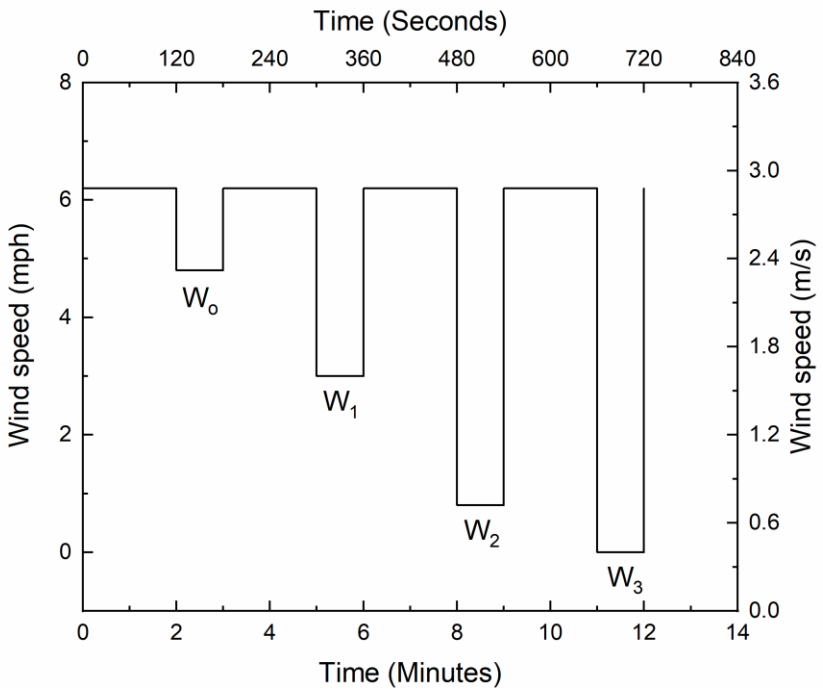

(a)

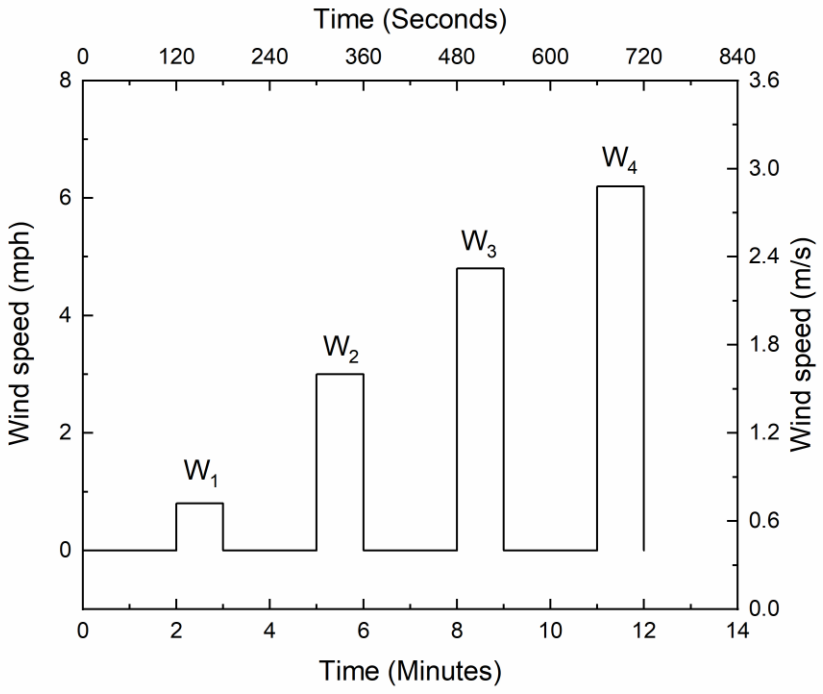

(b)

Figure 4- 28 (a) Step function for Rebound cycle, (b) Step Function for Dissipating Cycle

4.7.2. Thermal Dissipation and Rebound Cycles

Figures 4-29 (a) and (b) display the net change in temperature relative to the reference temperature at steady state corresponding to each alternating period (W_x). The net change due to rebound was roughly three (3) times less than the net change due to dissipation. If this relation holds for all Δw (mph), then the steady-state temperature will be highly sensitive to the upper bound corresponding to the maximum wind magnitude. This will imply that during the onset of a cold front, the slab temperature will converge within a marginal limit from the ambient temperature. Since thermal energy is translated below the surface of slab as wind is projected at slab, it will follow that the energy must translate back to the surface as wind magnitude is reduced. Therefore, there will exists some time lag due to the re-adjustment of thermal energy. The one limitation is that each cycle period had time constraints because the process was manually controlled. Thus, for a more accurate assessment, each time period should be extended such that initial conditions are satisfied for all cycles.

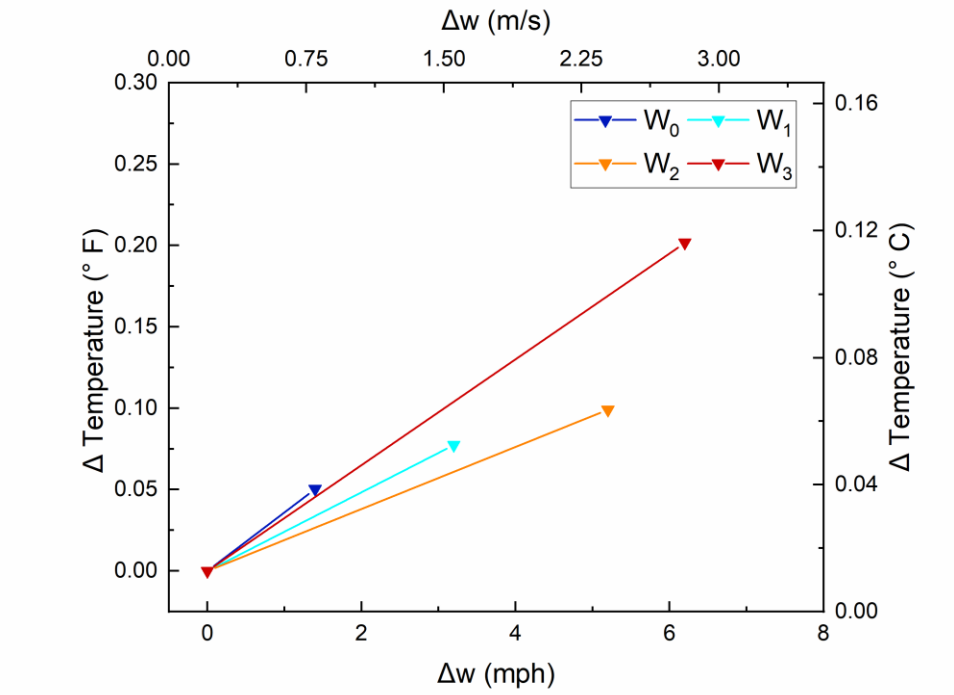

(a)

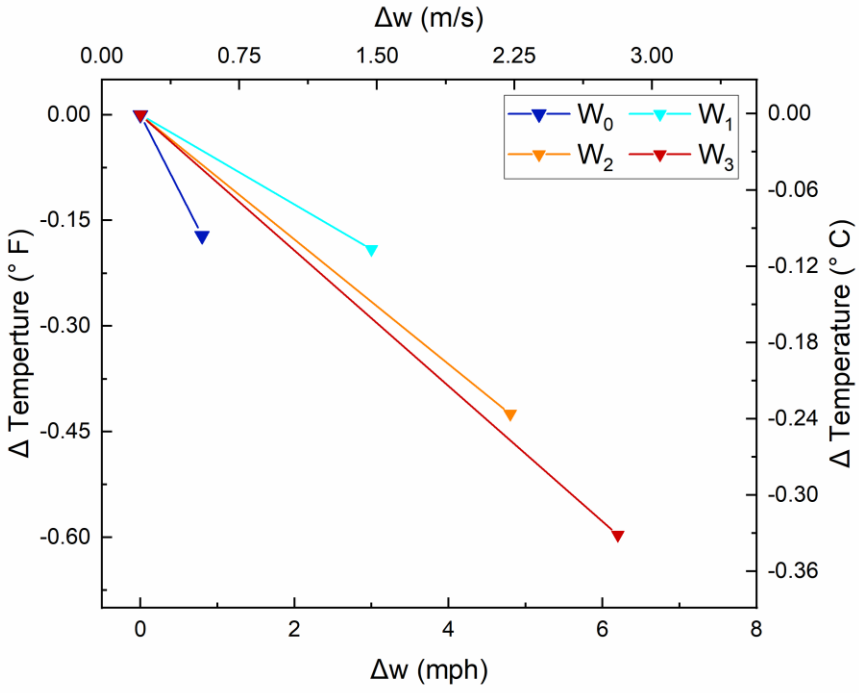

(b)

Figure 4- 29 (a) Thermal dissipating effect, (b) Thermal Rebound Effect

Conclusion

In conclusion, the temperature distribution within the slab follows a slight parabolic function in the lateral direction and a strong linear function in the vertical direction. Using these relations, the steady-state temperature at any depth interval within the slab can be reasonably estimated. Therefore, the thermal demands can be predicted to ensure de-icing is permissible. Using confidence intervals and hypothesis testing, a probable region in which the proportion may reside can be estimated. This ensures the prediction is constrained such that the margin of error in minimized. Sustained wind was determined to greatly compromise the performance of the system by minimizing the proportion of heat transferred to the slab surface. Since sustained wind conditions are only confined to controlled weather scenarios, a thermal rebound study was provided to prove the significance of cyclic wind initiation and cessation periods. The results showed that incremental increases in wind magnitude reduced that system performance to a higher degree than incremental decreases in wind magnitude, however, further testing must be conducted based on testing frequency.

Chapter 5: Performance of De-icing System Under Transient Conditions

5.1: Scope and Motivation

Based on the results attained from paper B, multiple Winter weather scenarios were analyzed to determine whether the de-icing system could counter conditions confined in the DFW area. The analysis was centered on sub-freezing events initiated by strong cold fronts. The sensitivity of the proportion due to an increase in wind conditions before the onset of a cold front was determined.

Abstract

The following study presents an experimental model of a geothermal bridge de-icing system in an outdoor environment during winter months. The overall performance of the system was analyzed using a variable, *p*, which represents the proportion of the heating load (I-A) transferred to the bridge slab for any depth, Z where I denotes Inlet temp. and A denotes ambient temp. Additionally, another variable defined as α represents the change in proportion per unit depth, Z ($\Delta p/\Delta Z$). These quantities are utilized to predict the steady-state temperature within the slab under varying environmental conditions. Generally, the proportion is fixed within a narrow range if the environmental conditions are constant for some duration, however, this study shows a transient relationship over time. The proportion is sensitive to the cyclic environmental conditions such as wind, which can negatively affect the performance of the system. Since the slab was positioned in an enclosed area, wind was not considered to be a major influence unless a severe cold front was initiated, which was shown to greatly suppress the proportion of heat within the slab. A winter event was simulated using a snow gun to determine whether the geothermal de-icing system was capable of countering induced icy conditions. A thermal imaging study was conducted to determine the efficiency of spray foam to prevent heat loss from base of slab, and to estimate the surface temperature of the slab with reasonable accuracy.

5.2. Introduction

To determine whether a geothermal bridge de-icing system can counter multiple winter events, it is imperative to study the thermal response of the slab to rapid fluctuations in environmental conditions. Prior to a cold front, warm air is converging toward the atmosphere at a fast rate, which causes the pressure to reduce at a faster rate. Consequently, the larger pressure gradient introduced by low pressure systems or cold fronts causes wind to gradually increase (Piggott, 1998). Therefore, the efficiency of the system will be compromised as a function of wind magnitude. For this reason, the thermal demands must be adjusted according to the anticipation of increased wind magnitude following a cold front. Another negative factor is that wind increasing evaporation rate at the surface, which induces a reduction in temperature due to energy demand. Without any wind travelling over the top of a water body, evaporation rates are low, because evaporated water vapor is not efficiently removed and remains in a relatively stationary state near the vicinity of the water surface (Peter et al., 2011). Thus, preferential ice build-up will be accelerated due to the onset of increased winds and hence, the potential for de-icing will decrease. By creating a relationship between heating efficiency and wind magnitude over a wide range, the thermal demands can be reasonably estimated to ensure de-icing is permissible. The aim of this study is to focus on the heating performance of the slab subjected to rather severe winter scenarios for the DFW area.

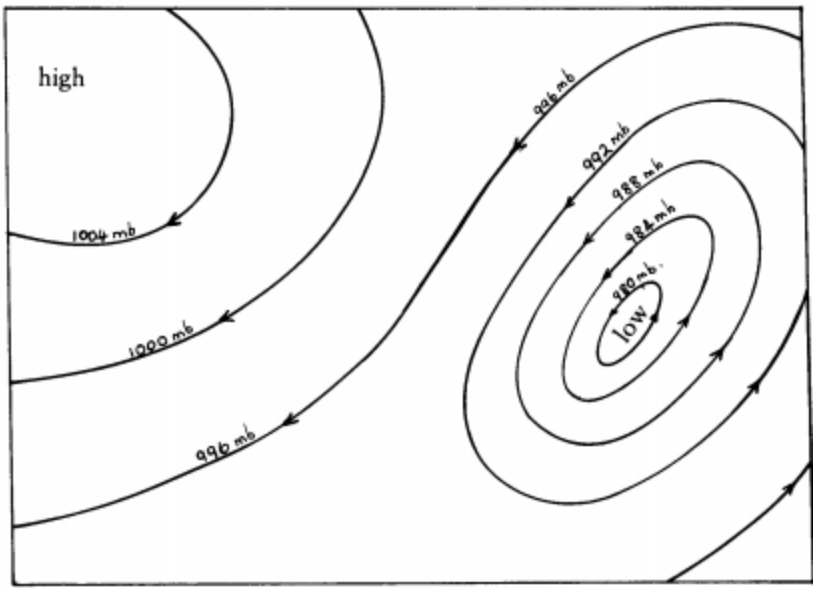

Figure 5- 1 High- and low-pressure areas (Piggott, 1998)

5.2.1. De-icing system

Prior to initiating the de-icing system, a 6' by 4' slab of 4" thickness was set in a confined area exposed to outdoor conditions. A water bath was utilized to provide the hydronic heating source, which was propagated throughout the slab via a water pump of 1.5 gpm capacity. A PEX pipe network consisting of multiple loops at the underside of the slab was assembled as the external carrier of heat as shown in figure 5-2. Thermocouples were installed within the slab at different depths to directly measure the performance of the system and relayed to a thermocouple chassis to export the recorded data to an excel spreadsheet per minute intervals. To minimize heat loss, closed cell spray foam was applied within an enclosed wooden framework as shown in figure 5-3 (a). The average thickness of the foam was roughly 4 inches to contain the heat source. Figure 5-3 (b) shows the thermocouple curing process after installation. Figure 5-4 (a) was utilized to measure the global temperature distribution across the slab at varying depths, thermocouple arrangement 1 was used where the first subscript denotes index and second subscript denotes depth within slab. Each set defines the corresponding depths at each location for thermocouple layout 1. The vertical temperature profile towards the inlet end of the slab was attained using thermocouple arrangement 2 as illustrated in figure 5-4 (b).

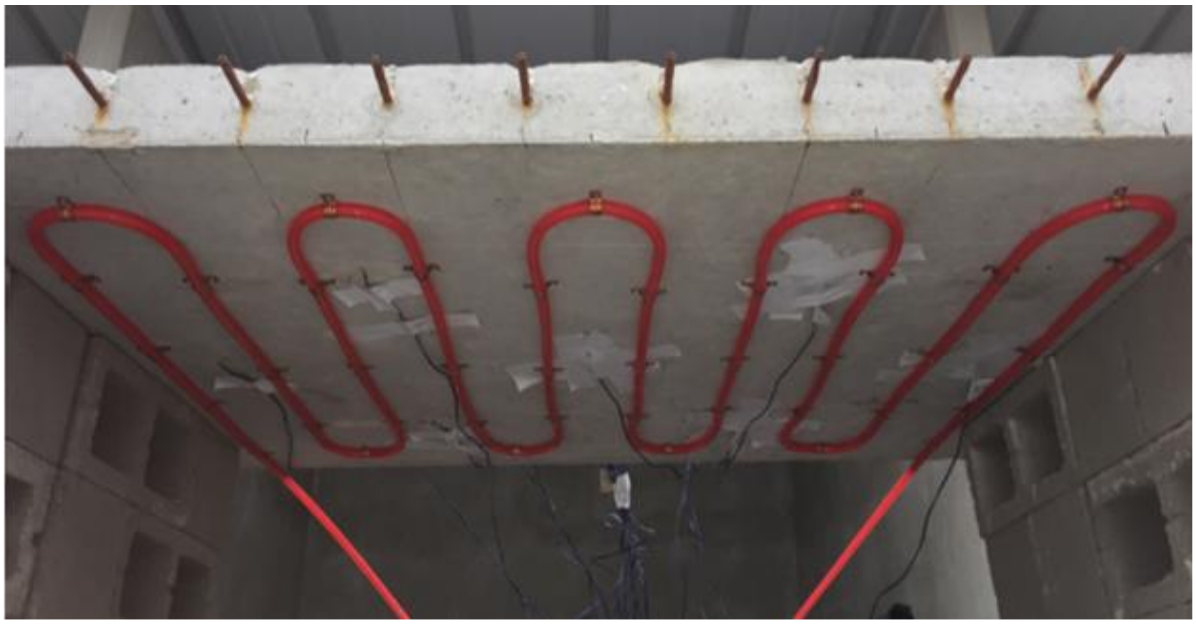

Figure 5- 2 Pipe Arrangement Prior to Framework Application

(a) (b)

Figure 5- 3 (a) Pipes Enclosed within Wooden Framework, (b) Complete thermocouple Set-up

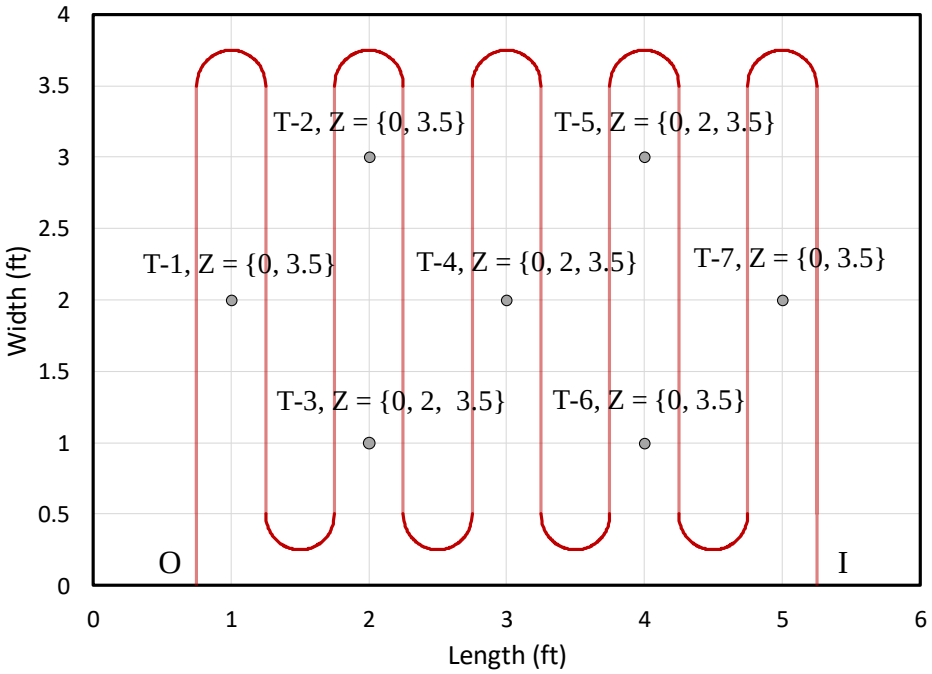

(a)

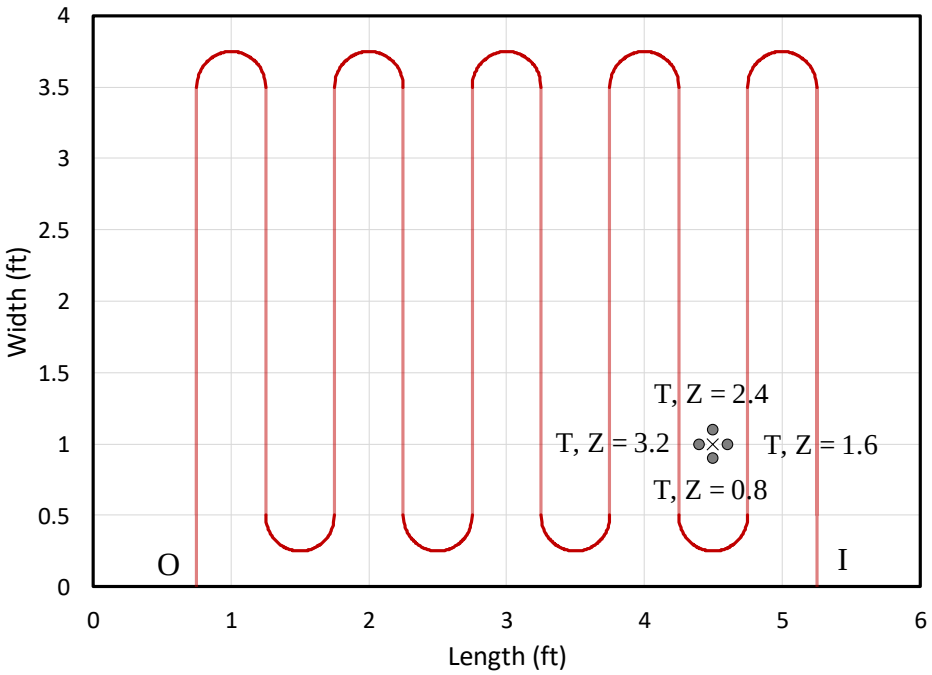

(b)

Figure 5- 4 (a) Thermocouple Numerical Plan 1, (b) Thermocouple Numerical Plan 2

5.2.2. De-icing System Performance under Transient Conditions

Prior to initiation of the system, it is important to gauge how the slab response to environmental conditions in the absence of external heat. A baseline measure as such provided key information regarding the response of the slab to alteration in environmental conditions in the absence of a heat input variable. Once a heat input was added via the transfer of heated water to the pipe network beneath the slab, the overall performance of the system could be directly recorded and analyzed. The following sub-tests were conducted to provide an indication of the overall performance of this system:

1) Pre-test
2) Slab Temperature Variation with Depth
3) Slab Response to Major Fluctuation in Environmental Temperature (Cold Front)
4) Effect of Wind Direction on Heat Dissipation
5) Thermal Imaging Comparison
6) Winter Simulation
7) Method to Predict Slab Temperature at any Depth

Result and discussion

5.3. Pre-Test

5.3.1. Introduction

Before the heating system was initiated, a pre-test was conducted to gauge how the concrete slab reacted to transient environmental conditions. The temperature within the slab follows a cyclic trend based on the daily diurnal cycle. The minimum slab temperature occurs at a time slightly later than the occurrence of the minimum daily temperature due to time lag, which is indirectly proportional to the magnitude of change in environmental conditions. Moreover, the maximum slab temperature occurs at a time slightly later than the occurrences of the maximum daily temperature. The morning cycle was defined as the period between the occurrences of the minimum and maximum environmental temperatures, respectively. Conversely, the nightly cycle was defined as the period between the occurrences of the maximum and minimum environmental

temperatures. Due to time lag, it follows that the proportion of heat transfer will be positive for majority of nightly cycle and negative for majority of daily cycle.

5.3.2. Initial Conditions

Figure 5-5 (a) shows the cyclic trend that corresponds to thermocouple layout 1 for depth, D = 0.5 inches. Figure 5-5 (b) shows the relationship between time lag and the initial negative change in ambient temperature per hour interval, which follows a negative exponential function. Therefore, the efficiency of the system will be greatly compromised during a severe cold front, in which the ambient temperature dissipates at a higher rate. Figure 5-5 (c) shows a comparison between the thermocouple (actual) and weather database measurements. The thermocouple measurement is more consistent with the sinusoidal transition between cycles and the steady reduction in temperature during the nightly cycle. The weather database measurements fluctuate on a continual basis, implying that the sensitivity is high.

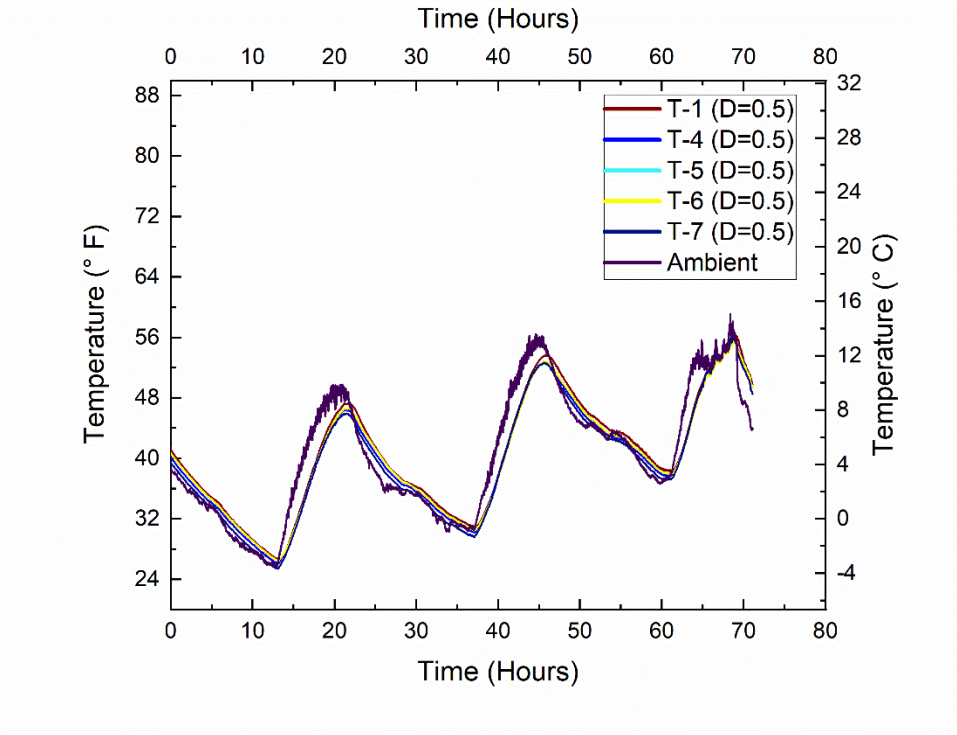

(a)

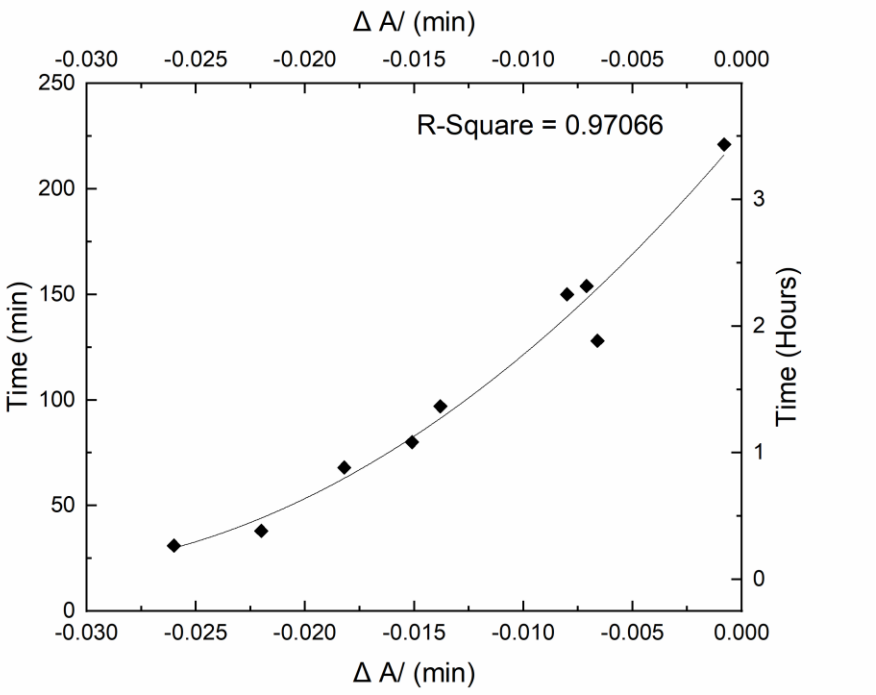

(b)

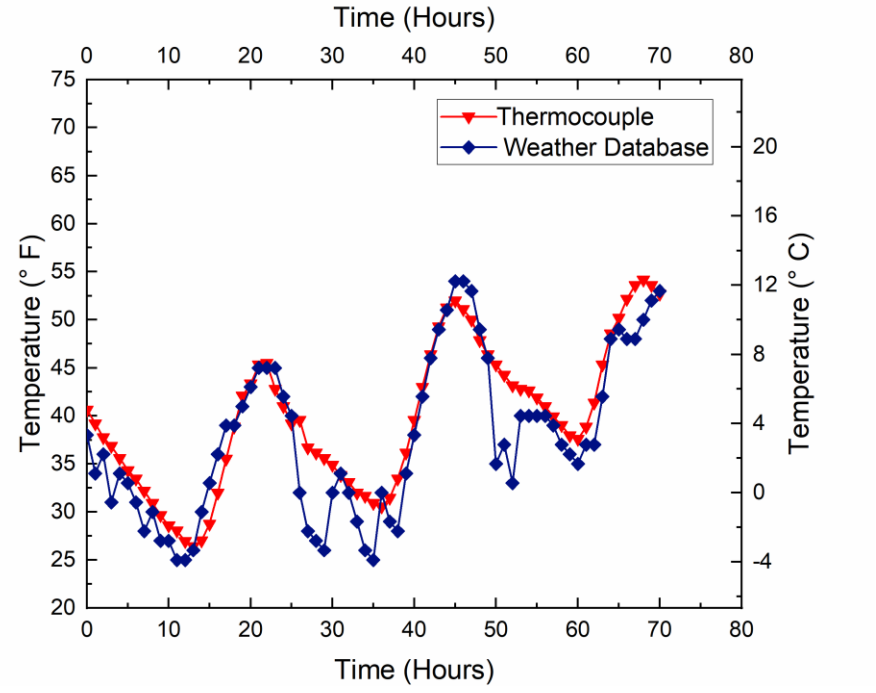

(c)

Figure 5- 5 (a) Slab Temperature Response in Absence of Heat Input (D = 0.5''), (b) Time Lag Associated with Initial Drop in Temperature during Nightly Cycle, (c) Ambient Temperature Comparison between Thermocouple and Weather Database

5.4. Slab Temperature Variation with Depth

5.4.1. Introduction

After the pre-test, the water pump was turned on to initiate the system into heating mode. The vertical change in temperature within the slab is an important measure of the efficiency of the system. The more efficient the heating system, the lower the heat input (water source) needs to be to satisfy de-icing of bridges. The greater the vertical change in temperature within the slab, the lower the efficiency and vice versa. Every material has a range in which the vertical change can reside, which means concrete will be fixed within a theoretical range of possible values. By idealizing the heating system, the efficiency can be maximized. During the nightly cycle, it will follow that $0 < p < 1$ unless a warm front occurs at night. The morning cycle was not analyzed unless a cold front occurred during the period. In the absence of a cold front during the morning cycle, the temperature will be steadily increasing, hence, there will be a higher likelihood of de-icing. The least likelihood for de-icing of bridges will typically occur during the night cycle for the opposite reason. Therefore, it is of high importance to analyze the degree at which a cold front may compromise the heating efficiency of the system.

5.4.2. Vertical Response to Initiation of System

Figure 5-6 (a) shows the variation in temperature at four equally spaced depths within the slab. The temperature within the slab is consistent in terms of decreasing as the depth approaches the top surface of the slab. The time lag steadily increases towards the base of the slab since there exists less influence from convective heat transfer. The rate of change in respect to the slab temp is lower relative to the ambient temp between cycles. Therefore, the proportion decreases during daily cycle and increases during nightly cycle. The proportion depends on thermal conductivity of the concrete which ranges from 1.2 to 3 W/m*k (Bošnjak, 2000). It is imperative to reasonably adjust the heat load depending on the environmental conditions so that enough energy can be utilized to melt ice on bridges, however, too much energy will be costly. Therefore, predicting the required heat load will be a useful measure for minimizing heating costs. Figure 5-6 (b) shows the proportion, p, increases rapidly during the initiation of the nightly cycle due to time lag, and

stabilizes during the re-adjustment period. Over the period, the proportion near the surface of the slab ranged from 0.2 to 0.33. Figure 5-6 (c) shows the change in proportion per depth interval, denotes as α. There is consistency til the first depth interval (near the surface) where there is a slight spike. A possible reason could be interference from the environment due to air pockets in the mortar as well as vibration. The thermocouples near the surface fluctuated to a higher degree than the sub-level thermocouples, which indicates that disturbance is likely.

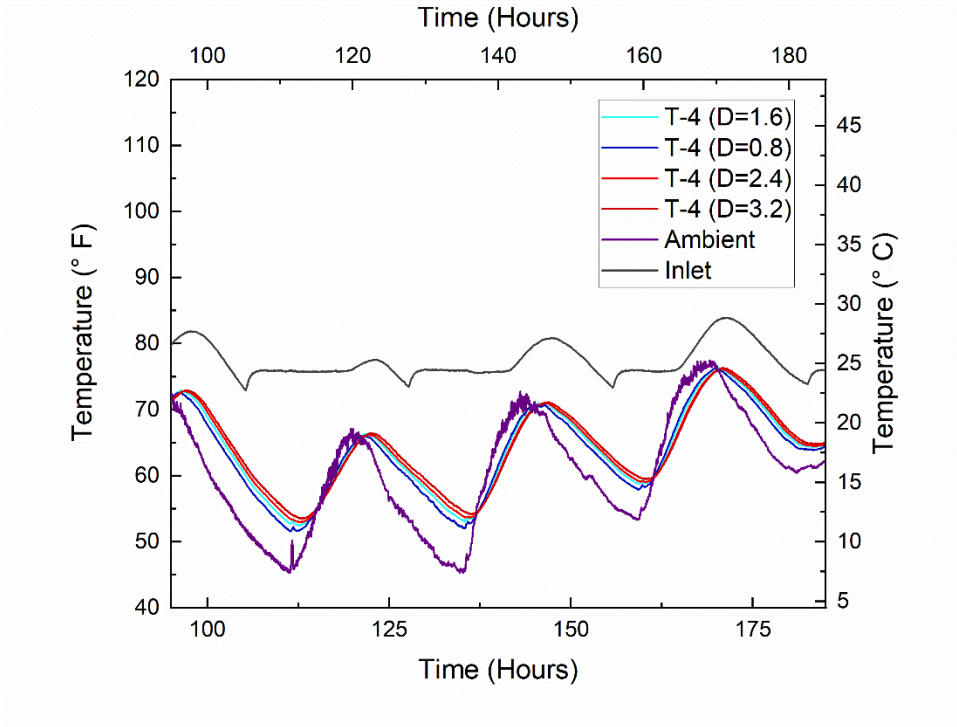

(a)

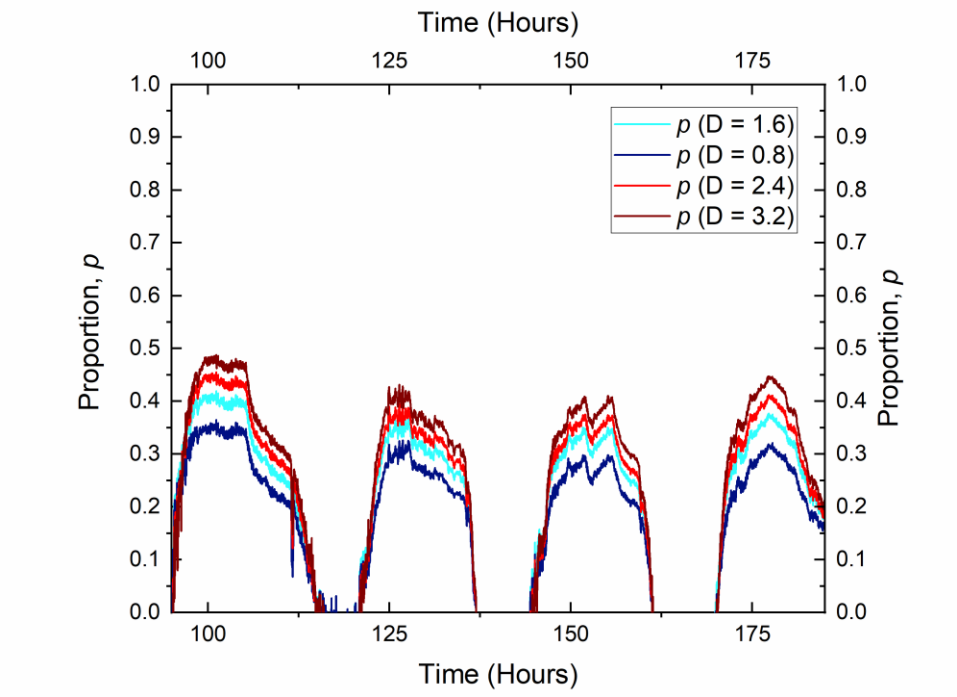
Time (Hours)
100
125
150
175
1.0
0.9
0.8
0.7
0.6
0.5
0.4
0.3
0.2
0.1
0.0
Proportion, p
p (D = 1.6)
p (D = 0.8)
p (D = 2.4)
p (D = 3.2)

(b)

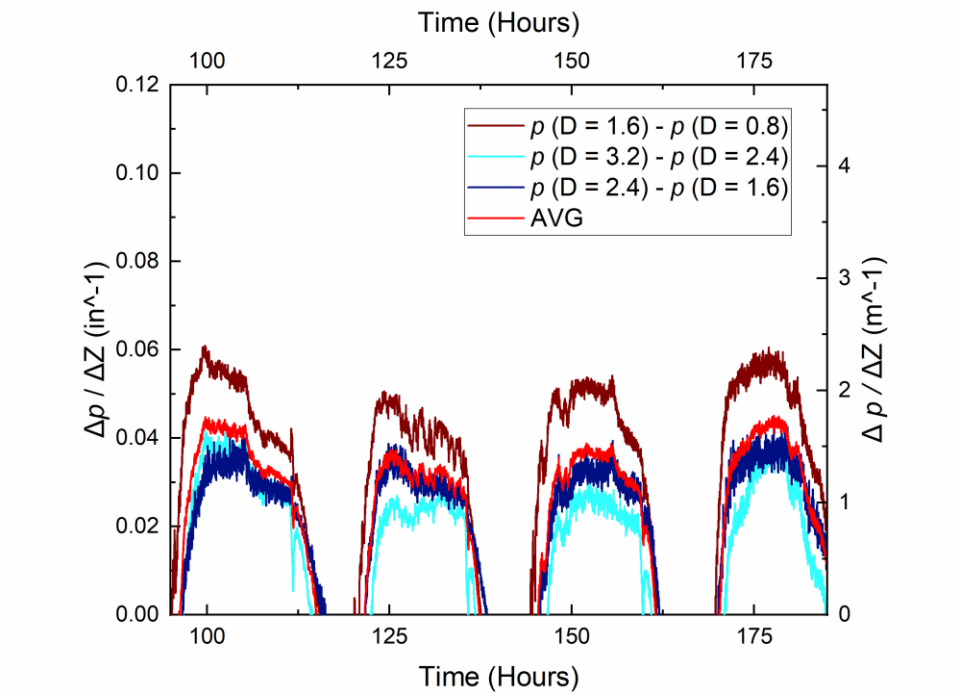

(c)

Figure 5- 6 (a) Temperature Response in Respect to Depth within Slab, (b) Proportion, p in respect to Depth, (c) Alpha Coefficient, α in respect to Depth

5.4.3. Thermal Divergence

Figure 5-7 shows the average temperature difference between the slab and ambient measurements in respect to the pre-test (a) and post-test (b). The measurements correspond to one nightly cycle period. The pre-test measurement is sensitive to the rate of change in the ambient temperature over time. That is, the spike is due to a rapid change whereas the dip is due to stabilization. The post-test shows that the heat introduced to the slab causes a divergence in respect to the slab and ambient measurements over one nightly cycle period.

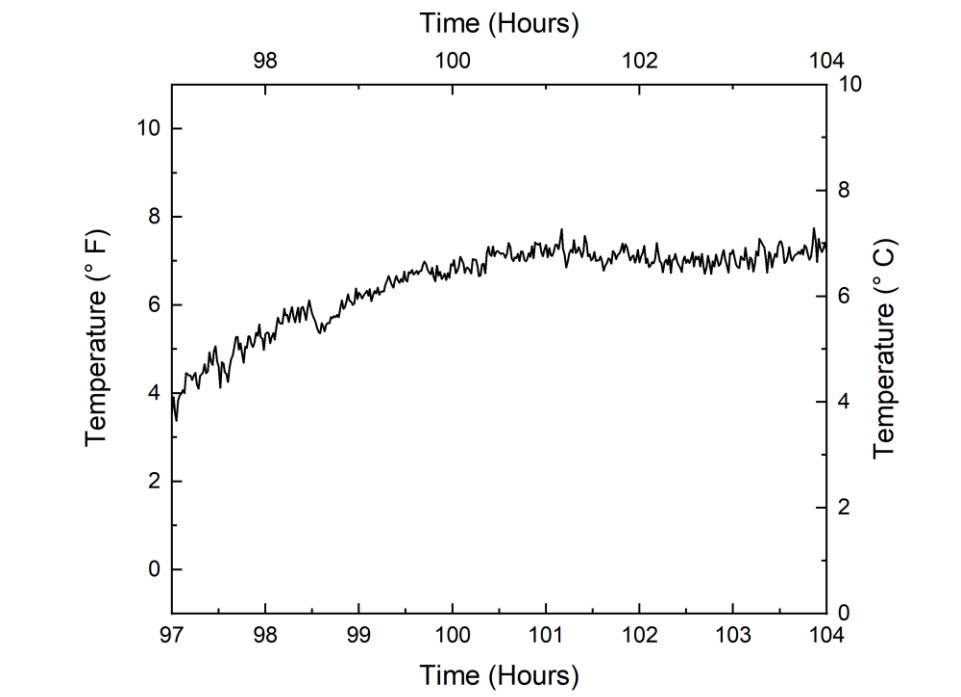

(a)

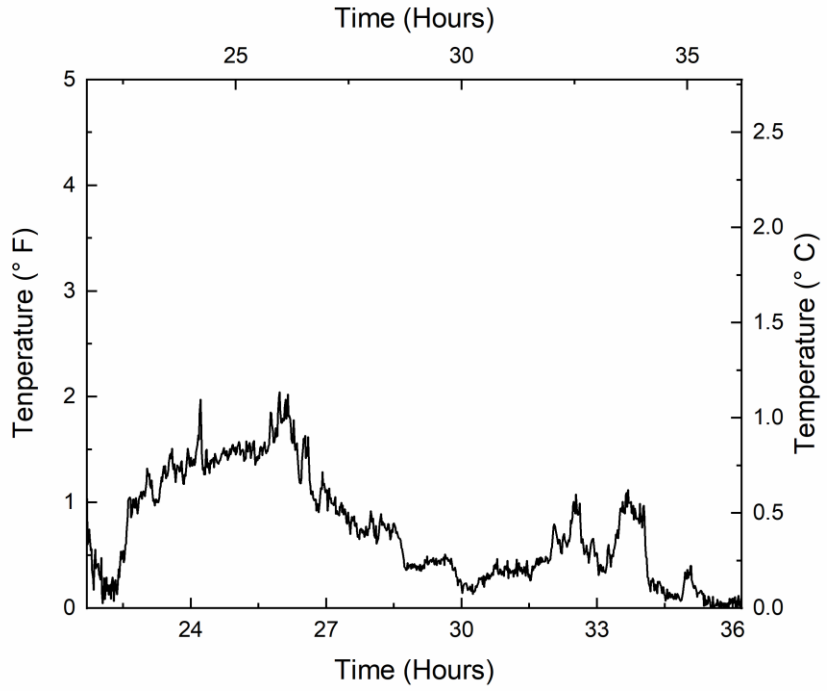

(b)

Figure 5- 7 Temperature Differential Between Average Slab Temp. and Ambient Temp. (D = 0.5"): (a) Pre-Test, (b) Post heated

5.5. Slab Response to Major Fluctuation in Environmental Temperature (Cold Front)

5.5.1. Introduction

The arrival of a cold front typically precedes a winter snow or ice event, so it is imperative that the heat input temperature is adjusted according to the severity of a cold front. Thus, a relatively strong cold front was analyzed, in which the temperature dipped from 70 to 32 degrees Fahrenheit within a 15-hour window on the night of February 20 followed by heavy rainfall. The wind and environmental conditions preceding, during, and after the event were recorded using Weather Underground Database.

5.5.2. Thermal Response to Extreme Cold Front

According to figure 5-8 a, the environmental temperature dipped rapidly for a 15-hour period following the cold front. The rapid dip in environmental temperature coupled with increased intensity and sustainment of wind resulted in a lesser time lag and hence, convergence was more eminent. The weather database readings were more sensitive to the rapid fluctuation in environmental temperature as indicated in figure 5-8 b. The temperature difference between the weather database and thermocouple (ambient) readings as illustrated by figure 5-8 c, was consistently between 0- and 2-degrees Fahrenheit, except during the onset of the cold front.

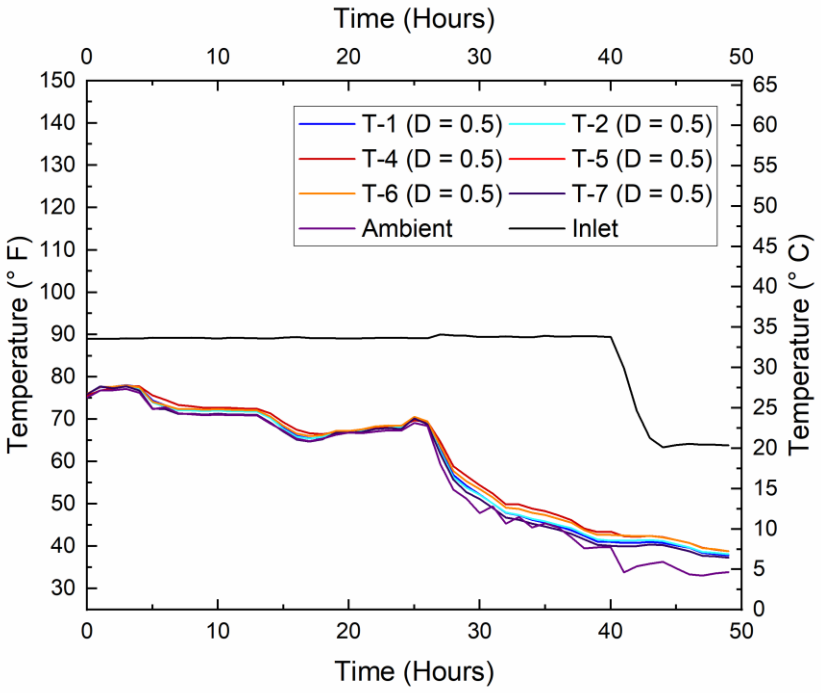
Time (Hours)
Temperature (° F)
Temperature (° C)
T-1 (D = 0.5)
T-2 (D = 0.5)
T-4 (D = 0.5)
T-5 (D = 0.5)
T-6 (D = 0.5)
T-7 (D = 0.5)
Ambient
Inlet

(a)

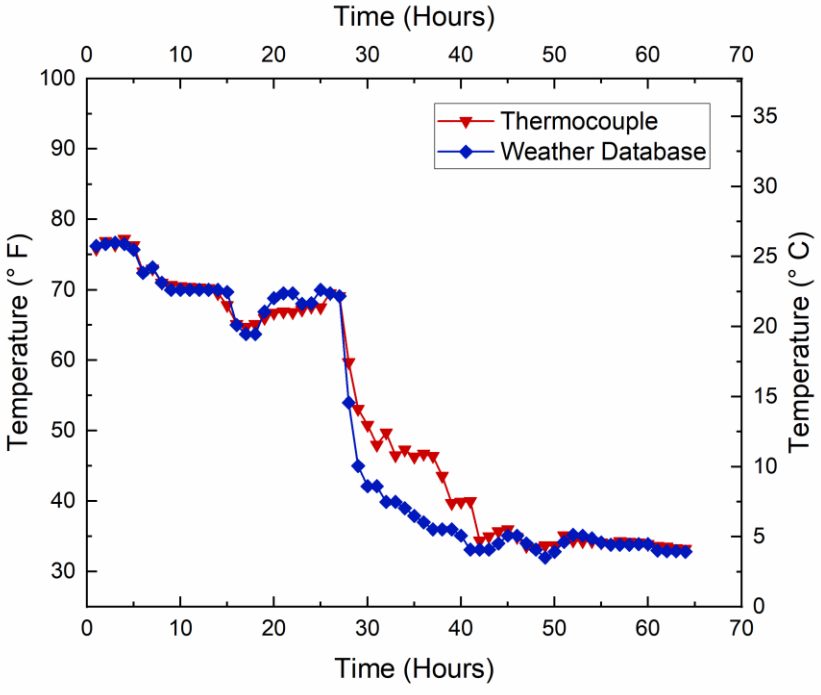
Time (Hours)
Temperature (° F)
Temperature (° C)
Thermocouple
Weather Database

(b)

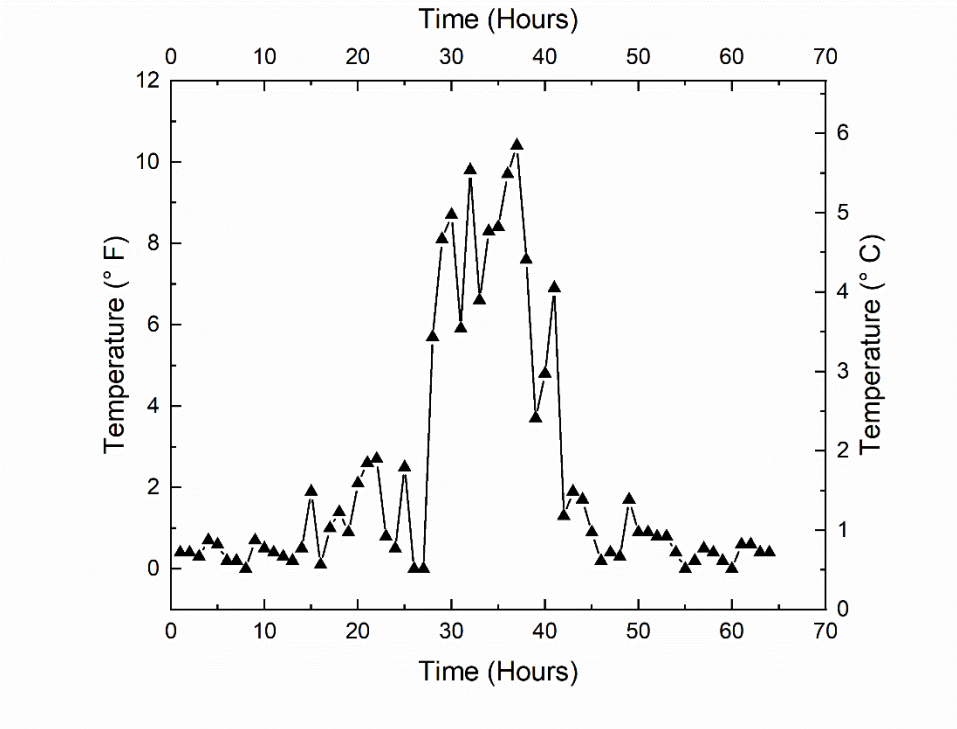

(c)

Figure 5- 8 (a) Thermocouple response to strong cold front, (b) Comparison between weather database and thermocouple readings, (c) Temperature difference between weather database and thermocouple reading

5.5.3 Wind Conditions

Figure 5-9 (a), (b), and (c) show change in wind conditions during different periods of transition for the duration of a strong cold front. As shown, the wind speed tended to decrease after the passing of the cold front, whereas the wind speed increased once the cold front was initiated. Preceding the cold front, the wind conditions will be more variable. The periods were defined based on the change in concavity corresponding to environmental conditions. Transient environmental conditions manifested for the duration of the cold front, however, conditions stabilized once the cold front was assumed to have passed.

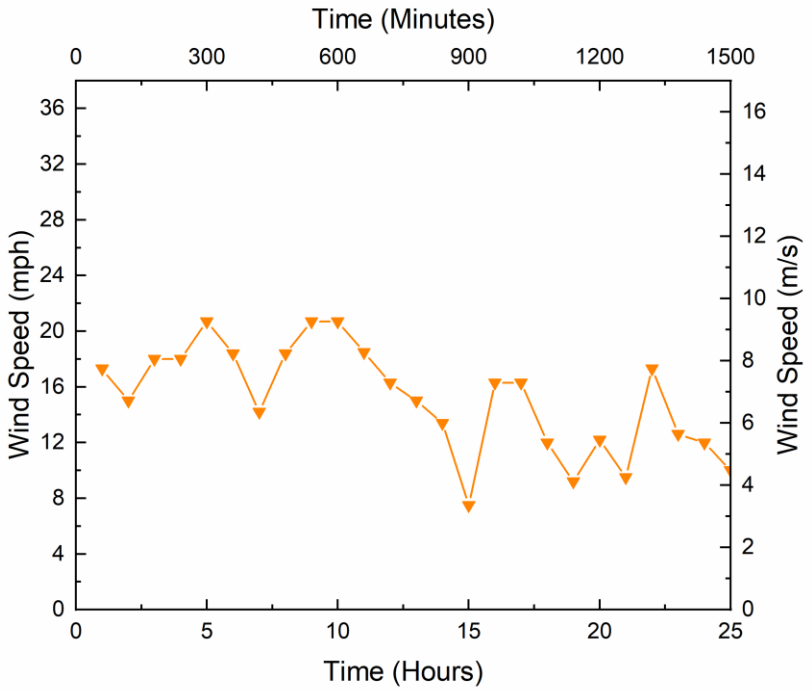
Time (Minutes)
0
300
600
900
1200
1500
Wind Speed (mph)
Wind Speed (m/s)
0
4
8
12
16
20
24
28
32
36
0
2
4
6
8
10
12
14
16
0
5
10
15
20
25
Time (Hours)

(a)

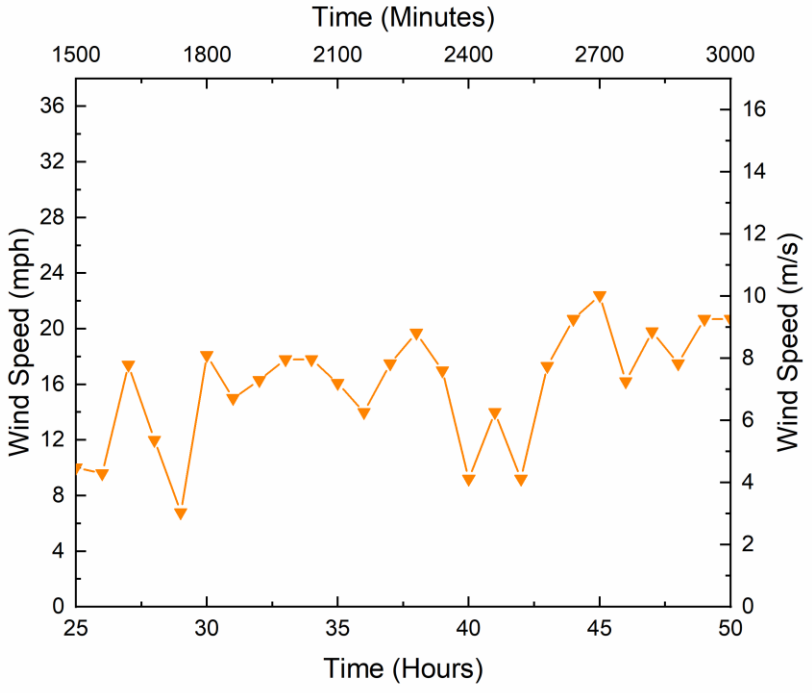
Time (Minutes)
1500
1800
2100
2400
2700
3000
Wind Speed (mph)
Wind Speed (m/s)
0
4
8
12
16
20
24
28
32
36
0
2
4
6
8
10
12
14
16
25
30
35
40
45
50
Time (Hours)

(b)

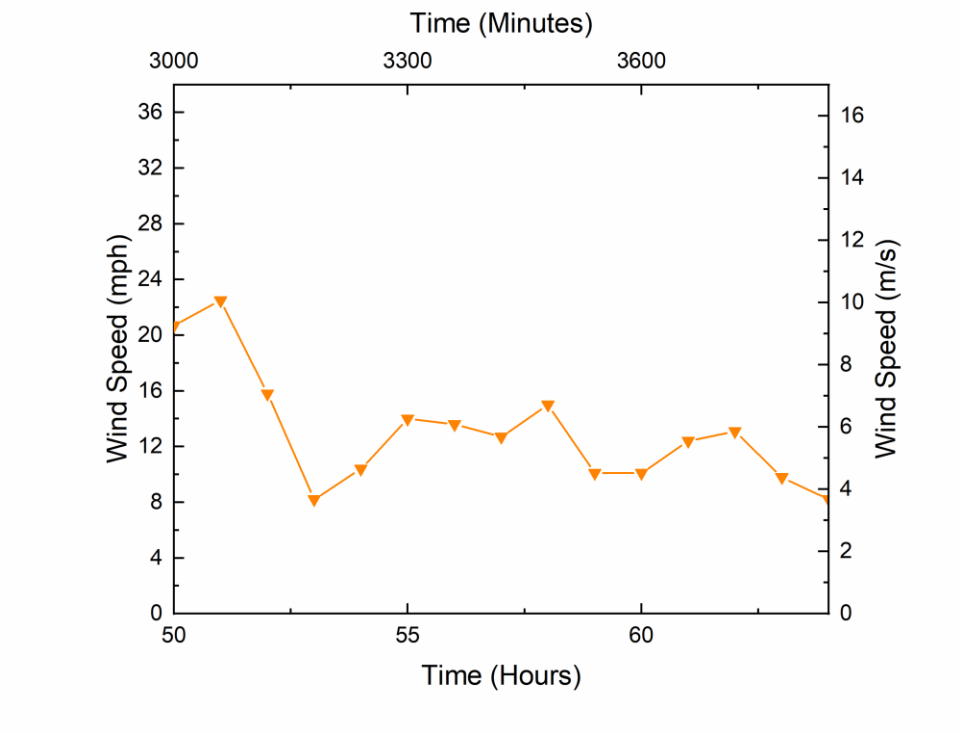

(c)

Figure 5- 9 (a) Wind Speed Prior to Cold Front (0 < time < 25), (b) Wind Speed during Cold Front (25 <= time <= 50), (c) Wind Speed after Cold Front (50 < time < 64)

5.6. Effect of Wind Direction on Heat Dissipation of Slab

5.6.1. Introduction

Due to the convective heat loss process, wind was an important parameter of interest, particularly in the East-West direction, because the slab was confined in an area blocked off to the North-South. It was determined that wind in the East-West direction significantly reduced the efficiency of the system by drastically decreases the proportion of heat transferred to the surface. Thus, a much higher heat load would be required to permit de-icing under the imposed conditions.

5.6.2. Effects of N to E Transition in Wind Direction

As shown from figures 5-10 (a), wind can have a significant effect on the slab temperature within a short period. In fact, the temperature at a depth of 0.8″ below the top surface of the slab

roughly converged within 1 degree Celsius from the environmental temperature after the wind shifted from North to East as indicated by figure 5-10 (b). Figure 5-10 (c) shows the proportion of heat transferred throughout the slab at different depths. There is roughly a 15% reduction in respect to the proportion near the surface of the slab implying that the heating efficiency is greatly compromised by wind exposure. Therefore, the thermal demands are highly sensitive to wind.

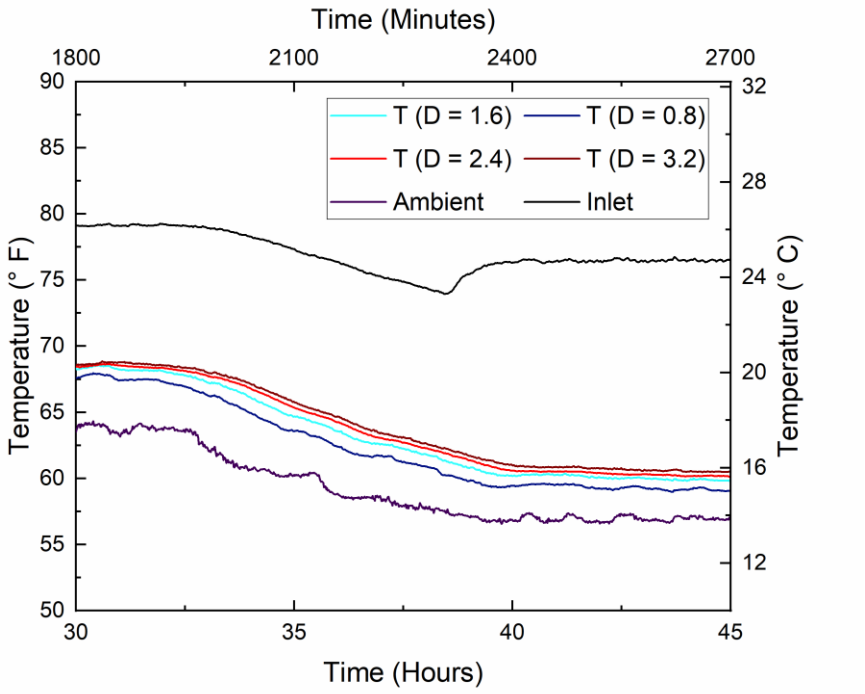

(a)

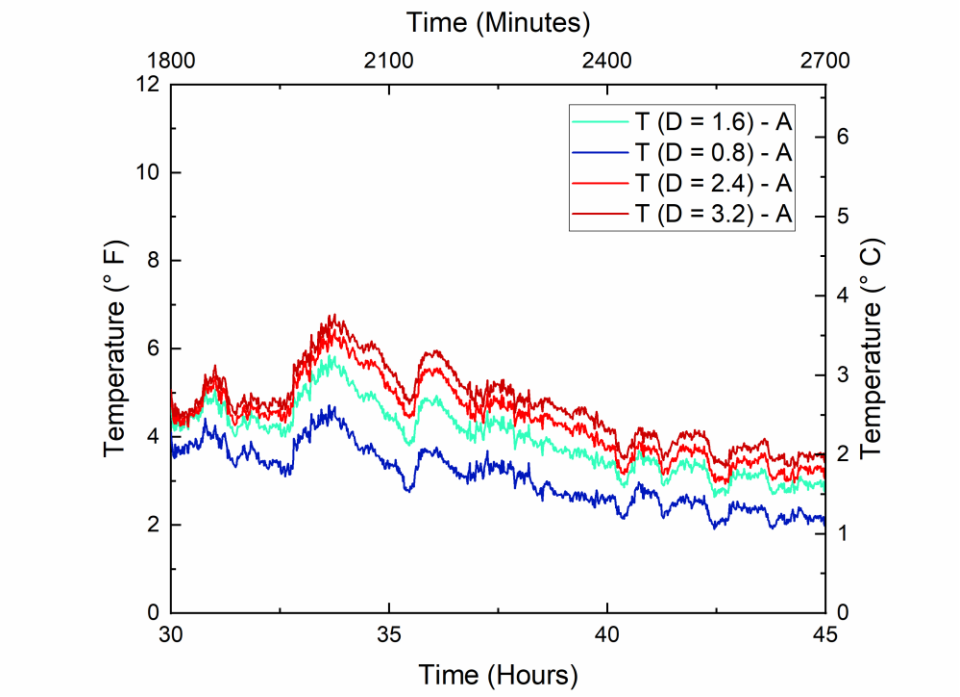
Time (Minutes)
1800
2100
2400
2700
T (D = 1.6) - A
T (D = 0.8) - A
T (D = 2.4) - A
T (D = 3.2) - A
Temperature (° F)
Temperature (° C)
Time (Hours)
30
35
40
45
0
2
4
6
8
10
12
1
3
5

(b)

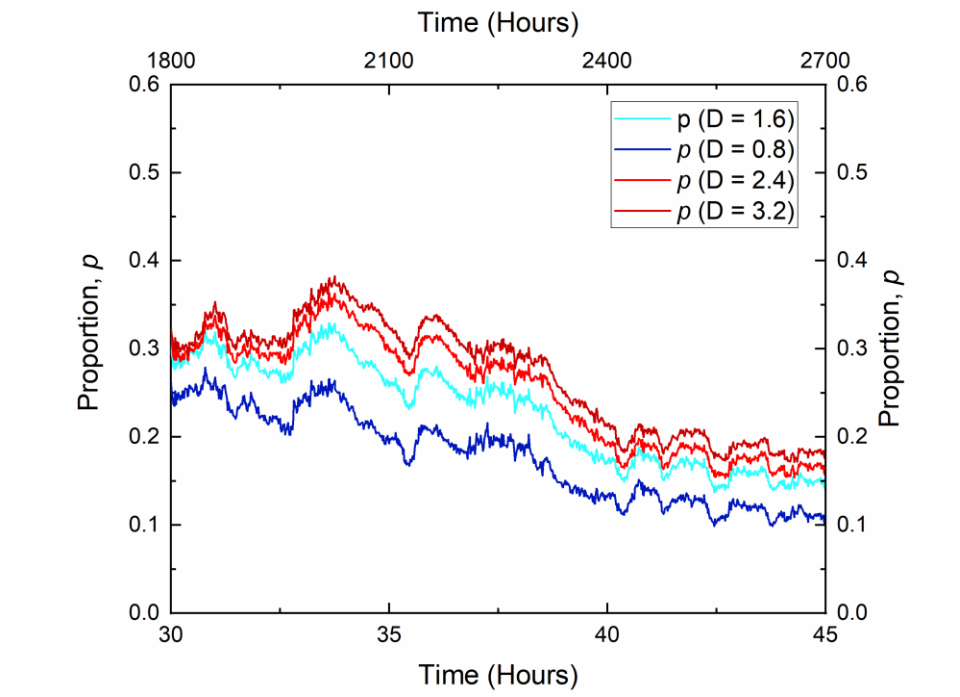

(c)

Figure 5- 10 (a) Thermocouple Response to Changing Wind Direction (North to East), (b) Temperature Difference between Thermocouples Embedded within Slab and Environment, (c) Negative Effect of Wind Shift on the Proportion, p

5.6.3. Wind Coordinate System

Figure 5-11 (a) shows the rapid change in wind direction as indicated by a coordinate system from table 3-1. The decrease in thermal efficiency of the system coincided well with the transition of wind from North to East. Figure 5-11 (b) shows the wind speed as a function of wind coordinates. As the wind shifted from North to East, the wind speed increased, which caused the temperature within the slab to converge toward the environmental temperature.

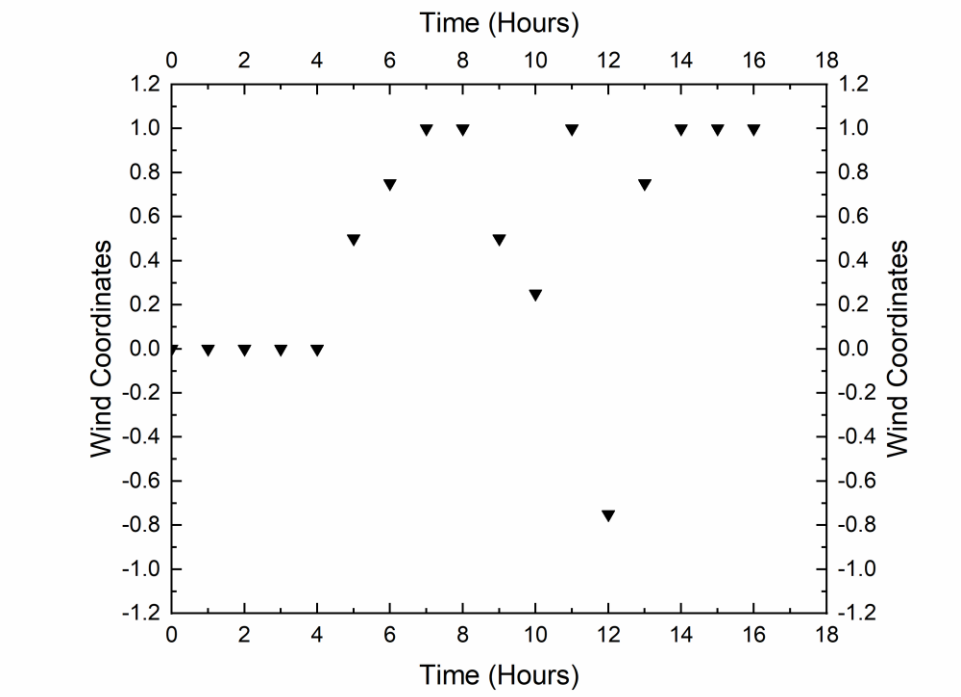

(a)

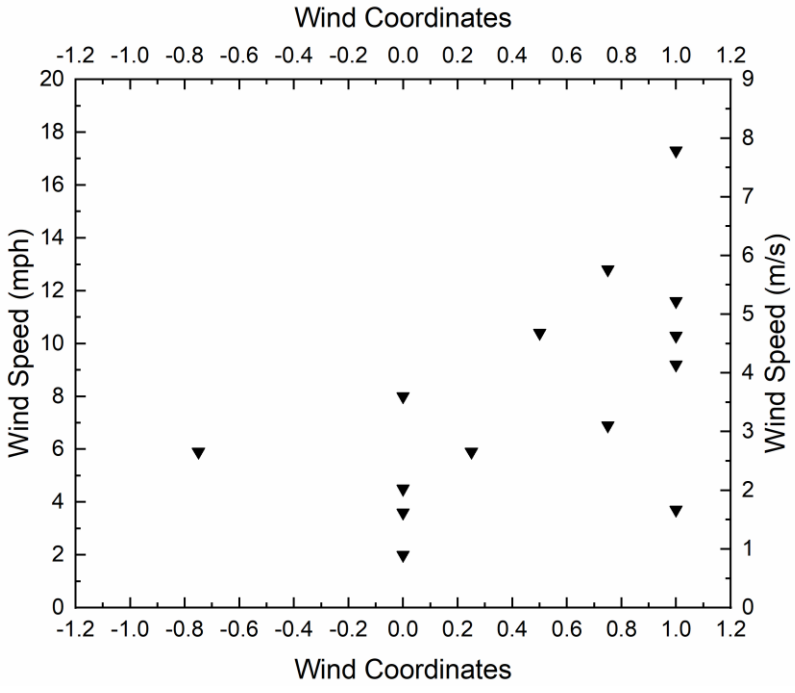

(b)

Figure 5- 11 (a) Wind Direction Corresponding to Figure 5.2, (b) Wind Speed Corresponding to coordinates displayed in Table 2

5.7. Thermal Imaging Comparison

5.7.1. Introduction

Another important aspect regarding the efficiency of the system is how much heat is retained at the base of the slab. That is, the thermal efficiency is a function of the spray foam's ability to resist heat flow. A Fluke thermal imaging camera was utilized to compare the spray foam temperature at the base of the foam relative to a thermocouple installed in proximity to the base. It is imperative to minimize the amount of heat loss at base of slab so that a maximum amount of heat can be supplied to the slab for de-icing. A second test was conducted to compare the surface temperature of the slab (via thermal camera) relative to an additional thermocouple, which was encapsulated by geo-foam to prevent disturbance from the ambient environment.

5.7.2. Spray Foam Imaging Study

Figure 5-12 shows an infrared image of the foam at the underside of the slab (a) and visible image (b). From figure 5-13, the difference between the temperature of the thermal image and thermocouple is relatively small. The inlet temperature and ambient temperatures were 31.8 and 13.2 degrees Celsius respectively. Hence, the heat load supplied to slab was 34.5° F (89.2 ° F – 55.7° F). Therefore, $p_{foam} = 0.142$, which implies that roughly 15% of the thermal load is transferred from heat source to the base of the foam layer, which is quite significant. The average thickness of the foam was 4", however, there are toughs and peaks, which yields a range of thickness that exceed or fall below the average. To minimize heat loss, the foam needs to be uniformly applied to the base to ensure even distribution of the thermal resistant material. Also, the thickness needs to be adjusted to maximize the thermal resistant properties of the foam.

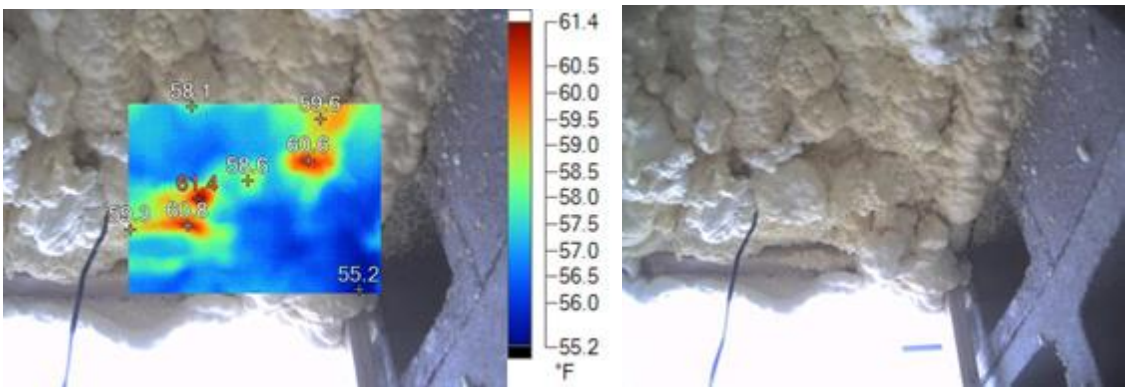

(a) (b)

Figure 5- 12 Thermal Camera Imaging of Spray Foam

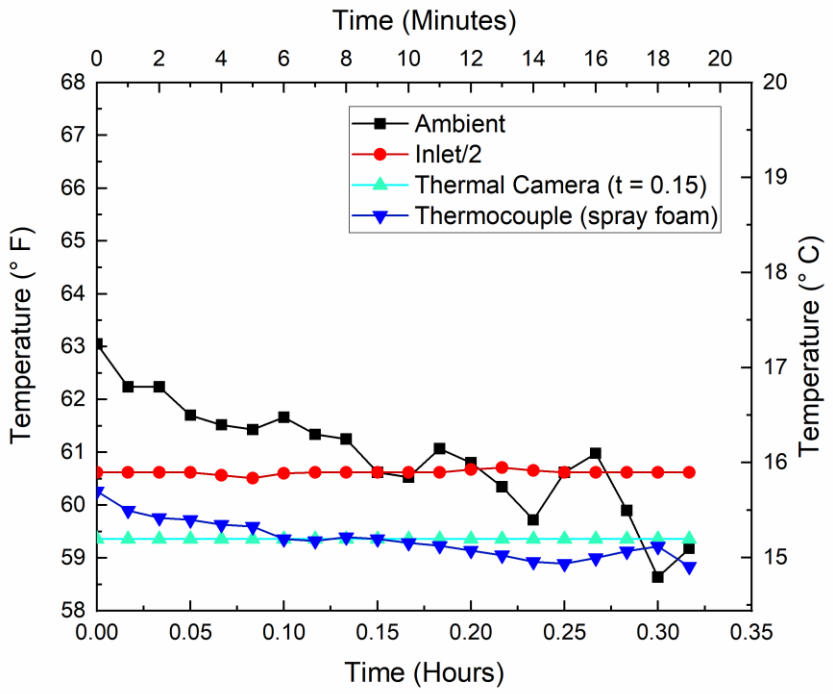

Figure 5- 13 Thermal Camera in Comparison with Thermocouples within Foam

5.7.3. Slab Surface Imaging Study

Figures 5-14 shows the infrared image of the slab surface (a) and the visible image (b). From Fig. 5-15 (a), the surface temperature reading via the thermal imaging camera is roughly 0.43°C

(~0.7°F) less than the temperature 0.5" below the slab at the time of measurement (10:50 P.M). The thermal camera is, however, subject to error. Figure 5-15 (b) shows the surface temperature of the slab is 0.4 ° C (~0.7 ° F) less than the temperature 0.5" below the surface as indicated by figure 12 (c). This is very consistent in respect to the thermal imaging readings. Therefore, the surface temperature of the slab can be estimated with reasonable accuracy because the variance in temperature is marginal regardless of the heat load. The average heat load corresponding to figure 5-15 (b) is 29.3 ° F. Thus, it can be determined that the deviation in the proportion for the upper layer of the slab, P_{dev} = 0.0238, which is marginal. The alpha coefficient, α, for this case is 0.0476, which is consistent with the upper depth interval via figure 5-15 (c). Therefore, the slab temperature profile can be reasonable estimated.

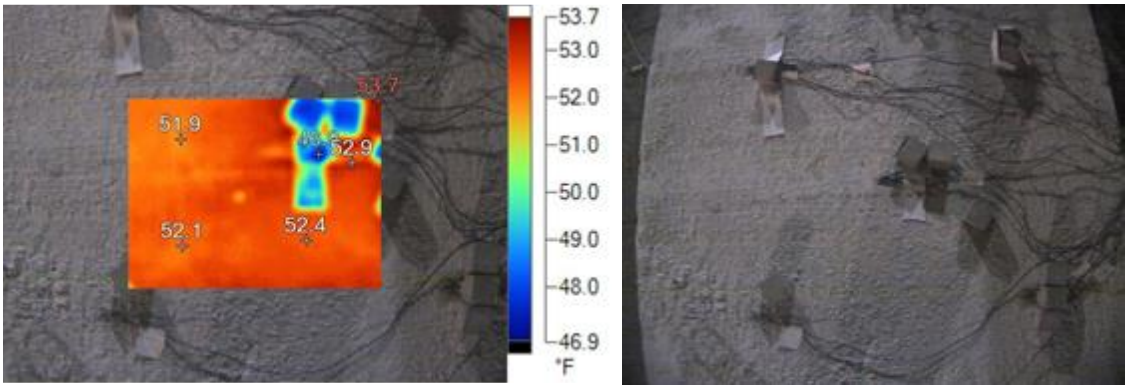

(a) (b)

Figure 5- 14 Slab Temperature in Vicinity of Thermocouple 4

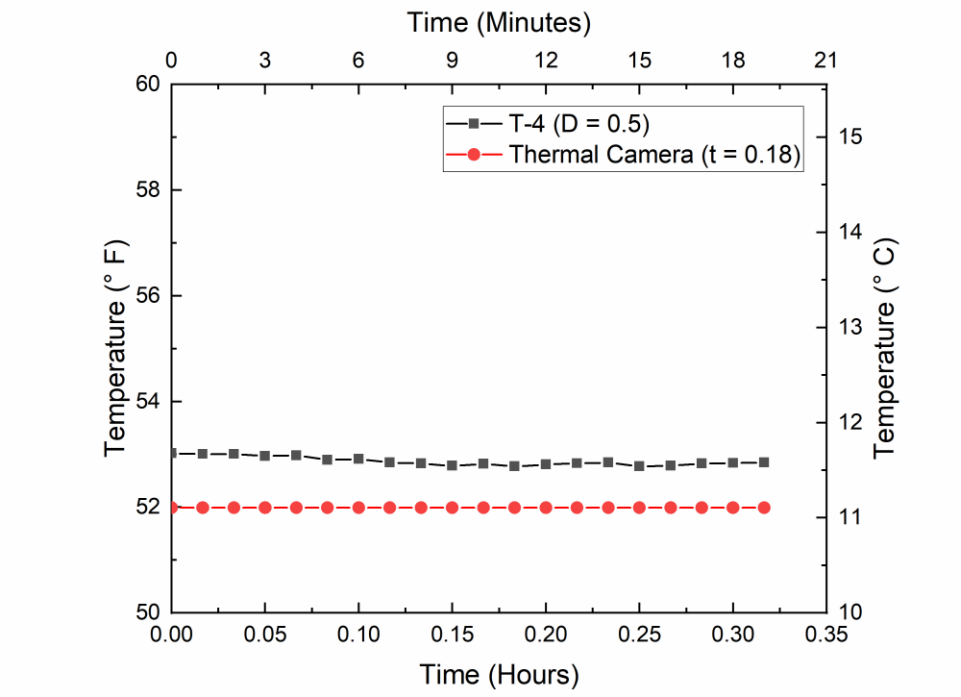
Time (Minutes)
0
3
6
9
12
15
18
21
T-4 (D = 0.5)
Thermal Camera (t = 0.18)
Temperature (° F)
Temperature (° C)
60
58
56
54
52
50
15
14
13
12
11
10
0.00
0.05
0.10
0.15
0.20
0.25
0.30
0.35
Time (Hours)

(a)

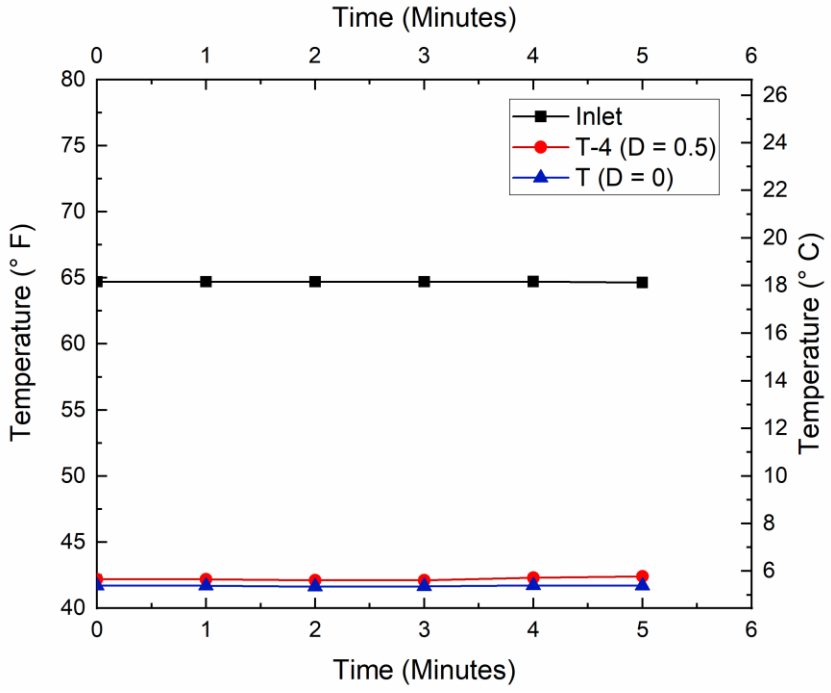
Time (Minutes)
0
1
2
3
4
5
6
Inlet
T-4 (D = 0.5)
T (D = 0)
Temperature (° F)
Temperature (° C)
80
75
70
65
60
55
50
45
40
26
24
22
20
18
16
14
12
10
8
6
Time (Minutes)

(b)

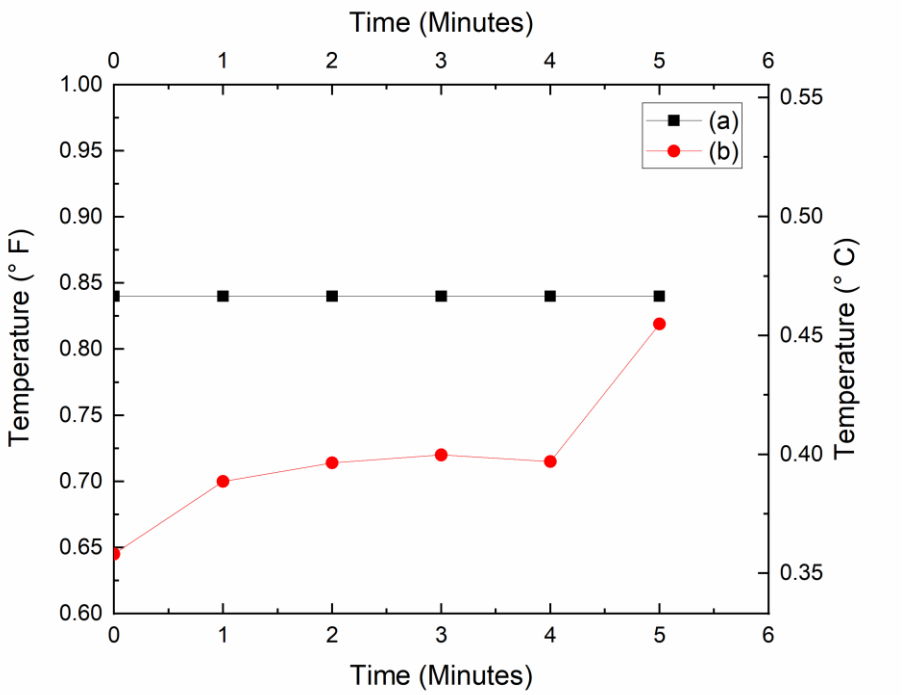

Figure 5- 15 (a) Comparison in temperature between T-4 and Thermal Imaging Camera, (b) Surface Temperature of Slab (Thermocouple Measurement), (c) Temperature Difference between T-4 (D= .5”) and T-4 (D= 0”)

5.8. Winter Simulation

5.8.1. Introduction

The validation of the de-icing system was determined during a Winter Event recorded on February 11-12 of 2018. A cold front passed a few nights prior to the event in which the temperature dipped slightly below 32 degrees Fahrenheit each night. A snow gun was utilized for the purpose of creating snow or ice over the slab to simulate a winter icing event. A washer and air compressor were used to project highly pressurized air through the snow gun to increase the surface area of water such that phase change is more likely. An additional study of the required heat flux needed to sufficiently melt the estimated ice accumulation during the winter event is analyzed. Figure 5-16 shows the complete assemblage of the snow gun attached to a air compressor of 125 psi capacity and pressure washer.

Figure 5- 16 Snow Gun Assemblage

5.8.2. Thermal Response for Winter Event

From figure 5-17 (a) and (b), the temperature immediately dissipated following the application of icy conditions to the slab. There was an immediate rebound in the slab temperature after the

cessation of the snow gun application. The measured environmental temperature fluctuated according to each cycle of ice/snow application via a snow gun, which was caused by warmer water entering the washer via a faucet. Therefore, each spike in environmental temperature corresponded to the fact that warmer water was initially projected towards the slab in a mist form. Conversely each dip in environmental temperature corresponded to the cessation of the snow gun, which resulted in ice accumulation along unheated portion of slab as the environmental temperature was around 25 ° F. Each thermocouple was able to maintain above freezing temperatures for the duration of the test as indicated by the freeing boundary line. Under the environmental conditions, a heat input of 70 ° F was sufficient to counter the event.

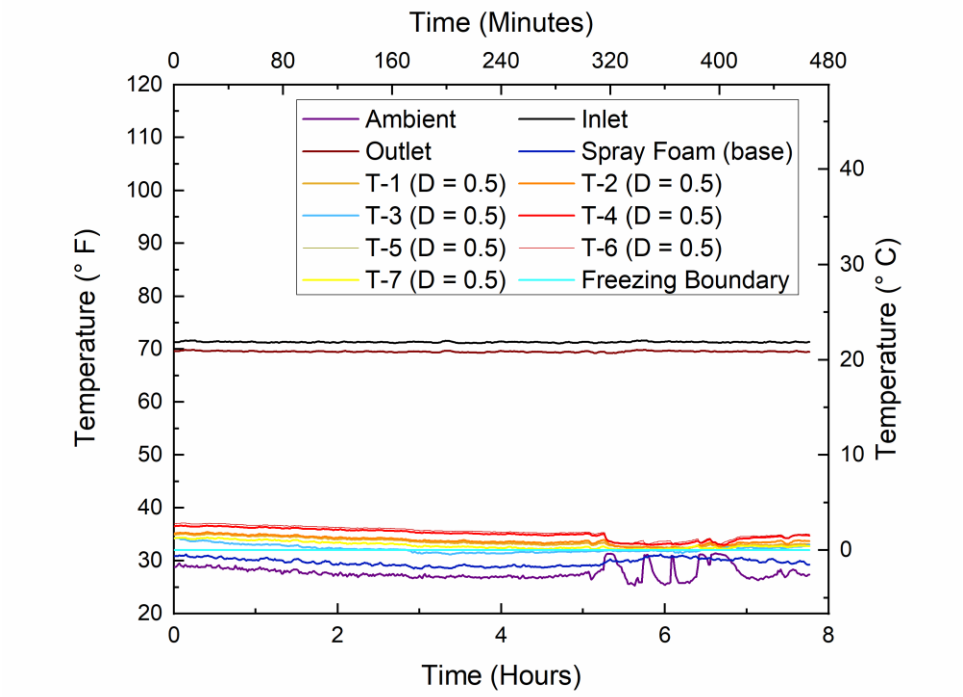

(a)

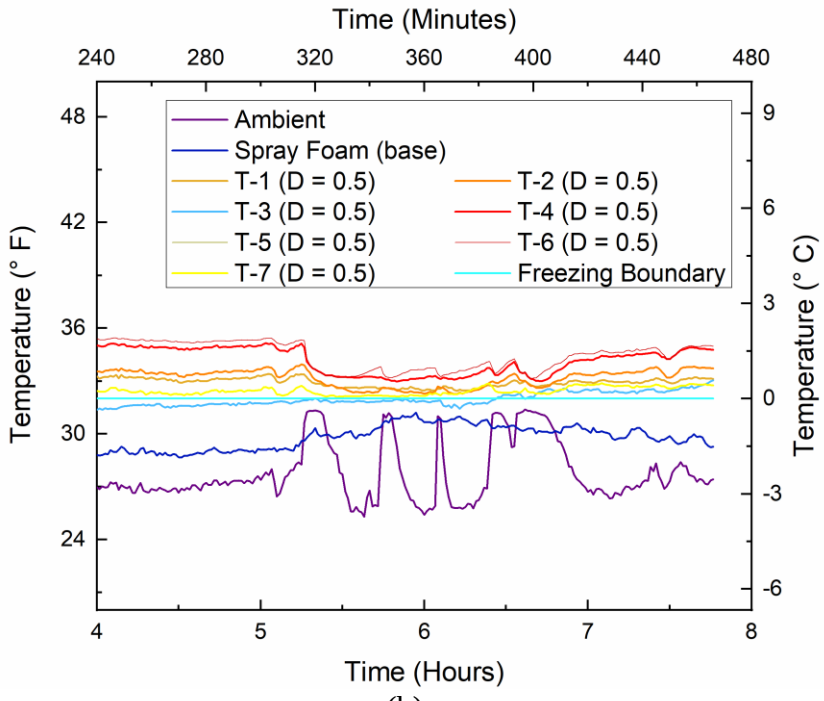

(b)

Figure 5- 17 (a) Winter Weather Event on February 11, (b)Winter Weather Even on February 11 (subset)

5.8.3. Thermal Imaging Comparison

According to figure 5-18 (a), the wind marginally and steadily increased during the event according to the weather underground database. Figure 5-18 (b) shows that the difference in temperature between the weather database and thermocouple is marginal. The study was performed to validate the thermocouple reading corresponding to ambient conditions. The outlier occurring around 8 A.M. is due to the snow making process, which was initiated around that time. This effect is a consequence of the oscillating ambient temp. due to mist exposure followed by brief cessation periods.

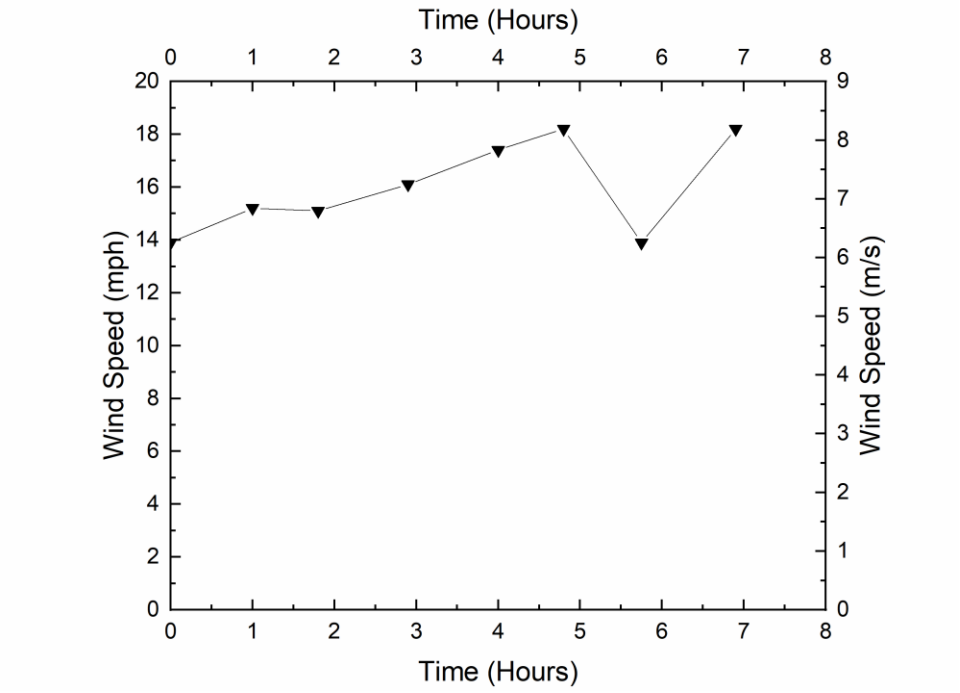

(a)

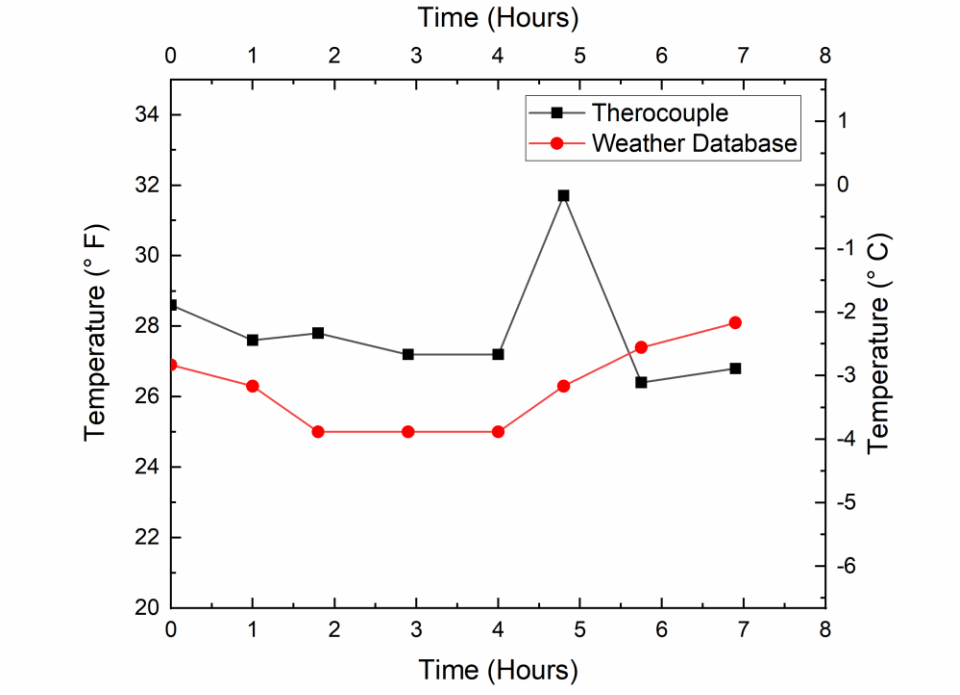

(b)

Figure 5- 18 (a) Environmental Temperature in respect to Weather Database and Thermocouple Measurements, (b) Wind Speed during Ice Event

5.8.4. Proportion as a Function of Depth, Z

According to figure 5-19 (a), the proportion, p, at thermocouple 4 varied from 0.18 to 0.28 in respect to different depths below the surface of slab. That is, roughly 20% of the heat load (I – A) is maintained near the surface. Figure 5-19 (b) shows the average proportion according to numerical plan 1. Figure 5-19 (c) shows the proportion as a function of depth below the slab surface. The upper and lower bounds are defined according to the variance in the proportion for numerical plan 1. There is less heat maintained towards the outer perimeter of the slab relative to the center, in consequence of the boundary effect. There is a near linear relationship for depths, --3.5 < Z < -0.5, and a large spike for D > -0.5. The reason for the spike is accounted for the placement of thermocouple T-4 at the base of slab, which was set at the interface between the pipe and slab. Thus, there is some offset from the vertical profile, which is at the midpoint between the pipe layout. The temperature at the midpoint will be lower since some heat is lost radially from the pipe network. Additionally, the thermocouples are likely offset by a marginal distance, which introduces some error. By extrapolating the data points for the surface and base along the vertical profile between the bounds, the heat flux can be estimated via equation (2). The average heat load corresponding to the event was 24.5 ° C (44 ° F). Therefore, the estimated heat flux at the surface is 2.38*24.5 = 58.3 W/m^2.

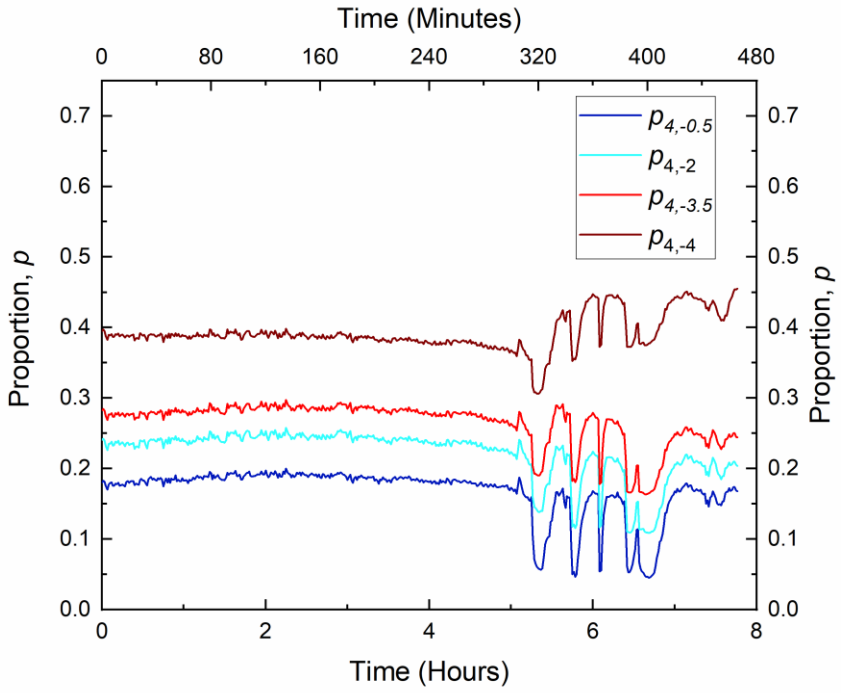
Time (Minutes)
0
80
160
240
320
400
480
0.7
0.6
0.5
0.4
0.3
0.2
0.1
0.0
Proportion, p
$p_{4,-0.5}$
$p_{4,-2}$
$p_{4,-3.5}$
$p_{4,-4}$
0
2
4
6
8
Time (Hours)

(a)

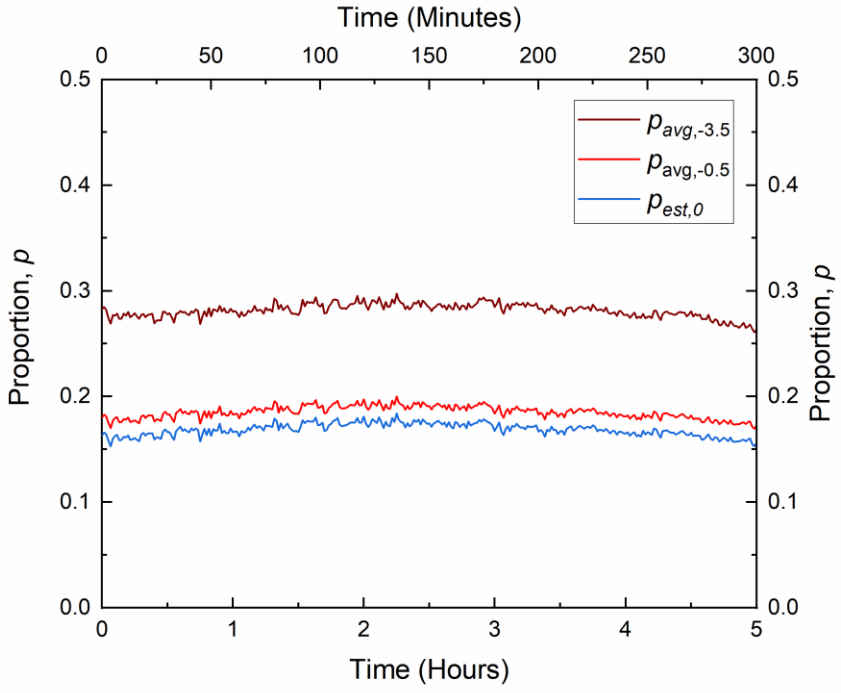
Time (Minutes)
0
50
100
150
200
250
300
0.5
0.4
0.3
0.2
0.1
0.0
Proportion, p
$p_{avg,-3.5}$
$p_{avg,-0.5}$
$p_{est,0}$
0
1
2
3
4
5
Time (Hours)

(b)

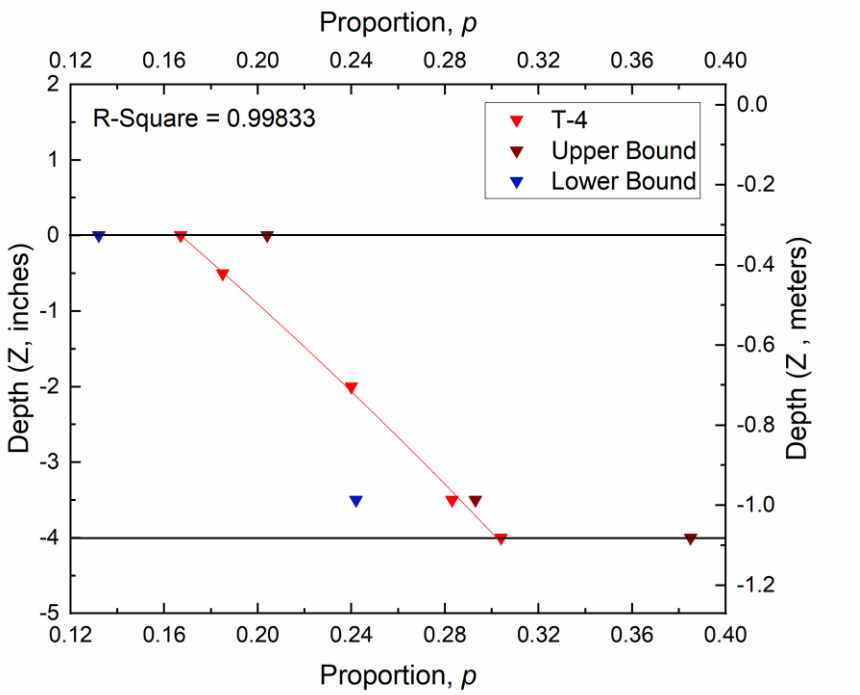

(c)

Figure 5- 19 (a) Proportion (P) during Ice Event (Thermocouple layout 1), b) Proportion (P) during Ice Event (Thermocouple layout 2) (c) 1D heat flux according to different snowfall rates

5.8.5. Heat Flux Analysis

Figure 5-20 displays the surface heat flux, required heat flux, and hydronic heat flux using equations (2), (3), and (5). The required heat flux to melt the imposed icy conditions was 51.2 W/m^2, which is an order of magnitude less than the estimated surface heat flux. The surface flux was sufficient for at countering the event, which was verified by figure 18. Some heat was lost at the boundaries as well as air pockets at interface between slab and foam. Figures 19 shows the extent of ice coverage along the slab. The ice was limited to the outer boundaries of the slab, which is cooler because of the pipe areal coverage at base of slab. Rocks were placed along the slab perimeter to show the boundary between ice and water coverage. Each thermocouple was measured within the inner region (melted region), which is consistent with estimated heat flux. The inlet temperature was set at 22 °C (71.6 °F) for the duration of the test, and the ambient temperature was maintained around -2.2 ° C (28 °F). Since the slab was only slightly above freezing during the test, a lower heat load (I – A) may not have been successful at countering the

event. By using equation (4), the estimated inlet temperature such that $T_{D=0} \geq 32$ ° for a 4" slab is 17.8 ° C (64 ° F).

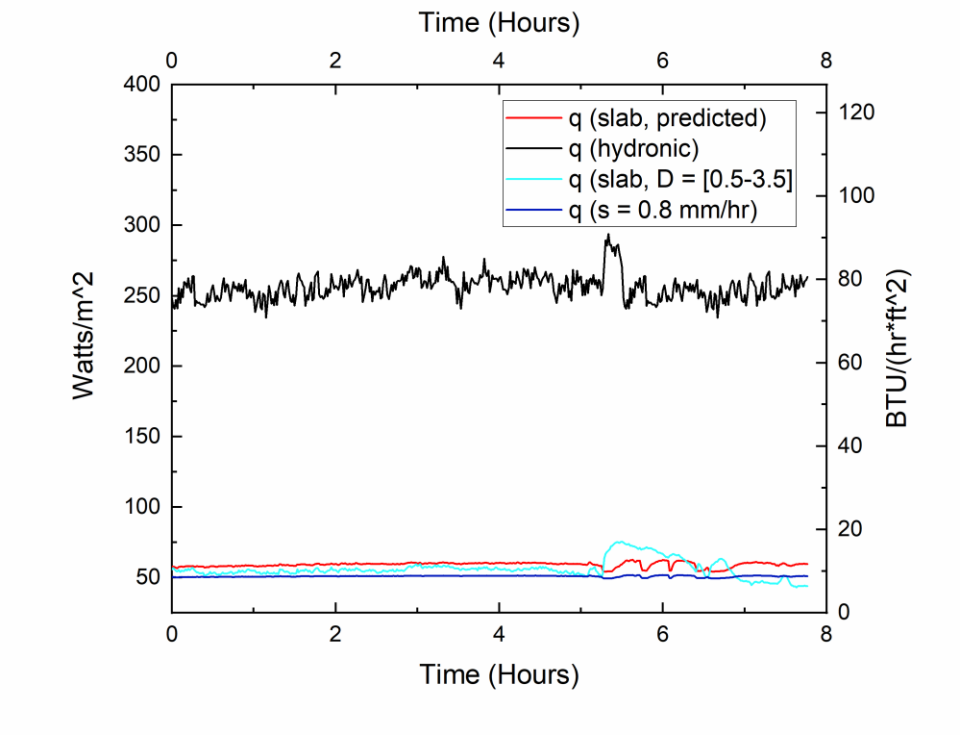

Figure 5- 20 Heat Flux during Winter Event

(a)

(b)

Figure 5- 21 (a) Creation of Freezing Mist via Snow Gun, (b) Icy Accumulation along Slab Boundaries Following Snow-gun Application

5.9. Method to Predict Slab Temperature at any Depth

5.9.1. Introduction

To predict the temperature at any depth below the slab surface, there must exist a consistent change in temperature between equal depth intervals. Since steady-state temperature is a function of the proportion, it follows that if $\Delta p/\Delta z = \alpha \in [a, b]$ where $|b-a|$ is reasonably small, then the prediction is valid. Let the number of depth intervals be defines as N and the number of thermocouples per set be defined as T. Then using thermocouple layout 2, it follows that the number of depth intervals is N = T-1 = 4-1 = 3. So, for each depth interval, α must deviate marginally from the mean for the prediction relationship to hold. Through trial and error, the alpha coefficient that minimizes the deviation in temperature between the actual and predicted results is 0.04/inch (1.57/meter) such that $|(P_{actual} - P_{predicted})|_{max} = 0.018$. The alpha coefficient corresponding to the Winter event is 0.036/inch (1.41/meter), which indicates that $\Delta p/\Delta z$ is consistent for steady-state and transient conditions (assuming Winter event is approx. at steady-state). By idealizing the thermal gradient profile using the alpha coefficient, the 1D heat flux at the surface of the slab can be reasonably estimated if the max proportion is known.

5.9.2. Estimation of Alpha Coefficient

To obtain an estimate for the alpha coefficient, it must first be verified that there exists a region of overlap corresponding to the variance from the mean. Thus, a 99% confidence region was used for each cyclic period to confirm that the possible mean coincides for each case. Figure 5-22 (a) shows the alpha coefficient corresponding to six nightly cycles. The calculated mean and standard deviation are 1.41 in^{-1} and 0.00452 respectfully. Figure 5-22 (b) shows the confidence bounds in respect to each depth interval for thermocouple arrangement 2. The variance is higher for the upper interval, which is constrained to the following depth range: $Z \in [-1.6,-0.8]$. This could be due to the upper interval being more sensitive to environmental conditions, which leads to a larger range of fluctuation over time. Since the confidence bounds are overlapped for each interval, the alpha coefficient is converging within a reasonable limit relative to the mean. Figure 5-22 (c) shows the that the mean alpha coefficient corresponding to each testing case deviates marginally from the predicted value, which was obtained by taking

the population average. This ensures that the predicted steady-state temperature can be reasonably estimated with minimal variance from the actual result. The alpha coefficient is, however, a function of wind magnitude. Thus, the limiting factor was that a wind sensor was not utilized to obtain such a relationship.

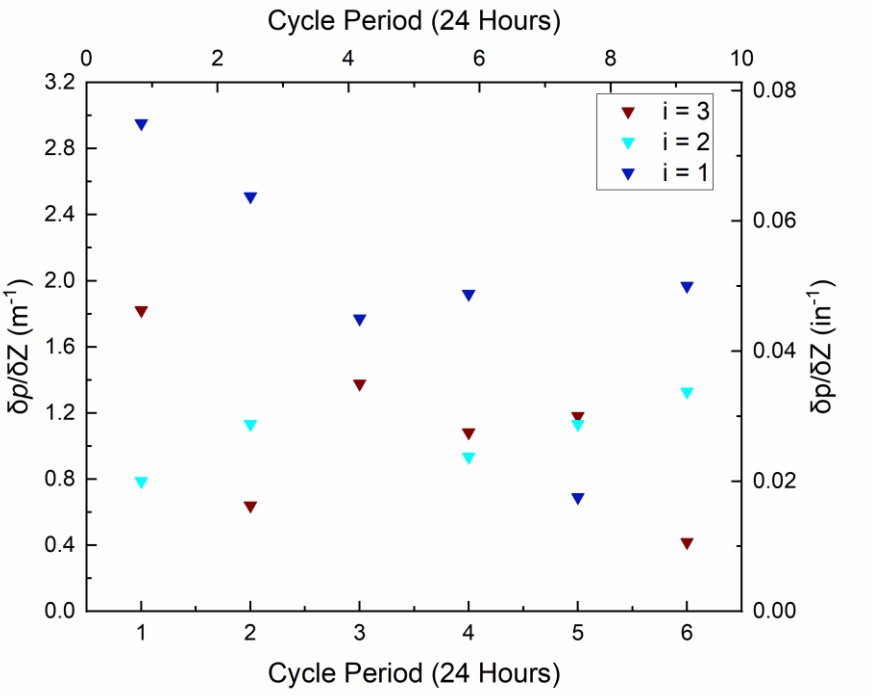

(a)

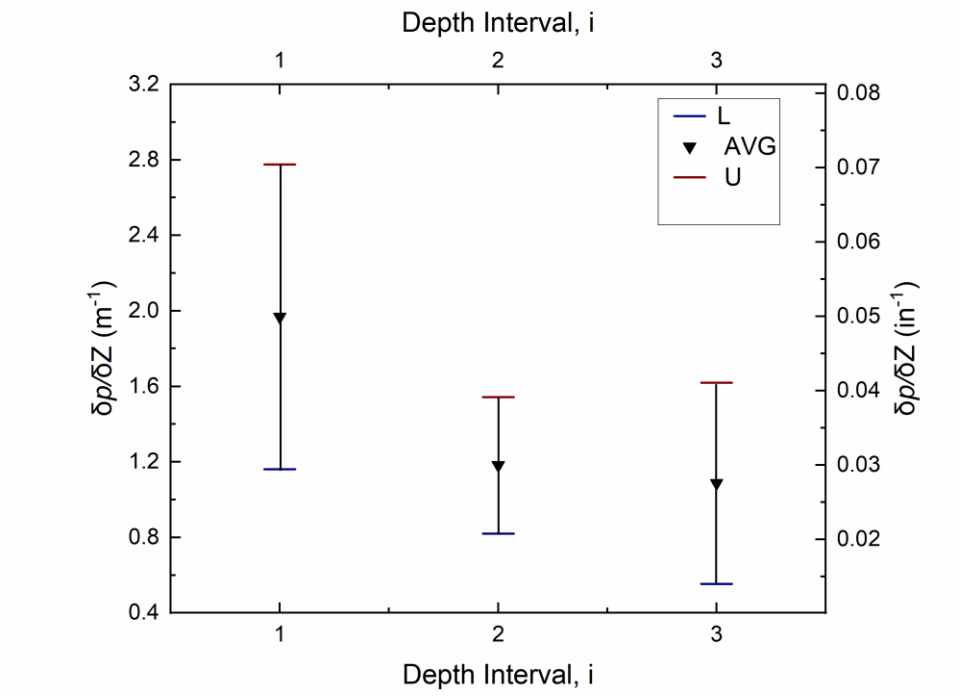

(b)

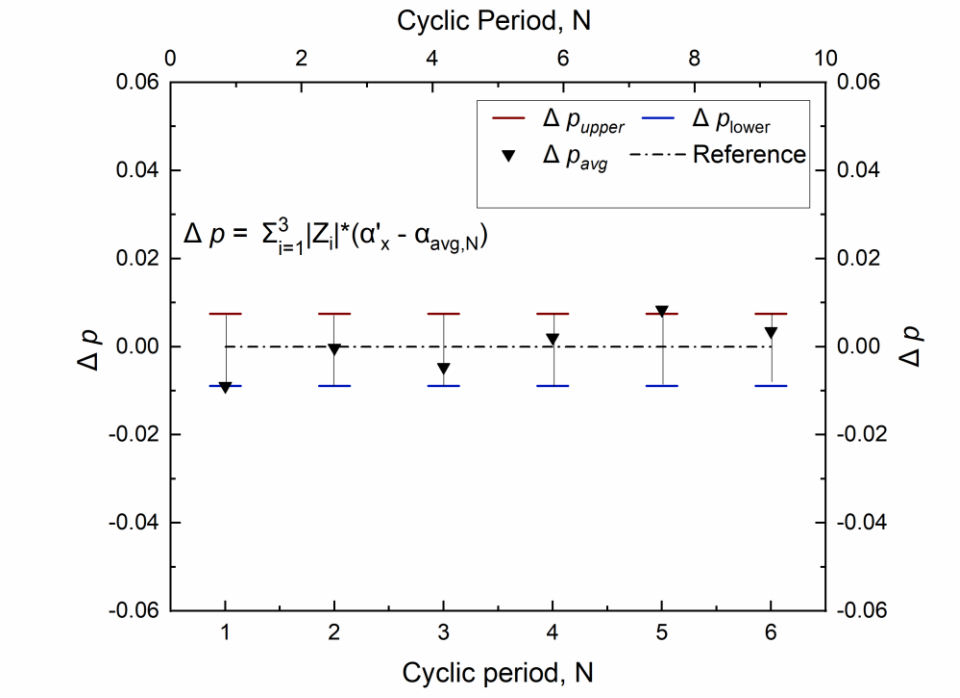

(c)

Figure 5- 22 Alpha Coefficient Estimation: (a) Variation in α for multiple cyclic periods (b) Vertical variation in α, (c) Deviation in the proportion relative to the mean over depth interval [-3.2,0]

5.9.3. Spread between predicted and Actual results

Figure 5-23 (a) shows that the temperature difference between the actual and predicted result using equation (9). There is a maximum spread of 0.35 ° F, which is insignificant across the slab length. This translates to a maximum difference of 0.018 between P_{actual} and $P_{predicted}$ via figure 5-23 (b). Figure 5-23 (c) shows the alpha coefficient range for multiple daily cycles. The maximum spread is approximately 0.03, which is amplified due to the increased reduction in temperature close to the surface of the slab. There are a few possible reasons for the relation: Air voids within the mortal paste near surface can introduce ambient air; There is increased noise (vibration) near the surface, which can cause increased thermocouple error; The depth at which the thermocouples were applied may be offset. By utilizing equation (13), the surface heat flux can be reasonably estimated if the heat load is known.

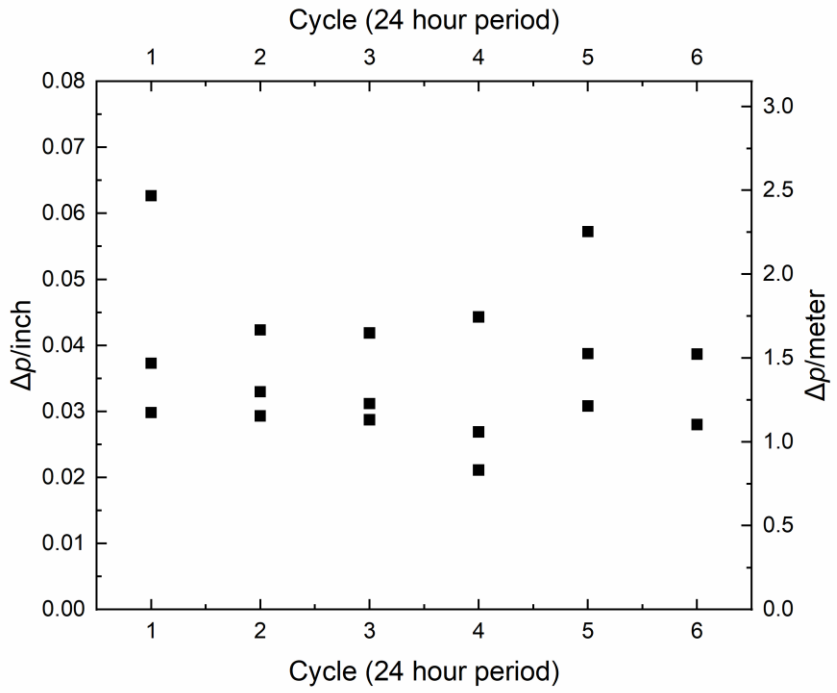

(a)

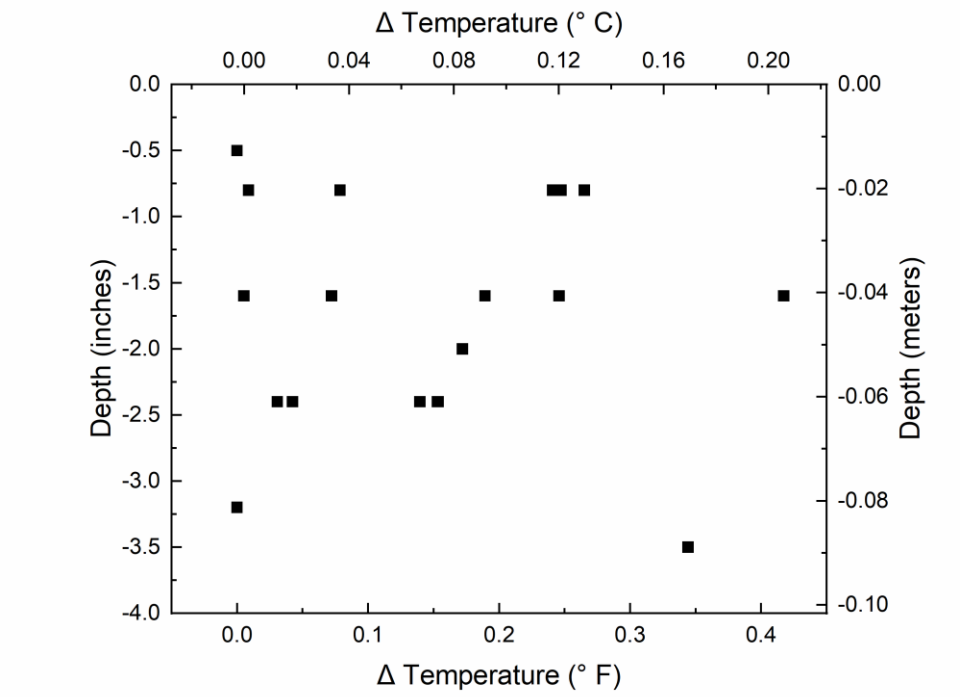

(b)

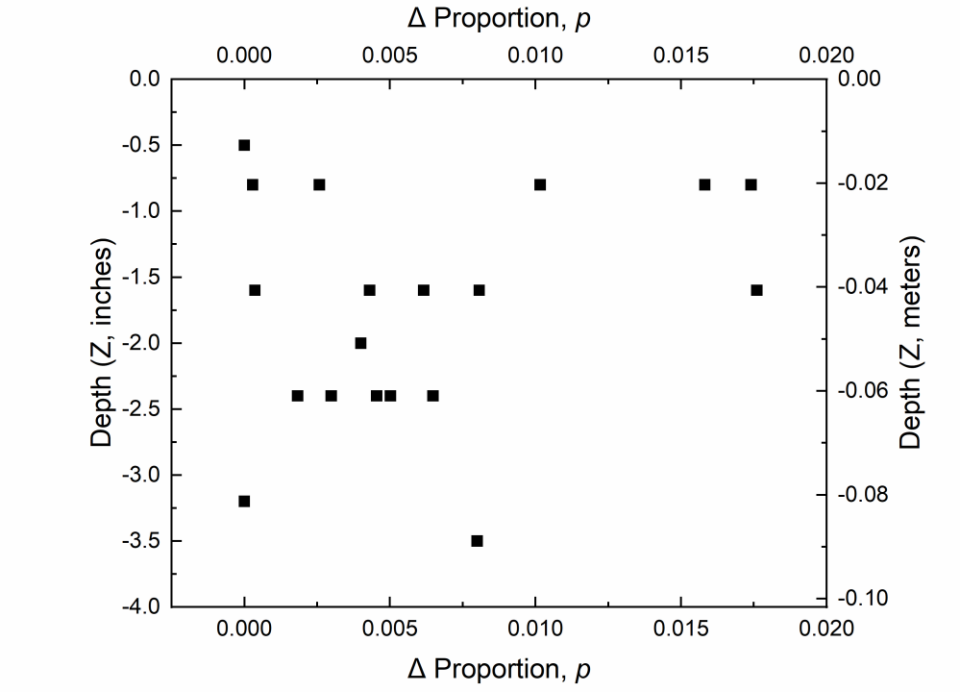

(c)

Figure 5- 23 (a) Minimum Temperature Change per Depth Interval (b) Minimum Change in Proportion per Depth Interval, (c) Minimum Alpha Coefficient per 24-hour Cycle

5.9.4. Prediction of Vertical profile for Nightly Cycle

As shown in figure 5-24 (a), there is an inverse relationship between wind speed and the quantity of heat transferred at different depths within the slab. Therefore, the heat input introduced into the system would need to be enhanced during winter storms because of increased wind. Hence, the minimum proportion must be considered to determine how much heat is enough to de-ice bridges. The proportion near the surface of the slab is a critical measure for potential de-icing. As shown in figure 5-24 (b), the proportion is highly variable depending on the wind conditions. Under very high wind conditions, the proportion dipped to a minimum of 0.115, which is significant reduction from the maximum (50%). Figure 5-24 (c) shows the proportion as a function of depth within slab, which strongly shifts to decreasing values as a function of cold front intensity. Thus, it is imperative to match the energy demands to some presumed environmental conditions to counter a possible icing event.

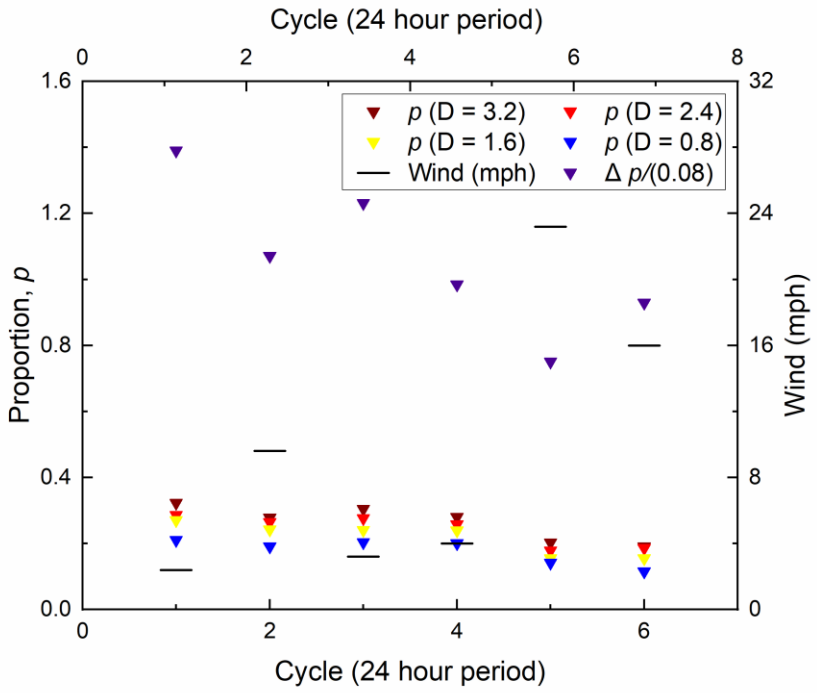

(a)

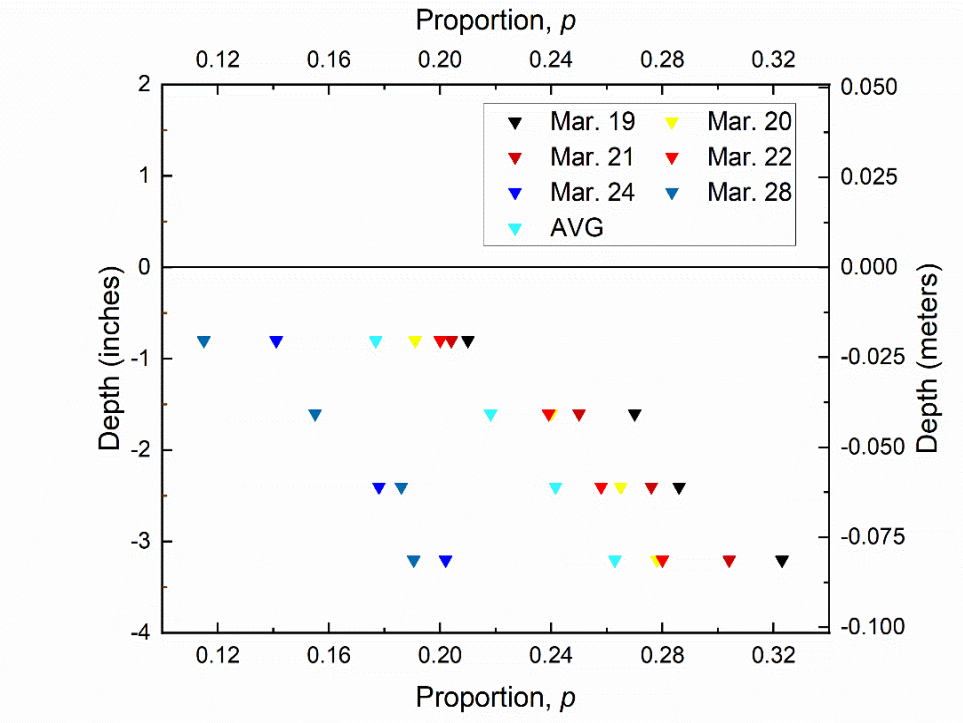
Proportion, p
0.12
0.16
0.20
0.24
0.28
0.32
2
1
0
-1
-2
-3
-4
0.050
0.025
0.000
-0.025
-0.050
-0.075
-0.100
Depth (inches)
Depth (meters)
Mar. 19
Mar. 20
Mar. 21
Mar. 22
Mar. 24
Mar. 28
AVG
Proportion, p

(b)

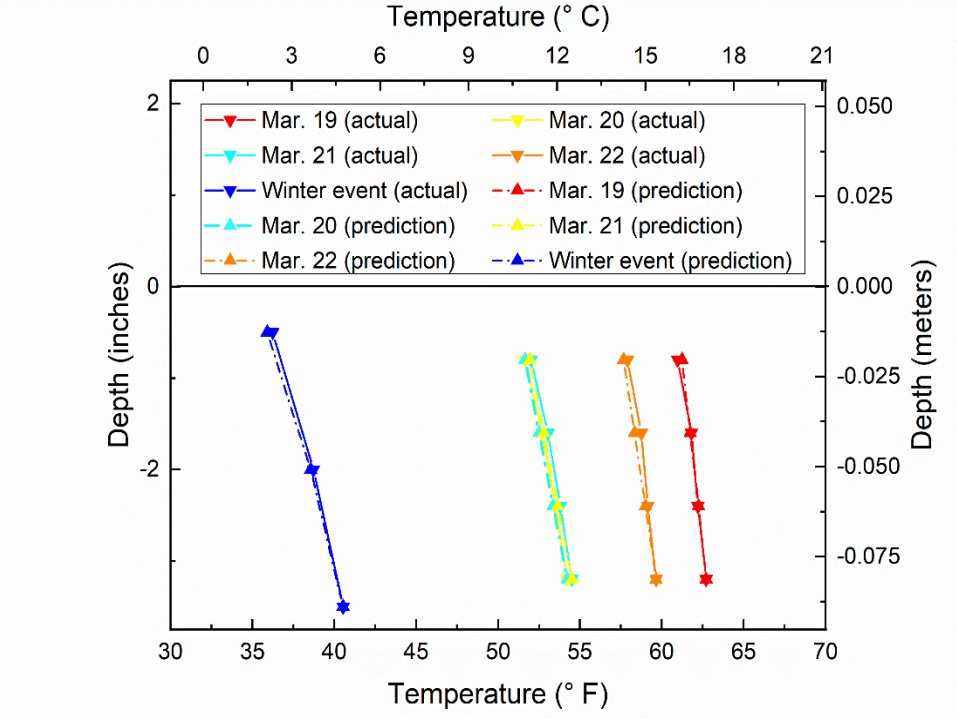

(c)

Figure 5- 24 (a) Proportion Range in respect to Depth and Wind Speed, (b) P as a Function of Wind Speed, (c) P as a Function of Depth

5.9.5. Proportion and Alpha Coefficient as a Function of Wind

The efficiency of the bridge de-icing system is greatly compromised by wind. The initial proportion obtained at a depth of 3.2" below the slab surface via thermocouple plan 2, was greatly reduced due to increasing wind magnitude. Because the surface of the slab is more sensitive to the negative effects of wind relative to the base, it will follow that the alpha coefficient will converge toward zero as wind tends to infinity. Thus, the heat flux will consequently decrease. Figure 5-25 exemplifies the aforementioned relation, which indicates that the thermal demands greatly increase due to wind. The wind magnitude, however, was attained using weather underground database. If an actual wind sensor was utilized, the results would be more consistent.

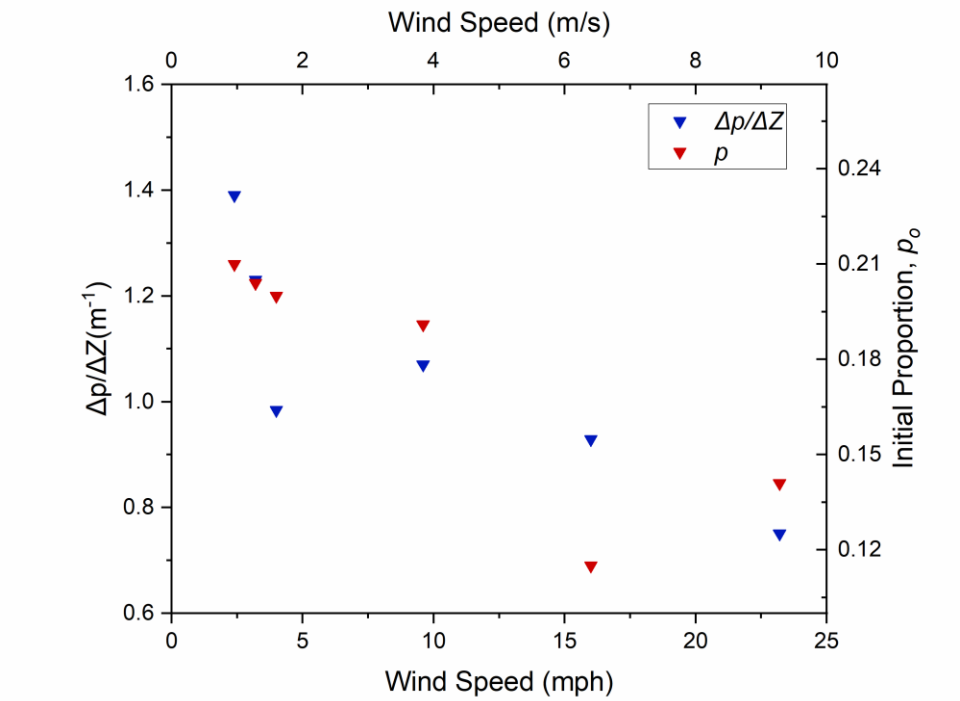

Figure 5- 25 p and α as a function of wind

Limitations and Recommendations

As the PEX pipe is attached to the base of the slab, only a point along the circumference of the pipe is in contact with the base. Hence, heat transfers to the slab along a line segment that extends from the inlet to the outlet. To maximize the flow of heat to the base, a thermal conductive paste or mortal should be applied such that the contact area becomes a rectangular region with a width equal to the diameter of the pipe. A small percentage of heat will be lost if insulation foam is injected within the void space occupied by the portion of the pipe not in contact with slab.

According to Fig. 5-26 (a), the spray foam injected at the base of the slab filled in between the void space at the contact zone between pipe and slab. This creates unnecessary tension to develop, which can cause separation of pipe from base of slab. Therefore, the surface area of contact (point contact) will be reduced overall implying that heat will be non-uniformly distributed. To correct this issue, mortar or thermal conductive paste can be injected into the void

space (≈ triangular regions) on both sides as illustrated from figure 5-26 (b) to prevent tensional forces from acting against the pipe network.

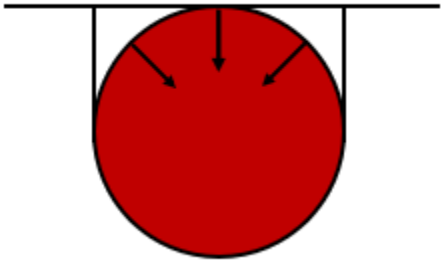

Figure 5- 26 (a) Pipe Injected at Contact Zone between Pipe and Base of Slab, (b) Tensional Forces Developed from Expansion of Spray Foam within void space

Conclusion

In conclusion, the experimental de-icing system perfumed quite well at countering icy conditions under various winter weather scenarios. The vertical temperature profile was consistent for each depth plane below the slab surface. That is, the change in the proportion per depth interval was confined within a narrow range. Moreover, the lateral variation in temperature across the slab length from sets 1-4 was relatively consistent in terms of heat being confined towards the center

of the slab. That is, the boundary effect due to the cooler outer perimeter of the slab will cause more heat to be lost toward at the boundaries of the pipe network. The surface temperature of the slab was consistent in respect to the fluke imaging camera and thermocouple measurement, implying that the imaging camera is accurate. Wind was determined to have major influence on the amount of heat retained within the slab. The proportion and alpha coefficient were found to be inversely proportional to wind magnitude. Thus, the efficiency of the system is greatly compromised by wind. By averaging the alpha coefficient for each depth interval for all cases, the steady-state temperature profile of the slab could be predicted to a reasonable degree. To maximize the transfer of heat to the slab, a thermally conductive paste or mortar should be applied within the void space occupied along the pipe length prior to the injection of spray foam at the base.

References

Alberdi-Pagola (2018). "Design and performance of energy pile foundations: Precast quadratic pile heat exchangers for shallow geothermal energy systems". Dissertation. Aalborg University, Denmark.

Bowers (2016). "Ground-Source Bridge Deck Deicing and Integrated Shallow Geothermal Energy Harvesting Systems." Dissertation. Virginia Polytechnic Institute and State University. Blacksburg, VA.

Brandl, H., (2006). "Energy foundations and other thermo-active ground structures". Geotechnique, 56(2), p.81-122.

Li, T., Lei, G., Yu, X., Zhang, N., & Puppala, A. J. "Numerical feasibility study of an externally heated geothermal bridge deck". In IFCEE 2018 p. 758-767. https://doi.org/10.1061/9780784481578.072

Brown, H., Kraus, M. and Bowders, J., (2014). "Decision methodology for temperature control of pavements. Transportation Research Record.:" Journal of the Transportation Research Board, 2403, p.45-51.

ECOMECH (2019). "Open Cell Spray Foam Insulation." http://www.ecomech.net/open-cell-spray-foam-insulation/

Eugster (2007). "Road and Bridge Heating Using Geothermal Energy. Overview and Examples". Proc, European Geothermal Congress. Unterhaching, Germany. Polydynamics Engineering, Malojaweg 19, CH-8048 Zurich, Switzerland

Fay, L., K. Volkening, C. Gallaway, X. Shi (2008). "Performance and impacts of current de-icing and anti-icing products: user perspective versus experimental data". TRB Committee AHD65. Prepared for the 87th annual meeting of the Transportation Research Board.

Fischel, M. (2001). "Evaluation of selected de-icers based on a review of the literature". Rep. No. CDOT-DTD-R-2001-15, SeaCrest Group, Louisville, CO.

Francesco Cecinatoa,c and Fleur A. Loveridge (2015). "Influences on the thermal efficiency of energy piles". Licensed under the Creative Commons Attribution-Non-Commercial-No Derivatives 4.0 International

Fahey (2008)." SNOWFALL RATE THRESHOLDS FOR LIGHT, MODERATE AND HEAVY. AERODROME METEOROLOGICAL OBSERVATION AND FORECAST STUDY GROUP" (AMOFSG). SEVENTH MEETING

Gangqiang Kong, Di Wu, Hanlong Liu, Lyesse Laloui ,Xiaohui Cheng , Xi Zhu (2018). "Performance of a geothermal energy deicing system for bridge deck using a pile heat exchanger." International Journal od Energy Research, 2019, Vol 43(1), p. 596-603.

Gode and Paeglitis, (2014). "CONCRETE BRIDGE DETEORATION CAUSED BY DE-ICING SALTS IN HIGH TRAFFIC ROAD ENVIRNMENT IN LATVIA". Institute of Transport Infrastructure Engineering, Riga Technical University

Graham Callum, Jessica Snow (2017). "De-icing Salts and Traditional Masonry. www.engineshed.org/publications

Isamu Yoshitake, Dr.Eng.; Narifumi Yasumura, Dr.Eng.; Masayuki Syobuzako;and Andrew Scanlon, Ph.D.,S.E., F.ASCE (2011). "Pipe Heating System with Underground Water Tank for Snow Thawing and Ice Prevention on Roads and Bridge Decks". Journal of Cold Regions Engineering. Vol 25 Issue 2

Jesús Chávez-Galán, Rafael Almanza and Neftalí Rodríguez Cuevas (2014). "Convective heat transfer coefficients: experimental estimation and its impact on thermal building design for walls made of different Mexican building materials" Concreto y Cemento. Investigación y Desarrollo Vol 5, No. 2, p. 26-38

K. Marita, M. Tago. (2000). "Operational characteristics of the GAIA snow-melting system in NINOHE, IWATE, JAPAN: DEVELOPMENT OF A SNOW-MELTING SYSTEM WHICH UTILIZES THERMAL FUNCTIONS OF THE GROUND". National Institute for Resources and Environment, 16-3 Onogawa, Tsukuba, Ibaraki 305-8569, Japan 2Akita University

Lei, G., Yu, X., & Li, T. (2018). "Design and numerical analysis of an externally heated geothermal bridge deck. In Civil Infrastructures" Proc, Confronting Severe Weathers and Climate Changes Conference, p.150-159.

Merrill (2002). " TEXAS' USE OF PRECAST CONCRETE STAY-IN-PLACE FORMS FOR BRIDGE DECKS." Texas Department of Transportation. Proc, Concrete Bridge Conference.

Minsk (1999)." Heated Bridge Technology.". Publication No. FHWA-RD-99-158. Federal Highway Administration. Washington, D.C.

Reysa, Gary (2005)." Ground Temperature as a Function of Location, Season, and Depth.". https://www.builditsolar.com/Projects/Cooling/EarthTemperatures.htm

Sirah Dubois (2019). "The Importance of Hypothesis Testing". https://sciencing.com/the-importance-of-hypothesis-testing-12750921.html

Omid Habibzadeh-Bigdarvish, Xinbao Yu, Gang Lei, Teng Li, Anand J. Puppala (2019). "Life-Cycle Cost-benefit Analysis of Bridge Deck De-icing using Geothermal Heat Pump System: A Case Study of North Texas" Sustainable Cities of Society, Vol 47

Piggott, Derek. "Understanding Flying Weather." Vol. 2, A & C Black Publishers Ltd, 2004.

Penn State University (2019). "Decision Making in Hypothesis Testing". https://newonlinecourses.science.psu.edu/stat500/node/44/

Yu, Puppala, Zhang (2017). "Use of Geothermal Energy for Deicing Approach Pavement Slabs and Bridge Decks, Phase 1": Final Report. TxDOT Report 0-6872-1